MECHANICAL PROPERTIES OF TRABECULAR MESHWORK

A Dissertation
Presented to
The Academic Faculty

by

Ke Wang

In Partial Fulfillment
of the Requirements for the Degree
of Doctor of Philosophy in the
Wallace H. Coulter Department of Biomedical Engineering

Georgia Institute of Technology and Emory University
May 2018

MECHANICAL PROPERTIES OF TRABECULAR MESHWORK

Approved by:

Dr. C. Ross Ethier, Advisor
Wallace H. Coulter Department of Biomedical Engineering
Georgia Institute of Technology and Emory University

Dr. W. Daniel Stamer
Department of Biomedical Engineering
Duke University

Dr. Machelle Pardue
Wallace H. Coulter Department of Biomedical Engineering
Georgia Institute of Technology and Emory University

Dr. Andres J. Garcia
George W. Woodruff School of Mechanical Engineering
Georgia Institute of Technology

Dr. Todd Sulchek
George W. Woodruff School of Mechanical Engineering
Georgia Institute of Technology

Date Approved: 12/15/2017

Dedicated to Ziping Xu and both our families

ACKNOWLEDGEMENTS

This dissertation would not have been possible without the generosity, support and help of many people.

First and foremost, I wish to express my gratitude to my advisor, C. Ross Ethier, for his great help, support and mentoring throughout my graduate studies. I met Ross during my Masters at Imperial Collage London. His vivid introduction of tissue mechanics is the reason why I decided to join his group and pursue a PhD afterwards. He is the most fantastically brilliant and incredible advisor I have ever seen, who cares about the well-being and intellectual advancement of his trainees. I have learned a lot from him in almost every aspect of doing research: tackling challenges, writing, presentation, peer-review, communicating, critical thinking and paying attention to the details, etc. Ross was incredibly patient with me especially when I was stuck in a situation where no progression was made for months. He inspired and encouraged me by suggesting a variety of solutions and meanwhile, searched for other resources as much as he can to help me get through the difficulties. I couldn’t have asked for a better advisor.

I would like to thank all the collaborators who help and support to my dissertation projects. Dr. Acott and Dr. Vranka at the Casey Eye Institute provided me with almost all the human samples for my study. Dr. Johnstone and Dr. Wang at the University of Washington were extraordinarily generous to help me with the OCT experiments and tissue structure delineation. Dr. Stamer and Dr. Li at Duke University were also extremely helpful in providing DEX treatment on mice and making measurements on IOP and facility.

To each of the members of my thesis committee, I am thankful for their advice on my research. Dr. Stamer provided me with valuable insights in experimental design and made me think through the rationality of each individual detail. Dr. Pardue always had great suggestions on how to think of differences between different strains of mice and the translational value of the research to the big picture. Dr. Garcia was always willing to provide more suggestions in the numerical methods and finite element models. Dr. Sulchek was extremely willing to sit down with me to discuss about details in AFM measurements and how to interpret the results. I cannot thank each of you enough.

I was very fortunate to be a member of the Ethier lab, not only because I have access to cutting-edge experimental instruments without worrying about the cost, but also because I have wonderful lab mates. Tom was extremely kind and helpful. He spent tons of hours helping me with AFM experiments, histology and microscopy. I could easily have spent 1 more year on TM stiffness measurements without his help. Baptiste, Andrew and Stephen have offered me tremendous help in the finite element models. They were willing to stop their work and provide solutions and suggestions to every single question of mine. I can’t list all of you here but you have all contributed to my happiness during the 5 years.

I would like to express my sincere gratitude to my family in China. My father Jiaping Wang and my mother Xiaoping Lu are always there for me. Your unconditional support and encouragement were essential to get myself through this work.

Last but not least, I would like to give my special thanks to my amazing husband, Ziping Xu. Thank you so much for your warm and lovely support. Without you, I would not have such real Chinese food with full of nutrition every night from the lab. You helped me stay positive and have a very happy home.

TABLE OF CONTENTS

LIST OF TABLES

LIST OF FIGURES

LIST OF SYMBOLS AND ABBREVIATIONS

AFM	Atomic Force Microscopy
AH	Aqueous Humor
α-SMA	α-Smooth Muscle Actin
C	Outflow Facility
CB	Ciliary Body
CC	Collector Channel
CTGF	Connective Tissue Growth Factor
DEX	Dexamethasone
DEX-PB-NPs	DEX-encapsulated Pentablock Copolymer-based Nanoparticles
E	Trabecular Meshwork Stiffness
ECM	Extracellular Matrix
ET	Endothelial Lining
EVP	Episcleral Venous Pressure
FEM	Finite Element Modeling
HF	High Flow
hTM	human Trabecular Meshwork
LF	Low Flow
LHS	Latin Hypercube Sampling
LPA	Lysophosphatidic Acid
NO	Nitric Oxide
IOP	Intraocular Pressure
OCT	Optical Coherence Tomography

OHT	Ocular Hypertension
POAG	Primary Open-angle Glaucoma
ROCK	Rho-associated Protein Kinase
SC	Schlemm’s Canal
SCE	SC Endothelial
SD-OCT	Spectral Domain Optical Coherence Tomography
SFRP1	Secreted Frizzled Related Protein-1
SIG	Steroid-induced Glaucoma
S1P	Sphingosine-1-phosphate
TGF- β_2	Tissue Growth Factor - β2
TLS	Transluminal Structure
TM	Trabecular Meshwork

SUMMARY

Glaucoma is the second leading cause of blindness. However, the precise mechanisms leading to vision loss in this group of diseases remain unknown. Increased intraocular pressure (IOP) has been recognized as the most important risk factor, and lowering IOP is currently the only effective treatment for glaucoma. Unfortunately, pressure lowering usually only slows progression and does not cure the disease. Interestingly, the mechanical properties of the trabecular meshwork (TM) have been suggested to differ significantly between glaucomatous eyes versus unaffected eyes. This is important because the TM provides major resistance to the conventional outflow of aqueous humor and thus has a major influence on IOP. The objective of this work is to develop computer modeling and experimental tools to characterize TM stiffness in situ for human and mouse eyes, and to evaluate the role of mechanical properties of TM in influencing IOP across different conditions.

We developed an inverse finite element method to estimate TM stiffness in dissected anterior wedges from 6 normal and 5 glaucomatous human eyes, in combination with optical coherence tomography (OCT) imaging. The results obtained from this method were also compared to direct measurements using atomic force microscopy (AFM). We showed that TM stiffness was higher, but only modestly so, in glaucomatous patients. Interestingly, outflow resistance in both normal and glaucomatous human eyes appeared to positively correlate with TM stiffness. We then went on to study TM in mice, first developing a cryosection-based AFM technique to localize and directly measure compressive Young’s modulus of TM. We found a significant correlation between TM stiffness and outflow resistance in wild-type mice. Further, we found that local DEX treatment of eyes in live mice can induce higher IOP, and that a significant correlation between TM stiffness and outflow resistance also existed in DEX-treated mice.

Together these findings suggest that TM stiffness is a surrogate marker for conventional outflow pathway function. This work motivates development of therapies to alter TM stiffness, or the factors underlying TM biomechanical property regulation, as potential novel alternative treatments for control of ocular hypertension in glaucoma**.**

CHAPTER 1. INTRODUCTION

Part of this chapter (Sections 1.4-1.6) is based on a published journal paper. Citation: Wang K, Read AT, Sulchek T, et al. Trabecular meshwork stiffness in glaucoma. Experimental Eye Research 2017, Vol.158, 3-12. doi: 10.1016/j.exer.2016.07.011

1.1 Anatomy of the Eye

The mammalian eye is a slightly asymmetrical globe largely filled with a clear gel called the vitreous humor (**Figure 1.1**). Light passes through the pupil and lens to reach the back of the eye. The retina (containing specialized light-sensing cells) converts incoming light into action potentials that are carried by the optic nerve to the visual cortex to generate vision.

The overall shape of the eye is maintained by its relatively stiff envelope, the so-called corneoscleral shell, and the intraocular pressure (IOP). The IOP is generated and maintained via the aqueous humor circulation system in the anterior part of the eye, which is divided into two chambers by the iris, namely the anterior and posterior chambers (**Figure 1.2**). The aqueous humor is a transparent fluid (98% water) that is secreted by the ciliary body into the posterior chamber at an approximately constant rate and then flows into the anterior chamber through the pupil. It then exits the eye through the so-called outflow pathway to return to the systemic circulation. There are two main outflow pathways, namely the conventional and unconventional outflow pathways (arrows in **Figure 1.2**).

In the conventional, or trabecular, outflow pathway, aqueous humor flows through a porous tissue called trabecular meshwork (TM), enters Schlemm's canal (SC) and then drains into the episcleral veins. In the unconventional, or uveoscleral, outflow pathway, the aqueous humor enters the ciliary muscle and reaches the vortex veins or permeates across the sclera [1]. The majority of aqueous humor outflow occurs through the conventional pathway, which is the primary pathway relevant to IOP maintenance under normal circumstances [1]. The bulk of the flow resistance provided by this pathway is thought to be located at TM and SC endothelium [2-4], and thus these tissues have a major role in the control of IOP. As such, they are a major focus of research efforts in multiple labs around the world.

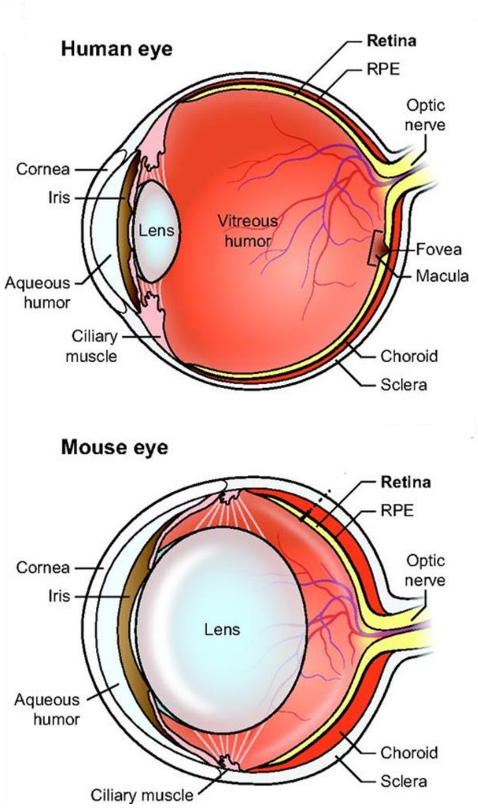

Figure 1.1: Schematic diagrams of cross-sections of human (top) and mouse eyes (bottom). Reproduced from Veleri et al. 2015 [5].

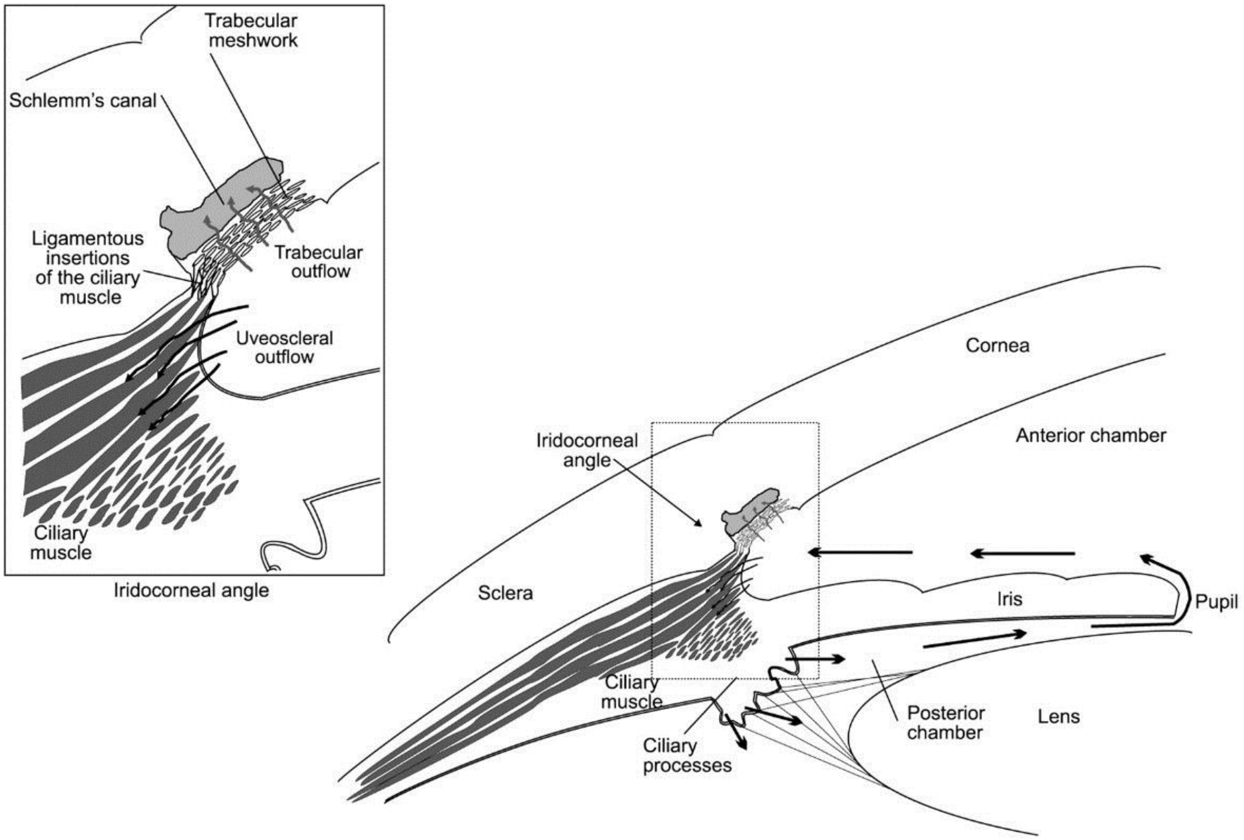

Figure 1.2: Schematic diagram of the aqueous humor circulation [6]. The aqueous humor is produced in the ciliary processes, flows into the anterior chamber through the pupil and exits the anterior chamber via either the trabecular or unconventional pathways.

1.2 Mouse Eyes vs. Human Eyes

Mice are important animal models for eye-related research, in part because their eyes share similarities with human eyes in both anatomy and function. For example, previous studies have shown that the conventional outflow pathway of mouse eyes resembles that of primate eyes in both their well-developed continuous SC and lamellated TM, and in their network of elastic fibers which tether the TM and SC inner wall to the ciliary muscle tendons [7]. In both humans and mice, the trabecular beams exhibit a central core of collagen oriented parallel with the long axis of the beam. A layer of basal lamina material surrounds the core on all sides. Usually adjacent trabecular beams are separated by a space about the same width as the beams. The spaces get quite narrow in the region directly adjacent to SC.

On the other hand, there are differences between mouse and human eyes, in addition to size. (1) The interior of the mouse eye is mostly occupied by the lens (**Figure 1.1**, bottom) and there is no macula lutea or lamina cribrosa in the mouse eye. (2) The number of trabecular beans are also different. In mice, there are 3-4 anterior and 7-10 posterior trabecular beams, which is about 1/3 – 1/2 the number in human eyes [8, 9]. (3) Further, in mice, iris processes can attach to the termination of Descemet's membrane known as Schwalbe's line, which is rarely seen in the human eye [8].

Functionally, mouse eyes are similar to human eyes, in that they have no detectable washout while all other species studied to date show washout (time-dependent outflow facility increase with perfusion) [10]. Further, mouse eyes of the C57BL/6 strain respond to all conventional outflow active drugs tested to date (including sphingosine-1-phosphate (S1P) and PG-EP_4 receptor agonist) in a similar manner as for human eyes [11]. Specifically, S1P decreases outflow facility in mouse eyes by 39% and PG-EP_4 causes a facility increase of 106% in mice, both of which are consistent with previous reports in human eyes [12, 13].

1.3 Glaucoma

1.3.1 Pathophysiology

Glaucoma is the second most common cause of blindness worldwide. It is characterized by damage to the optic nerve (composed primarily of retinal ganglion cell axons), which transmits visual information from the retina to the brain. Unfortunately, optic nerve damage in glaucoma causes irreversible vison loss. Elevated intraocular pressure (IOP) is one of the most important risk factors for glaucoma [14]. It is caused by an increased outflow resistance (or decreased outflow facility) to drainage of aqueous humor (AH) via the so-called conventional outflow pathway (**Figure 1.2**). As explained in greater detail in Section 1.3, this increased resistance is thought to be due to changes in the trabecular meshwork and/or inner wall of Schlemm's canal which hinder the normal drainage of aqueous humor.

1.3.2 Treatments for Glaucoma

The goal of current treatments for glaucoma is to preserve vision by reducing IOP to a target value, using either medication or surgery. Common classes of medications used to lower IOP include prostaglandin analogues (to increase unconventional aqueous humor drainage), beta-adrenergic blockers (to reduce aqueous humor production), alpha-adrenergic agonists (to reduce aqueous humor production, with a minor increase in outflow) and cholinergic agonists (to increase conventional aqueous humor outflow). However, these drugs can have both local and systemic adverse effects [15], such as ocular irritation and dry eye. Thus, some of these drugs are contraindicated, e.g. beta-adrenergic blockers are inappropriate for patients with diseases like chronic pulmonary obstruction or asthma.

Surgically, laser trabeculoplasty is widely used to lower IOP by inducing biological changes in the trabecular meshwork (TM), resulting in increased aqueous outflow. Additionally, trabeculectomy is a commonly performed incisional surgical procedure that reduces IOP by excising a small portion of the TM or adjacent corneoscleral tissue to provide an alternate drainage route for aqueous humor. However, all of those treatments usually only slow progression and do not cure the disease. The pathobiology of elevated IOP in glaucoma is still poorly understood and the factors contributing to its progression have not been fully characterized. Thus, there is a pressing need for deeper knowledge of mechanisms that influence IOP in health and disease so as to develop new treatment strategies.

1.4 The Trabecular Meshwork (TM)

The TM can be divided into three parts according to tissue ultrastructure: the uveal meshwork, the corneoscleral meshwork and the juxtacanalicular connective tissue (JCT, also known as the cribriform meshwork; **Figure 1.3**). The uveal meshwork is the layer closest to the anterior chamber. It is formed by connective tissue extended from the iris and ciliary body. The intercellular spaces in this region are relatively large, so that it provides little resistance to the outflow of aqueous humor. The layer adjacent to the uveal meshwork is the corneoscleral meshwork. This layer is composed of lamellae and perforated plates covered by TM cells standing on a basement membrane [6]. The intercellular spaces in the corneoscleral meshwork are narrower than that in the uveal meshwork, although still not thought to be small enough to contribute the major resistance to the aqueous humor outflow. The JCT, which has direct contact with the inner wall of endothelium of SC, is an amorphous layer consisting of cells interspersed amongst ECM. It has the smallest flow passageways in the TM, and thus it has been suggested to be the major site providing resistance to outflow within the TM [2, 16].

The lamellae or beams and plates in the uveal and corneoscleral meshwork are covered by TM cells. TM cells are similar to endothelial cells in some ways, but also demonstrate additional phenotypical features, such as phagocytosis, migration and contractility [17]. The main components of ECM in the TM are collagens, elastin, proteoglycans and glycoproteins [18-21] and they provide the scaffold for TM cells to reside on and also interact with the cells. More specifically, the stroma of the beams in the uveal and corneoscleral meshwork exhibits typical collagen fibrils (type I and III), elastic fibers and microfibril sheath-derived (SD) material [18]. Additionally, the basement membrane proteins, type IV collagen and laminin, and basement membrane proteoglycans have been identified in the JCT region [22].

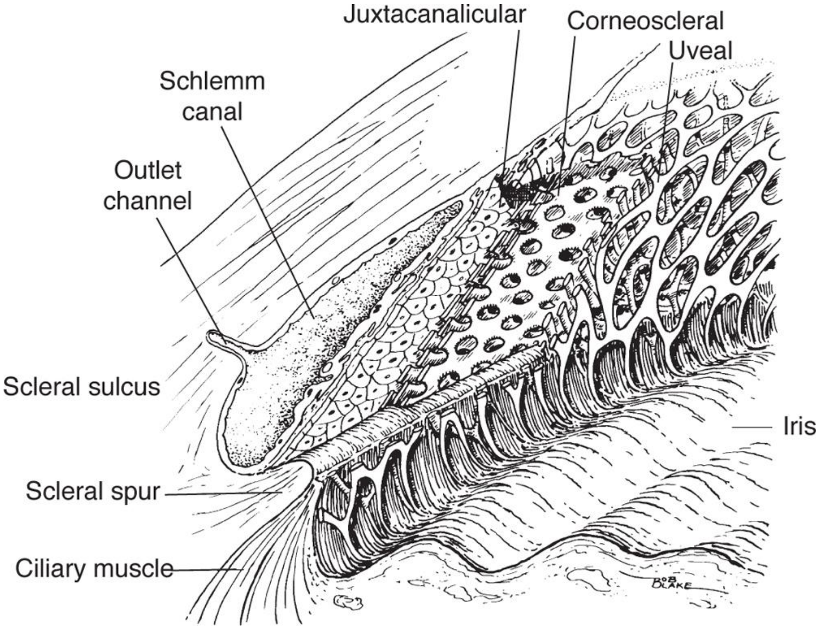

Figure 1.3: Schematic diagram of the TM. The arrows indicate the direction of the aqueous humor flow, from the anterior chamber toward Schlemm's canal (SC). The different regions of the TM are the uveal meshwork, the corneoscleral meshwork and the juxtacanalicular (or cribriform) meshwork. Resistance to aqueous humor flow increases progressively from the anterior chamber to SC as intercellular spaces narrow (reproduced from Textbook of Glaucoma. 3rd ed. Baltimore: Williams & Wilkins; 1992).

The resistance provided by the TM is quantified by the outflow facility, which is the mathematical inverse of the outflow resistance. Outflow facility $\boldsymbol{C}$, is defined by the standard Goldmann's equation:

$$\boldsymbol{C} = \frac{\boldsymbol{Q}-\boldsymbol{Q_u}}{\boldsymbol{IOP}-\boldsymbol{EVP}} \qquad (1)$$

where $\boldsymbol{Q}$ is total aqueous humor outflow rate, $\boldsymbol{Q_u}$ is the unconventional outflow rate, and EVP is episcleral venous pressure. Goldmann's equation simply states that outflow facility is the flow rate of aqueous humor through the trabecular meshwork divided by the pressure drop across this pathway.

In normal human eyes, the typical EVP is approximately 7-8 mmHg [23] and IOP ranges from 10-20 mmHg [24], which results in a pressure difference across the trabecular outflow pathway of around 8 mmHg. The aqueous humor is produced at an average rate of 2.75 µl/min [25] and normal outflow facility is around 0.23 µl/min/mmHg [26, 27]. The percentage of unconventional outflow of aqueous humor ranges from 0-62% of total outflow depending on measurement approaches (direct or indirect) and age [28].

1.4.1 TM Stiffness

There are several observations which suggest that TM stiffness may be important in ocular hypertension associated with glaucoma. For example, pharmacologic modulation of TM cell actomyosin tone has a significant effect on outflow facility [29]. Further, using direct measurements of TM biomechanical properties, Last et al. (2011) reported that the compressive stiffness of TM was 20 times greater in post mortem glaucomatous human eyes compared to ostensibly healthy eyes [30]. These findings have motivated us to study how TM stiffness and fluid flow resistance are interrelated.

Stiffness is a measure of the tendency of a material to resist deformation when it is loaded, i.e. when a force is applied to it. There are many types of forces acting on tissue, including forces that pull or push perpendicular to the tissue surface (i.e. tensile forces or compressive forces) and shear forces which are parallel to the surface. Those forces can apply stress (unit: Pascals) on the tissue, defined as the force (unit: Newtons, N) normalized by the area over which it acts. Tissue stiffness can be formally quantified through the elastic modulus, which is the magnitude of a stress divided by the strain (deformation) induced by the stress. More specifically, Young's elastic modulus describes the resistance to compressive or tension forces while shear elastic modulus describes the resistance to shear forces.

In the simplest case, strain ($\boldsymbol{\epsilon}$, quantifying the extent of tissue deformation) is defined by

$$\boldsymbol{\epsilon = \frac{tissue\ deformation}{tissue\ original\ length}}$$

Similarly, the load is quantified through the stress, $\boldsymbol{\sigma}$

$$\boldsymbol{\sigma = \frac{force}{tissue\ cross\text{-}sectional\ area}}$$

A measure of tissue stiffness is then Young's modulus, $\boldsymbol{E}$, defined as:

$$E = \frac{\sigma(\epsilon)}{\epsilon}$$

Here we explicitly note that the stress depends on the strain; in fact, for soft tissues, this dependence is usually non-linear so that Young's modulus is not a constant value, but one that varies with the strain. In this case, we can describe tissue stiffness by an effective Young's modulus, or more simply, by "the modulus". The implication is that comparison of stiffness values from different studies is strictly only valid when the extent of tissue deformation is comparable between studies.

In addition to the magnitude of strain, the effective Young's modulus of soft tissues typically depends on a number of other factors, including how the external force is applied (i.e. direction, rate of application) and whether the tissue is in tension or compression. Importantly for any discussion of TM stiffness, it should be noted that soft tissues are much softer when they are loaded in compression vs. when they are loaded in tension.

Taking all the above into consideration, the actual value of the effective Young's modulus should be interpreted as a general indication of tissue stiffness that may not be relevant in all situations. More realistic descriptions of tissue biomechanical behavior require more complex formulations that are beyond the scope of this thesis [31, 32]. Nonetheless, measured modulus values are still useful since they can be used for relative comparisons of tissue stiffness between samples (e.g. normal vs. glaucomatous) if the testing conditions are identical between samples.

1.4.2 Tissue Constituents Contributing to TM Stiffness

In general, tissue stiffness depends on both cells and extracellular matrix (ECM), and it is important to note that these two components interact in multiple ways in all tissues. Notably, in addition to matricellular signaling pathways and modification of the matrix by the resident cells, it is well known that cells directly sense and respond to the stiffness and topography of their underlying substrate [33-36]. For example, fibroblasts change their internal stiffness to try to match that of a stiffer substrate by enhancing actin polymerization and cross-linking [37]. Similarly, airway smooth muscle cells increase their baseline contractile tone in response to increased substrate stiffness by upregulating their contractile protein expression [38].

Accordingly, we expect the stiffness of human TM to depend in a complex fashion on the resident TM cells, the ECM, and the interactions between the two [39-43]. It is known that TM cells are contractile [44] and that elevated outflow resistance can be partly due to an increase in TM tone [45]. Further, TM cell contraction can direct ECM reorganization, and thus it has been hypothesized that the increased contraction state of TM cells in POAG might be associated with a stiffer TM [42]. Additionally, it is suggested that stiffness changes in the ECM of TM may in turn induce alterations in the mechanical properties of the TM cell itself [30]. The biomechanical interaction between cells and ECM, and the likely modulation of this interaction in disease, make it difficult to “cleanly” determine the relative contributions of cells and ECM to overall TM stiffness and stiffness changes.

1.5 Measurements of TM Stiffness in Different Species

1.5.1 Human

The stiffness of human TM has been determined directly and indirectly in several studies. There are currently two approaches for direct measurement: compression (indentation) testing and tensile testing. In view of the Discussion in Section 1.4.1, modulus values obtained from these two techniques are not expected to be of comparable magnitudes. Atomic force microscopy (AFM) is an example of a compressive testing modality, with the details of the cellular deformation field depending strongly on factors such as cantilever tip geometry and indentation depth [46].

In an important early study, the compressive modulus of human TM was measured using AFM by Last et al. (2011). They found that TM stiffness was 20 times greater in glaucomatous eyes compared to normal eyes (glaucomatous eyes: mean, 80.8 kPa, range, 0.5 – 565.3 kPa; normal eyes: mean, 4.0 kPa, range, 0.5 – 10 kPa). However, in this study, measurements were performed on excised TM, which may affect stiffness, due for example to the loss of ciliary muscle attachments and tension. Furthermore, it was possible that the cyanoacrylate glue, used to secure the tissue for AFM, may have affected the measurements [47-49]. Most importantly, and relevant to the interpretation of all measurements on human glaucomatous TM samples, are the possible confounding effects of glaucoma medications. Post mortem glaucomatous donor eyes have almost inevitably been treated with outflow drugs (to increase unconventional outflow and/or suppress AH production), and the long-term effects of these drugs on TM stiffness, either to stiffen or soften the TM, is unknown but potentially significant due to e.g. sustained under-perfusion of the TM as secondary effects of prostaglandins or beta-blockers. Previous studies have shown that prostaglandins led to loss of ECM components from the cribriform region and disconnection of the TM cells from the ECM, which may soften the TM [50]. Further, timolol, a type of beta-blocker, induced degeneration of TM endothelium in some regions, which would presumably soften the TM, while in other areas, the TM was densified and collapsed with accumulation of pigment granules within TM cells [51], which would presumably increase TM stiffness. Thus, we must bear in mind the possibility that any reported stiffness alterations in glaucomatous TM could be epiphenomenon unrelated to the pathogenesis of glaucoma per se, underscoring the importance of making similar measurements in animal models so as to potentially uncover mechanistic links between TM stiffness and outflow resistance.

Camras et al. [52, 53] subsequently measured the tensile stiffness of both normal and glaucomatous human TM via uniaxial tension testing, and found that Young’s modulus of glaucomatous TM was approximately one-fifth that of normal TM, contradicting Last et al.’s (2011) results. A partial explanation for this difference may be related to the different modes of testing used (tensile vs compressive). Additionally, different tissue structures were involved in those two studies. In Last’s study (2011), the stiffness of the JCT and inner wall of SC was primarily measured, while in Camras’ study, TM stiffness was likely determined primarily by the corneoscleral portion of the TM, since it makes up the majority of TM volume. It is also notable that the stiffness values reported by Camras et al. were extremely large (many times stiffer than sclera), which is hard to understand and to reconcile with experience gained from direct manipulation of the very soft TM.

Turning now to indirect methods, Johnson et al. (2015) used an analytical beam-bending model to obtain an estimate of TM stiffness. They visualized in vivo changes in TM and SC thickness by optical coherence tomography (OCT) as IOP was increased, and then used this information to estimate the elastic modulus of the TM. They calculated an average elastic modulus for the human TM of 128 kPa, a value between that measured by Last et al. and Camras et al. Another recently published paper [54] proposed a new theoretical framework for mechanical analysis of the TM, asserting the meshwork to be anisotropic and significantly stiffer in the circumferential direction compared to the transverse direction. This model demonstrated that large discrepancies in the reported Young’s modulus of TM could be due to the anisotropy of the tissue.

Because the inner wall of SC is potentially important in determining outflow resistance, the stiffness of SC endothelial (SCE) cells has also been specifically investigated. Overby et al. [55] measured the stiffness of both the cortical and subcortical components of the cytoskeleton by AFM in cultured SCE cells. Importantly, the stiffness of SCE cells from glaucomatous human eyes was found to be higher than those from healthy eyes using a 10-µm AFM tip (glaucomatous eyes: mean ± SEM, 1.24 ± 0.11 kPa; normal eyes: 0.79 ± 0.10 kPa). One possible explanation for this finding may be that the ECM underlying SCE cells is stiffer in the glaucomatous TM vs normal eyes, since as noted above, the mechanical properties of a cell's microenvironment affect cell stiffness [37, 56]. In fact, Overby et al. (2014) investigated the influence of substrate stiffness on SC cells using AFM and optical magnetic twisting cytometry, and discovered that both normal and glaucomatous SC cells stiffen in response to increasingly stiffer substrates. More interestingly, glaucomatous SC cells exhibited higher degree of stiffening than normal SC cells. They also examined the expression of genes related to ECM remodeling and found that DCN and BMP4 had lower expression in glaucomatous SC cells compared to normal SC cells, but that DCN and CTGF were strongly up-regulated by increased substrate stiffness in glaucomatous SC cells. This confirms that substrate stiffness affects SCE cell behavior, which may in turn lead to changes in SCE cell stiffness.

1.5.2 Non-human primates

A recent study measured TM stiffness in laser-induced experimental glaucoma monkeys, and observed softening of the unlasered parts of the TM compared to untreated controls [57]. Those data suggest that a compensatory mechanism may exist in the TM, whereby unlasered (ostensibly uninjured) TM may adaptively soften to increase local outflow in response to increased IOP after laser damage. Combined with the findings observed in human eyes, it may be the case that this compensatory mechanism is somehow impaired in human glaucoma patients.

1.5.3 Pigs

Porcine TM stiffness has been investigated by both compressive and tensile testing. The average compressive modulus was found to be 1.38 kPa, as measured by AFM [58]. However, the tensile stiffness reported by Camras et al. [52, 59] was 2490 kPa, which is three orders of magnitude higher than the compressive modulus. The huge discrepancy may again be partly due to different measurement techniques used; however, as was the case for human tissue, the TM stiffnesses measured by tensile testing were surprisingly large.

1.5.4 Rabbits

The mean (± SD) stiffness of rabbit TM was measured by AFM as 1.03 ± 0.55 kPa [60]. Unfortunately, no detailed description of AFM measurement was provided in this study, such as tissue preparation protocol and measurement locations (e.g. which part of the TM was indented). The same study reported that after topical administration of 0.1 % dexamethasone (DEX) in vivo for 3 weeks, the elastic modulus of TMs in DEX-treated eyes was 3.89 ± 2.55 kPa, which was significantly larger than that in control eyes. This is particularly interesting in view of the known tendency of DEX to increase intraocular pressure [61, 62].

1.5.5 Rats

TM stiffness was measured in rats using AFM by Huang et al. [63]. In their study, Evans blue dye was perfused into the eye before measurement to help locate the TM. The anterior segment was then dissected and flat-mounted with the TM facing upwards. They found the geometric mean TM stiffness to be 162 Pa; however, there were some limitations to this study. Evans blue is not specific to the TM, making it difficult to definitively identify the TM location under the AFM microscope. Also, the integrity of the TM was not examined at locations where measurements were made. Finally, it is conceivable that Evans blue dye itself may affect stiffness as it binds to the tissue.

1.5.6 Mice

In a glaucoma mouse model (overexpression of BMP-2 in conventional outflow tissue), Young's modulus of the TM was estimated by means of spectral domain optical coherence tomography [64]. In this study, the relationship between IOP and SC lumen area was used to determine TM stiffness, using the same beam deflection model described by Johnson et al. [65]. TM stiffness was estimated to be 2.16 kPa in control eyes; in BMP-2 treated eyes this value increased by approximately 20% on day 7 and more than doubled on day 10 after treatment. One limitation of the theoretical model used in this study is that all parameters were assumed to be identical for all SCs, which is likely not valid, since in reality, variations in parameters such as the undeformed height of the SC (SC height when IOP equals collector channel pressure) will occur from one eye to another.

1.6 Factors and Agents Affecting TM Stiffness

In addition to disease state, there are a number of factors and agents that are known to alter TM stiffness; here, we selectively review several important studies in this area.

1.6.1 Lysophospholipids

Two lysophospholipids, lysophosphatidic acid (LPA) and sphingosine-1-phosphate (S1P), are known to increase outflow resistance and thus have the potential to be involved in the regulation of aqueous humor outflow. In TM cells, it has been shown that LPA increased the expression of proteins such as α-smooth muscle actin (α-SMA), fibroblast specific protein-1 [66], and connective tissue growth factor (CTGF) [67]. Although the influence of LPA or S1P on TM stiffness has not been directly measured, it has been suggested that both may activate a wide variety of intracellular signaling pathways (such as Rho/Rho kinase and protein kinase) that would affect contraction and actin cytoskeletal organization, which would in turn affect TM cell stiffness [68]. Consistent with this understanding, S1P and LPA caused an increase in cell stiffness of up to 200 per cent in primary cultures of human SCE [69].

1.6.2 Rho-associated Protein Kinase Inhibitors

The TM is known to express many components of the Rho signaling pathway such as ROCK1 and ROCK2 [70]. In recent years, Rho-associated protein kinase (ROCK) inhibitors have emerged as a potential treatment option for glaucoma due to their IOP lowering effect [49, 71]. Specifically, the ROCK inhibitors Y-27632, H-1152 and AR-12286 have been shown to induce IOP lowering [72-74]. The exact mechanism by which ROCK inhibitors work on the TM to increase outflow facility is not completely understood. Nevertheless, it has been shown that ROCK inhibitors increase matrix metalloproteinase expression in TM cells which may reorganize ECM and widen intracellular spaces in the TM, especially in the JCT region [75]. Most relevant to this review, evidence suggests that ROCK inhibitors work by relaxing the TM through reduction of actomyosin contractile tone [76].

1.6.3 Cytoskeletal Disrupting Agents

Latrunculin B and the serine-threonine kinase inhibitor H-7 are cytoskeletal disrupting agents that dramatically increase outflow facility in human and monkey eyes [77, 78]. Latrunculin-B substantially decreased human TM cell stiffness after 30 min of exposure in vitro [79], while H-7 has been shown to inhibit cell contractility, and expand the intercellular spaces in the JCT, accompanied by removal of extracellular material, which likely affected TM stiffness [80].

1.6.4 Dexamethasone

Treatment with ocular glucocorticoids such as DEX causes increased IOP in approximately one third of the normotensive human population. Studies have shown that human TM cell stiffness increased approximately two-fold after just three days of treatment with DEX, and this was correlated with activation of extracellular signal-related kinase 1/2 and overexpression of α-SMA [60]. Furthermore, the matrix deposited by DEX-treated human TM cells was approximately four-fold stiffer than that deposited by control cells, and there was increased expression of matrix proteins such as fibrillin, myocilin and decorin [60], demonstrating that chronic treatment with DEX can alter TM cell and matrix stiffness. This is consistent with whole tissue measurements in rabbit eyes described above.

1.6.5 Transforming Growth Factor-β_2

Several investigators have found that the concentration of TGF-$\boldsymbol{\beta_2}$ is significantly increased in the aqueous humor of POAG patients [81-83]. Early studies demonstrated that TGF-$\boldsymbol{\beta_2}$ stimulates a very significant increase in the expression of ECM molecules by TM cells [84-89], and importantly, is also involved in the induction of irreversible cross-linking of TM fibronectin [85]. Moreover, TGF-$\boldsymbol{\beta_2}$is known to induce the expression of cross-linking enzymes for elastin and collagen [90]. It is possible that this increase in cross-linking and deposition may have contributed to the increased TM stiffness observed by Last et al. (2011) in glaucomatous eyes.

1.6.6 Nitric Oxide

Several studies have indicated that nitric oxide (NO) has an important role in IOP homeostasis. A study using isolated strips of bovine TM also indicated that TM contracts in response to L-nitroarginine, an inhibitor of NO formation [91]. A more recent study using a gel contraction assay demonstrated that NO donors could relax human TM cells [92]. Thus, one possible mechanism proposed for the increase in outflow facility induced by NO is via TM relaxation [93].

1.6.7 Senescence

A recent study [94] demonstrated that senescence may be a causal factor in human TM stiffening. They found that the stiffness of senescent TM cells increased approximately two-fold, indicating that such cells are intrinsically stiffer as measured by AFM. Further, it has been shown that secreted frizzled related protein-1 (SFRP1), a potent inhibitor of a key pathway involved in proliferation regulation, can induce human TM cell stiffening [95]. Increased expression of SFRP1 has also been observed in TM cells grown on substrates that mimic the stiffness of glaucomatous TM [79, 96].

1.7 Objectives of this Dissertation

When the author began her Ph.D., there were only two papers (and one erratum) published on mechanical properties of TM at the tissue level [30, 52, 59]. However, there were methodological concerns with the above studies, including:

- the dissection procedure, which required excision of the entire TM, which may have damaged/altered the TM, and
- the mechanical loading conditions, which in some cases did not replicate the loads that occur in vivo.

Thus, it is important to explore alternate approaches for TM stiffness estimation to determine whether TM stiffness is truly altered in eyes with ocular hypertension.

Further, the above studies did not address the question as to whether any observed differences between normal and glaucomatous eyes are primary causes of elevated IOP, or are epi-phenomena, since post mortem human glaucomatous eyes have typically been treated with anti-glaucoma medications. Thus, it is possible that measured stiffness differences were not directly related to the pathogenesis of glaucoma. In 2014, Boussommier-Calleja et al. found that there were spontaneous differences in IOP and outflow facility between mouse strains [97], and this observation suggests using different mouse strains could provide a way to study the relationship between facility and TM stiffness in the absence of medications. However, the technique of measuring TM stiffness in mouse eyes had not been presented in the literature likely due to the significant challenge of obtaining measurements on the small, delicate TM of this species.

Finally, patients treated with DEX can suffer from steroid-induced ocular hypertension, which can in turn lead to steroid-induced glaucoma (SIG). SIG has commonalities with primary open-angle glaucoma, and thus an understanding of TM changes in SIG may shed light on TM dysfunction in glaucoma in general. It had been reported that the stiffness of cultured TM cells and of their extracellular matrix were elevated when treated with DEX [98]. However, whether the increased TM stiffness contributes to altered IOP remains unknown.

From the above, we identified a specific set of questions that need to be answered:

1. Can we measure human TM stiffness without excising the TM from its physiological environment?
2. Is there a significant correlation between outflow resistance and TM stiffness in human eyes?
3. Can we measure TM stiffness in mice?
4. Is there a significant correlation between outflow resistance and TM stiffness in wild-type mice?

5. Is there a significant correlation between outflow resistance and TM stiffness in a single mouse strain after DEX treatment?

This dissertation addressed these questions by developing improved measurement approaches to better understand the role of TM biomechanics in the pathogenesis of glaucoma. We propose the following objectives:

Objective 1: Develop a specimen-specific inverse finite element modelling approach to deduce mechanical properties of human TM, and compare the differences in TM stiffness between normal and glaucomatous eyes. This work will provide a novel and improved approach for TM stiffness estimation in human eyes which does not require excision of the TM. Additionally, this model can be used for predicting stiffness of other outflow structures/tissues (such as transluminal structures across SC and septae at collector channels (CC)), which may also play a role in influencing aqueous humor drainage and are difficult to assess experimentally. The objective aims to answer questions 1 and 2.

Objective 2: Develop a cryosection-based AFM technique to measure TM stiffness in mice and study the correlation between TM stiffness and outflow resistance across different strains of mice. This work will provide a way to directly measure TM stiffness in mice where the TM can be clearly localized. It could be used in future work to study issues such as identification of molecular factors and associated genes involved in TM stiffness regulation. The objective aims to answer question 3 and 4.

Objective 3: Apply the same AFM technique to measure the change of TM stiffness in DEX-treated mice and its correlation with outflow resistance. The objective aims to answer question 5.

This dissertation is organized around those 3 objectives, and each of the following chapters address one of the three objectives.

Chapter 2 describes the development of a specimen-specific inverse finite element model to deduce the material properties of normal and glaucomatous human TM (Objective 1). This work was carried out in collaboration with Dr. Murray A. Johnstone and Dr. Ted S. Acott. This study showed that combining OCT and inverse FEM could be an alternative approach to measure human TM stiffness in a less invasive way. En face AFM was also performed on the same tissue, validating the trend of TM stiffness difference between normal and glaucomatous eyes observed by computer modeling. This chapter was published in September 2017.

Chapter 3 describes the development of a method to directly measure mouse TM stiffness using AFM and investigates the relationship between TM stiffness and aqueous outflow dynamics in wild-type mice (Objective 2). It is worth mentioning that the idea of using cryosections was partially inspired by previous studies in which tissue stiffness was measured by AFM on cryosections, e.g. human lamina cribrosa, porcine cornea and pericellular matrix of porcine articular cartilage [99-101].

A detailed protocol is described for outflow facility and TM stiffness measurements in mice, which has been published in Experimental Eye Research [102]. It revealed that outflow resistance was positively correlated with compressive TM stiffness. This represents the first experimental characterization of the relationship between mechanical properties of TM and outflow dynamics. This chapter and chapter 4 were combined as a paper and have been submitted for publication in November 2017.

Chapter 4 illustrates the application of the AFM method developed in Chapter 3 to evaluate the effects of DEX treatment on TM stiffness in mice (Objective 3). This work was carried out as a collaboration with the lab of Dr. W. Daniel Stamer at Duke University. It details how DEX was delivered to the eyes and how IOP, facility and TM stiffness were changed by the treatment. This study confirmed the positive correlation between IOP and outflow resistance that we discovered using mice with different genetic backgrounds. In addition, a significant correlation between aqueous outflow resistance and TM stiffness was found in DEX-treated mice. Together with chapter 3, these results demonstrate that the mechanical properties of the TM are closely involved in the function of the outflow pathway across a range of conditions.

CHAPTER 2. ESTIMATING HUMAN TRABECULAR MESHWORK STIFFNESS BY NUMERICAL MODELING AND ADVANCED OCT IMAGING

This chapter is based on a published journal paper: Wang K, Johnstone MA, Xin C, et al. Estimating human trabecular meshwork stiffness by numerical modeling and advanced OCT imaging. Investigative Ophthalmology & Visual Science September 2017, Vol.58, 4809-4817. doi:10.1167/iovs.17-22175

2.1 Abstract

Purpose: To estimate human trabecular meshwork (hTM) stiffness, thought to be elevated in glaucoma, using a novel indirect approach and to compare results with direct en face atomic force microscopy (AFM) measurements.

Methods: Post mortem human eyes were perfused to measure outflow facility and identify high- and low-flow regions (HF, LF) by tracer. Optical coherence tomography (OCT) images were obtained as Schlemm’s canal (SC) luminal pressure was directly manipulated. TM stiffness was deduced by an inverse Finite Element Modeling (FEM) approach. A series of AFM forcemaps was acquired along a line traversing the anterior angle on a radially cut flat-mount corneoscleral wedge with TM facing upward.

Results: The elastic modulus of normal hTM estimated by inverse FEM was 70±20 kPa (mean ± SD), while glaucomatous hTM was slightly stiffer (98±19 kPa). This trend was consistent with TM stiffnesses measured by AFM: normal hTM stiffness =

1.37±0.56 kPa, lower than glaucomatous hTM stiffness (2.75±1.19 kPa). None of these differences were statistically significant. TM in HF wedges was softer than that in LF wedges for both normal and glaucomatous eyes based on the inverse FEM approach, but not by AFM. Outflow facility was significantly correlated with TM stiffness estimated by FEM in 6 human eyes ($p = 0.018$).

Conclusions: TM stiffness is higher, but only modestly so, in glaucomatous patients. Outflow facility in both normal and glaucomatous human eyes appears to associate with TM stiffness. This evidence motivates further studies to investigate factors underlying TM biomechanical property regulation.

2.2 Introduction

The cause of increased outflow resistance leading to ocular hypertension in glaucoma remains unknown. However, several intriguing studies suggest that human trabecular meshwork (hTM) stiffness may differ in glaucomatous vs. unaffected eyes [102]. These studies raise the possibility that TM stiffness might be involved in the pathogenesis of ocular hypertension in glaucoma. Last et al., in an important early study, used atomic force microscopy (AFM) in dissected TM samples from postmortem eyes to show that TM stiffness was markedly elevated in glaucomatous vs. normal eyes [30]. Subsequently, Camras et al. examined the tensile stiffness of dissected human TM [52, 53, 59] via uniaxial testing. This study found that the glaucomatous TM was softer than normal TM, contrary to the results of the AFM testing. This discrepancy might be in part due to different testing modes used (tension vs. compression). Johnson et al. [65] estimated hTM stiffness in vivo in normal eyes using OCT imaging and an indirect method based on changes in TM geometry. In all of the above studies, there were methodological concerns, including: dissection that may have damaged/altered the TM; different mechanical loading conditions which in some cases did not replicate the loads that occur in vivo; and/or over-simplified modeling assumptions. In view of the limitations of the above studies, it is important to explore alternate approaches for TM stiffness estimation to determine whether TM stiffness is truly altered in eyes with ocular hypertension.

Optical coherence tomography (OCT) is a cross-sectional, three-dimensional imaging technique with high spatial resolution (<20 um) [103]. Recent studies have used OCT for characterization of tissue structure and movement inside the eye [104-108]. Specifically, spectral domain OCT (SD-OCT) was used to image radial limbal segments in ex vivo primate eyes. A cannula was inserted into SC to control pressure inside SC lumen. A pressure gradient was introduced across the TM that differed from the gradient expected due to standing, sitting, supine or prone positions. Instead, pressure gradients were typical of those encountered during body inversion, e.g. gymnastics, yoga and the spectrum of partial inversions that occur in daily life. SD-OCT was able to capture the dynamic motion of the TM, SC and collector channels (CCs) as SC luminal pressure was changed.

The inverse finite element method (FEM) is a computer modeling technique that has been widely used to estimate tissue biomechanical properties. The basic idea behind inverse FEM is to select input parameters for computational simulations that minimize the difference(s) between simulated and measured outcomes (e.g. tissue displacement, strain, etc.), thereby allowing indirect determination of such parameter values from experimental data [109-111].

The goal of this paper was to determine human TM stiffness in normal and glaucomatous eyes using a novel approach combining OCT and the inverse FEM. We reasoned that this technique would be less disruptive to TM structure than previous approaches. Additionally, we carried out en face AFM stiffness measurements on the same hTM samples to compare with results obtained from the OCT/inverse FEM approach. Finally, stiffness data were correlated with outflow facility in some eyes.

2.3 Methods

In brief, human eyes were obtained from eye banks, and anterior segments were perfused in Portland at OHSU under organ culture conditions [112] to measure outflow facility and identify high- and low-flow (HF, LF) regions of the TM. Anterior segment HF and LF wedges in culture medium were then sent on ice to Seattle by overnight express and received by 10 AM the next day for OCT scanning. Finally, the same wedges were sent to Atlanta where AFM measurements on the TM were carried out, and post hoc analysis of the OCT scans was undertaken.

In more detail, human eyes (5 normal and 3 glaucomatous; ages 74-88 years) were obtained within 72 hours postmortem from Oregon VisionGift eye bank. All research followed the tenets of the Declaration of Helsinki. Details on the glaucoma or normal donors included medications, but not detailed Ophthalmologist’s records. Anterior segments were immediately dissected, gently removing the lens, iris, ciliary body and posterior pole, while retaining the cornea, approximately 5-10 mm of sclera, the TM and SC. These anterior segments were immediately placed in stationary anterior segment organ culture and maintained for approximately 5 days [112]. Media and conditions were the same except a 1:1 mix of high glucose:low glucose DMEM was used. Anterior segments were then mounted on perfusion chambers and perfused at a constant pressure of 8.8 mm Hg (corresponding to approximately 15 mmHg in vivo), with gravimetric fluid flow rates assessed using minor modifications from the original method [113]. After flow rates had stabilized, we averaged the perfusion outflow facility (Cpf = flow rate in µl/min / perfusion pressure in mm Hg) over 2-3 days. To mark high flow areas in a manner that did not affect the AFM measurements, CellMask plasma membrane stain (ThermoFisher Scientific) was perfused for 1 hour prior to termination of flow experiments. HF and LF wedges approximately 4 mm wide were cut, based on relative CellMask staining intensity, and sent to Seattle for OCT scanning. OCT scanning was performed the following day using the same formulation of culture media used at OHSU.

2.3.1 OCT

Anterior segment wedges encompassing the cornea, limbal region with TM, SC and approximately 5 mm of sclera were mounted in a petri dish with pins, with the inner TM surface facing upward. The entire wedge was submerged in a saline bath, eliminating possible surface tension effects on the open end of SC. This uniform and stable saline bath surface also helped to eliminate surface motion artifacts when dynamic TM motion occurred (**Figure 2.1**). A crucial factor in the protocol was a previously described [104] custom-made steeply tapered and flexible insertion cannula fashioned from PE 60 tubing with an outside diameter of 1.22 mm a taper length of 4.5 mm and an outside diameter at the tip of 130-150 µm that provided a tight fit when inserted into SC.

The cannula was inserted into SC with the help of a dissecting microscope and a micromanipulator while the other end remained free (open). The tip of the cannula slid into, and made a tight contact with, the canal lumen. The other end of the cannula was connected to a reservoir filled with saline, so that SC lumen pressure could be controlled by changing the height of the reservoir. To capture the dynamic movement of tissues along the SC lumen at high resolution, the SD-OCT imaging probe was adjusted to face the TM. A series of cross-sectional scans of the wedge were captured at multiple locations for different reservoir pressures (e.g. 0, 5, 10, 20, 30 and 50 mmHg). The distance between two adjacent scans was about 10 µm. The central wavelength of the SD-OCT system was 1310 nm and the spatial resolution in each scan was 5 and 5.75 µm in axial and lateral dimensions, respectively. The imaging was performed through air without the OCT probe touching on the sample. The system was capable of an imaging speed of 92 kHz, i.e. 92,000 A-scans per second. At this speed, a system sensitivity (or dynamic range) of 105 dB was measured when the light power on the sample was 5 mW. Thus, for each location along TM/SC (typically 1-3 random locations were scanned for each wedge), a set of images were obtained for assessment of tissue configuration at several pressure levels (**Figure 2.1**).

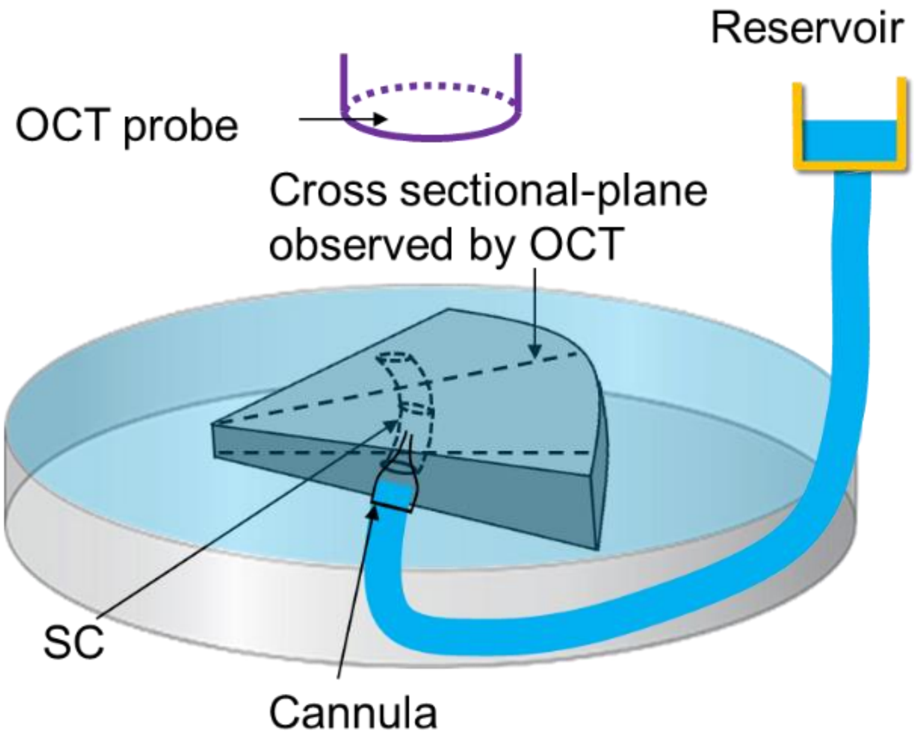

Figure 2.1: Schematic overview of experimental setup, including the SD-OCT system, a reservoir used for controlling pressure in Schlemm's canal (SC), a cannula and a Petri dish. The triangular-shaped object is a wedge of limbal tissue.

2.3.2 Inverse FEM

For 2-3 wedges per eye and 1-3 cross-sectional locations per wedge, we created a pseudo-2D FEM geometry in Abaqus (version 6.16, Simulia Corporation, Providence, RI). This pseudo-2D model was formed by "extruding" the 2D cross-section for a distance of 10 microns from a single OCT scan at a low SC pressure (**Figure 2.2**). OCT scans were used only if a clear, open SC lumen could be identified.

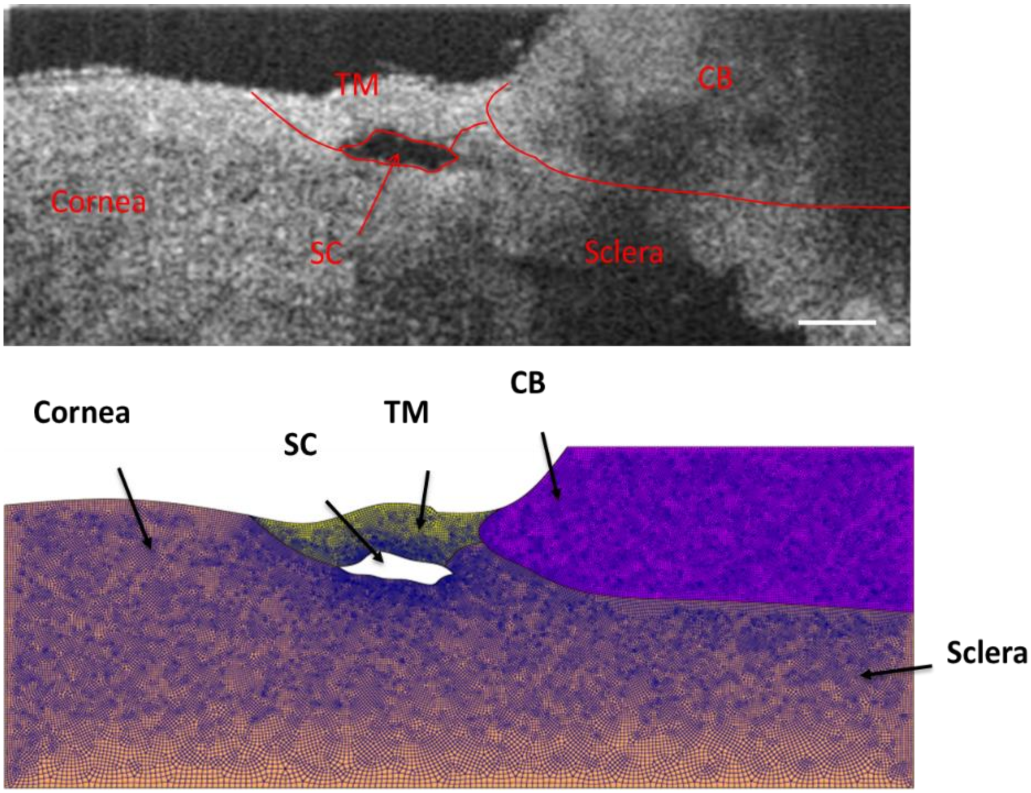

Figure 2.2: (Upper) Representative OCT image at a low SC luminal pressure (here, 0 mmHg) with delineated tissue structures superimposed. (Bottom) Geometry created in Abaqus with mesh superimposed. The total number of hexahedral elements for this mesh was 55358, with typical edge lengths from 5-10 µm. Scale bar: 250 µm. Sample: inferior temporal quadrant of Eye 77R.

In more detail, tissue components including TM, SC, sclera/cornea and ciliary body (CB) were first delineated from the OCT scan and verified by one co-author (MAJ) by carefully looking at the relative deformation of outflow tissues from the 3D OCT videos of SC lumen during the pressurization interval. The model was then meshed with 8-node hexahedral elements (edge lengths from 5 to 15 µm, as justified in the Supplementary Methods). The meshed model was then imported from Abaqus into PreView (FEBio package) [114]. Tissues were treated as incompressible, isotropic and nonlinearly hyperelastic (neo-Hookean material model) [115]. The strain energy density function for such a material is:

$$\boldsymbol{W} = \boldsymbol{C_1}\,(\boldsymbol{I_1} - \mathbf{3}) \qquad (2)$$

where $\boldsymbol{C_1} = \frac{\boldsymbol{E}}{\mathbf{4}(\mathbf{1}+\boldsymbol{v})}$ is a stiffness parameter (with $\boldsymbol{E}$ representing Young's modulus and $\boldsymbol{v}$ representing Poisson's ratio) and $\boldsymbol{I_1}$ is the first invariant of the deviatoric component of the right Cauchy-Green deformation tensor.

A tissue-specific fixed value for the parameter $\boldsymbol{C_1}$ was assigned to each tissue component (except TM) according to either literature reports, or, for tissues lacking literature reports of their stiffness, our best estimates. Specifically, sclera/cornea stiffness ($\boldsymbol{E}$) was taken as 2700 kPa [116], while CB stiffness was estimated as 100 kPa, close to the stiffness of vessels [116], since CB contains the ciliary muscle, vessels, and fibrous connective tissue. Poisson's ratio was assumed to be 0.5. Fortunately, a sensitivity analysis (see Supplemental Materials) demonstrated that the assumed CB stiffness value had a limited impact on the resulting estimated TM stiffness. Unlike the rest of the tissue components, the stiffness of the TM ($\boldsymbol{E}$) was allowed to vary over a range of values, typically from 18-300 kPa.

Loading conditions were specified based on those that were imposed experimentally. The plane strain assumption was made when imposing boundary conditions, suitable for the case in which SC cross-section shape changed slowly over axial distances comparable to the characteristic dimensions of the SC cross-section. The bottom surface of sclera was fixed in all three directions and one of the two side faces containing TM and SC was fixed in its normal direction. A pressure load was applied to the walls of SC lumen, carefully corrected for losses in the delivery tubing, the cannula and the distance from the tip of cannula to the OCT scan location (see Appendix A). Due to the small cross-sectional area of the SC lumen, the majority of the computed pressure drop typically occurred within SC. Young’s modulus for TM was allowed to vary over a certain range in steps of 6 kPa, and tissue deformations were computed for each TM stiffness using the open source FEBio package (version 2.2.2, Musculoskeletal Research Lab at the University of Utah) [114]. Differences in SC lumen size (area) between simulations and experiments were then calculated as

$$\text{Area difference} = \sqrt{(\boldsymbol{Area_{OCT}} - \boldsymbol{Area_{FEM}})^{\mathbf{2}}} \qquad (3)$$

where subscripts “OCT” and “FEM” refer to experimentally measured and numerically simulated cross-sectional areas, respectively. The TM stiffness value that gave the minimum difference in SC cross-sectional area was then taken as the estimated local TM stiffness for that model/cross-section (**Figure 2.3**).

As a quality control step, SC lumen contours were compared between OCT images and simulations at the corresponding elevated pressure (**Figure 2.3**, Left). We excluded a total of 2 quadrants when the match in contour shape was poor even if the SC cross-sectional area agreed well between the numerical simulation and the experimental data (**Figure 2.4**).

Finally, the average value of estimated TM stiffnesses over all modeled quadrants in one eye was taken as the TM stiffness of that eye.

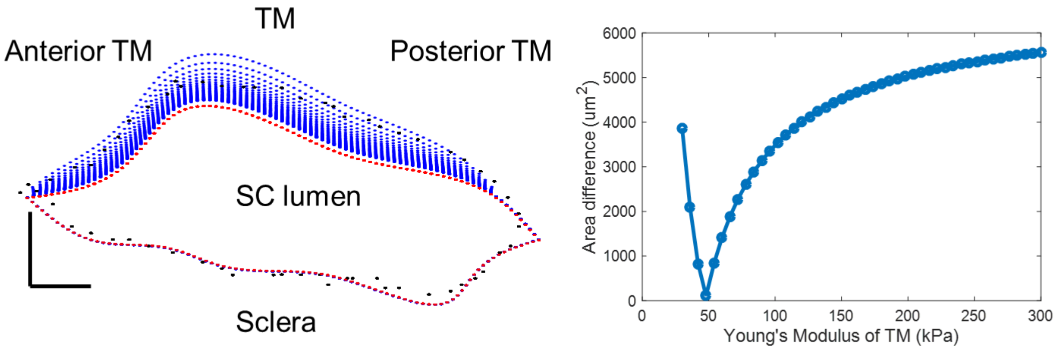

Figure 2.3: Comparison between SC contours as measured by OCT and as computed for a range of TM stiffnesses. (Left) SC contours at reservoir pressures of 0 mmHg and 20 mmHg are shown in red and black, respectively. The trabecular meshwork lies above SC lumen, with sclera immediately below. The blue dots represent a set of computed SC contours from simulations at 20 mmHg over a range of TM stiffnesses. Blue dots are not visible along the lower portion of the figure because there was essentially no computed deformation of the SC outer wall, i.e. blue dots are overlain by the red dots in this region. (Right) Quantification of SC lumen area difference, as computed from equation (2), at a reservoir pressure of 20 mmHg for different numerically specified Young's moduli for the TM (x-axis). A minimum difference was observed at 48 kPa, which was therefore taken as the best estimate of Young's modulus for the TM at this location. Scale bar: 50 µm. Sample: inferior temporal quadrant of Eye 77R.

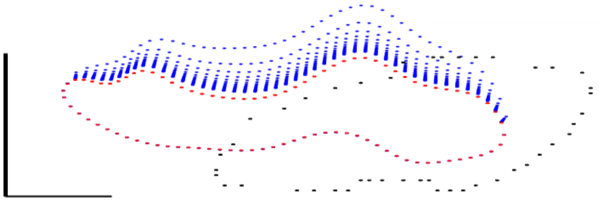

Figure 2.4: A representative poor match of SC contours. Red and black dots are SC contours at reservoir pressures of 0 mmHg and 10 mmHg, respectively. Tissue orientation and symbols are the same as those in Figure 3. Scale bar: 50 µm. Sample: High-flow quadrant of Eye 111.

2.3.3 AFM

The wedges, immersed into centrifuge tubes containing organ culture media, were then shipped overnight from Seattle to Atlanta on wet ice (typical postmortem time on receipt: 15 days). Upon receipt, each wedge was glued (Super glue, Loctite, Germany) onto a Petri dish with the same orientation as in the OCT experiment (glue was applied at the three corners of the wedge which were far from the limbal region). Samples were transferred to a MFD-3D AFM (Asylum Research, Santa Barbara, CA) and immersed into the same organ culture media. Silicon nitride cantilevers with an attached borosilicate sphere (radius, 5 µm; nominal spring constant, 0.1 N/m; Novascan Technologies, Inc., Ames, IA) were used. Cantilevers were calibrated by measuring the thermally induced motion of the unloaded cantilever before measurements. A series of forcemaps were obtained in regions located along a line starting on the cornea and ending on the sclera. The starting location for this line was determined visually with the aid of markers on the Petri dish. Specifically, the markers were several grids which were drawn on the bottom of the Petri dishes using a “Sharpie” marker that could be seen through the transparent cornea. Even with marker’s help, there was still some uncertainty in measurement location due to the thickness of the samples. When observed from the bottom camera, the cantilever tip and tissue were usually not focused on the same plane. Thus, the desired measurement location and the cantilever tip may not have been in the same spot. To estimate the uncertainty in measurement location, the cantilever tip was first moved to barely touch the surface of a glass slide and the bottom camera was focused on that surface. Then the cantilever tip was raised by 0.8 mm (typical wedge thickness at the limbus) and the camera was refocused on the cantilever tip. The distance between cantilever tip before and after the refocusing was used to estimate the uncertainty of the measurement location.

Each forcemap region consisted of 16 force curves in a 4 × 4 grid covering a scan region of 20 µm x 20 µm. The center-to-center distance between adjacent forcemap regions was 20-80 µm. Each force curve was taken at a rate of 8 µm/s and a typical indentation depth was 0.5-1 µm. The indentation depth was controlled in this relatively narrow range for all the AFM measurements to avoid substrate effects, since using larger indentations resulted in much larger tissue stiffnesses. For the 16 force curves in each forcemap region, those lacking either linear behavior or a clear cantilever contact point were discarded from the analysis. The remaining force curves were fit to a Hertz model (Equation 4) for a sphere in contact with a flat surface to determine the local compressive modulus (Igor Pro software, 6.34A; **Figure 2.5**)

$$\boldsymbol{E} = \frac{\boldsymbol{3(1-v^2)F}}{\boldsymbol{4R^{1/2}\delta^{3/2}}} \tag{4}$$

In Equation 4, $\boldsymbol{E}$ is Young's modulus, $\boldsymbol{F}$ is the force applied by cantilever bending, $\boldsymbol{R}$ is the radius of the sphere on the cantilever tip, $\boldsymbol{\delta}$ is the actual sample indentation, and $\boldsymbol{v}$ is the sample's Poisson's ratio, taken as 0.5. In **Figure 2.5** [102], the force experienced by the cantilever tip is zero when the cantilever is far from the sample surface. The force increases as the cantilever tip touches and indents the sample surface. The cantilever starts to retract once it reaches a maximum force, leading to a decreasing force.

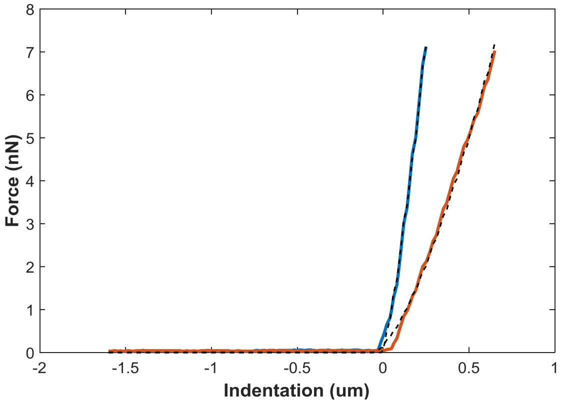

Figure 2.5: Typical force-indentation curve and fitting to raw data. Red and blue are advancing curves for soft and stiff locations respectively. Dashed lines are curve fit.

The average modulus from the valid measurement points within a forcemap region was taken as the compressive modulus of that region. These moduli from all forcemap regions in one sample were then plotted as a function of region location along the measurement line (cornea to sclera). The TM region was putatively defined as the anterior-most pigmented area that was adjacent to the cornea plus the narrow white band, representing the scleral spur (shown as the region between the two dashed lines in **Figure 2.6**). The mean of the modulus values along the measurement line traversing the TM region was taken as the TM stiffness of that location. Typically, 2-3 such locations were measured for each wedge, and the average was taken as the TM stiffness for that wedge (quadrant), as shown in **Table 2.1**. Usually, tissue was stiffest in the cornea and softened gradually as the measurement location moved posteriorly. Surprisingly, in most cases, the sclera had a lower modulus than the cornea. However, it is very likely that there was some residual iris root, ciliary body, retinal pigment epithelium or choroid left near the limbal region since we didn’t aggressively clean or scrape the sclera during dissection. These tissues are expected to be soft and could explain the low “scleral” modulus.

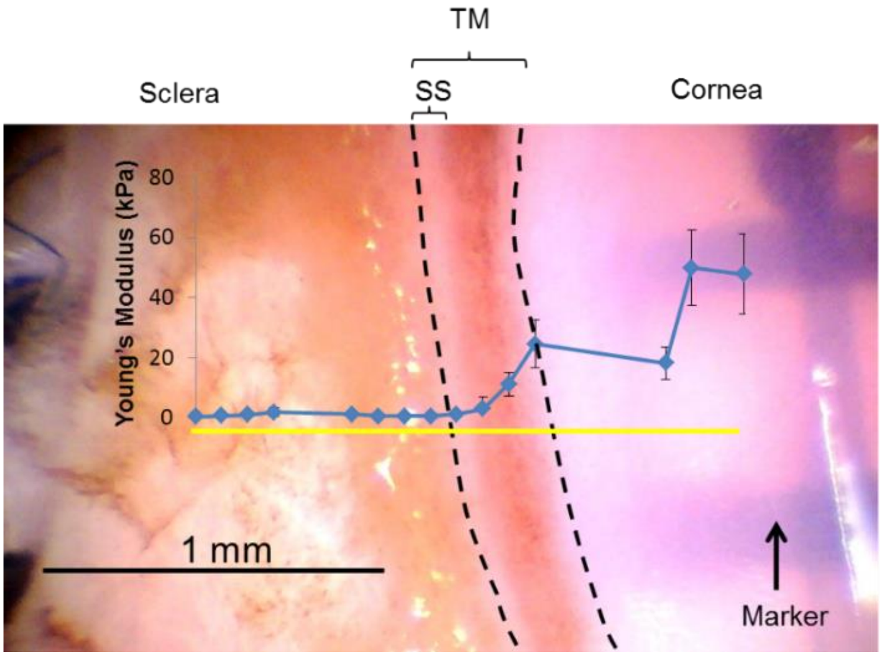

Figure 2.6: A representative top view of a wedge (Glaucomatous eye 122) from the dissection microscope with TM facing upward. AFM measurements started in the cornea on the right side, along the measurement line (yellow solid line) and towards to the sclera. The measured compressive modulus of each location along the measurement line is indicated in blue dots. The area between the two dashed lines is taken as the TM region. Error bar: standard deviation. Tissue was stiff in the cornea and decreased gradually as the measurement location moved posteriorly. Relatively low modulus was obtained in sclera region probably due to measurements on residual iris root or ciliary body. Sclera, cornea, TM and sclera spur (SS) are labeled.

2.4 Results

TM stiffnesses for 6 normal and 4 glaucomatous human eyes were successfully estimated using the inverse FEM method (**Table 2.1**). We were unable to use this approach for one (Eye 121) out of the five glaucomatous eyes due to the lack of a clear and open SC lumen at the OCT scan locations. The elastic modulus determined in this way in normal hTM ranged from 42 to 102 kPa (mean, 70±20 kPa, **Table 2.1**), while glaucomatous hTM samples had slightly larger elastic moduli, ranging from 79-123 kPa (mean, 98±19 kPa, **Table 2.1**).

This trend of a slightly stiffer glaucomatous TM was consistent with TM stiffness measured by AFM, where hTM stiffness in normal eyes (mean, 1.37±0.56 kPa) was lower than that in glaucomatous eyes (mean, 2.75±1.19 kPa). AFM measurements were performed on a total of 4 normal and 5 glaucomatous human eyes. We were unable to make stiffness measurements on 2 of the 6 normal eyes due to logistical issues. None of the above differences between normal and glaucomatous TM stiffness reached statistical significance (Mann-Whitney U-test, FEM $p = 0.051$, AFM $p = 0.127$); however, we suggest it is reasonable to call the p-value of 0.051 associated with the difference in TM stiffness estimated by inverse FEM a 'borderline significant' result.

TM stiffness measured by AFM was approximately 1/40 of that estimated by inverse FEM. This difference is almost certainly due, at least in part, to different modes of testing (compressive in AFM vs. primarily tensile by SC luminal pressurization), since it is known that the type of mechanical load applied to a tissue can result in very different mechanical behavior [117]. Specifically, soft tissues are usually much stiffer in tension, consistent with our results. Further, the length scales of the two measurement techniques were quite different, which could contribute to the discrepancy. The FEM involved deformation of the entire TM, while AFM measurements were very local. It has been reported that elastic properties of soft tissues can strongly depend on the length scale of the measurement technique, since different tissue structural components can be involved at different length scales [118]. We examined the correlation between TM stiffnesses determined by inverse FEM vs. that determined by AFM (**Figure 2.7**). Interestingly, there was a strong positive correlation ($p = 0.009$) between TM stiffness measured by AFM and that estimated by inverse FEM (n=8, 4 normal and 4 glaucomatous eyes were both measured by FEM and AFM). From the above evidence, it appears that combining numerical modeling and OCT has the potential to provide an alternative indirect approach to assess hTM stiffness which does not require excision of the TM.

Outflow facility (Cpf) was measured for 4 normal and 5 glaucomatous eyes (**Table 2.1**). We excluded Cpf values for 2 eyes (eyes 125, 126) from further analysis since, although they were documented as glaucomatous eyes, they had abnormally high facilities (0.54, 0.46 µl/min mmHg, respectively) [27, 52, 119]. After excluding these eyes, Cpf of normal eyes was higher (0.24±0.15 µl/min mmHg) compared to that in glaucomatous eyes (0.15±0.02 µl/min mmHg), but this difference did not reach statistical significance. We then plotted Cpf versus TM stiffness as estimated by inverse FEM (**Figure 2.8**). Despite the limited number of eyes (n=6), the Cpf and TM stiffness were significantly correlated (p = 0.018; $\boldsymbol{r^2}$ = 0.79) suggesting that nearly 80% of the variation in Cpf was associated with variation in TM stiffness. None of the two eyes were from the same individual, so that the statistical confounding effect of non-independence of paired eyes was avoided.

Table 2.1: TM stiffness in normal and glaucomatous human eyes obtained by inverse FEM and AFM.

Identifiers							FEM		AFM		C_{pf} at 8.8 mmHg (μl/min mmHg)
		Eye #	Age	Gender	PT (hours)	Quadrants	TM E for each quadrant (kPa)	TM E for each eye (kPa)	TM E for each quadrant (kPa)	TM E for each eye (kPa)	
Normal eyes	1	77R	79	M	10	IN	120	78	ND	ND	ND
						IT	48		ND		
						ST	66		ND		
	2	80R	74	M	25	SN	60	60	ND	ND	ND
						ST	60		ND		
	3	111	78	F	29	HF	(24)	102	3.15	1.92	0.11
						LF	102		0.68		
	4	115	54	M	43	HF	36	69	0.35	0.73	0.17
						LF	102		1.11		
	5	116	89	M	45	HF	60	42	0.27	1.09	0.45
						LF	24		1.9		
	6	124	78	F	55	HF	66	66	2.62	1.75	0.23
						LF	(108)		0.89		
Glaucoma eyes	1	118	84	F	24	HF	57	79	1.27	1.45	0.14
						LF	100		1.63		
	2	121	88	M	27	HF	ND	ND	4.98	4.23	0.13
						LF	ND	ND	3.47		
	3	122	77	M	22	HF	ND	90	2.13	1.75	0.17
						LF	90		1.36		
	*4	125	80	F	67	HF	108	102	3.12	2.72	(0.54)
						LF	96		2.32		
	*5	126	80	F	67	HF	90	123	3.25	3.62	(0.46)
						LF	156		3.99		

*PT, Postmortem Time from death to stationary culture in Portland; IN, Inferior Nasal; IT, Inferior Temple; SN, Superior Nasal; ST, Superior Temple; HF, High-flow; LF, Low-flow; E = Young's modulus; ND = not determined; (): discarded value; *: eyes from the same individual.

TM stiffness in HF and LF regions was also compared for both normal and glaucomatous eyes (**Figure 2.9**). TM stiffness determined by inverse FEM was higher in LF wedges than that in HF wedges, both in normal and glaucomatous eyes. However, AFM measurements did not show the same trend. In fact, on average, AFM measurements of TM stiffness in HF wedges were fairly close or even higher than those in LF wedges. However, none of the above comparisons reached statistical significance. A power analysis indicated that a total of 42 normal eyes and 12 glaucomatous eyes would be needed to reach statistical significance in TM stiffness between HF and LF regions for the inverse FEM approach (α = 0.05, power = 0.8; for normal eyes, effect size = 0.39; for glaucomatous eyes, effect size = 0.80). A similar analysis for the AFM approach indicated that a total of 100 normal eyes and 114 glaucomatous would be needed.

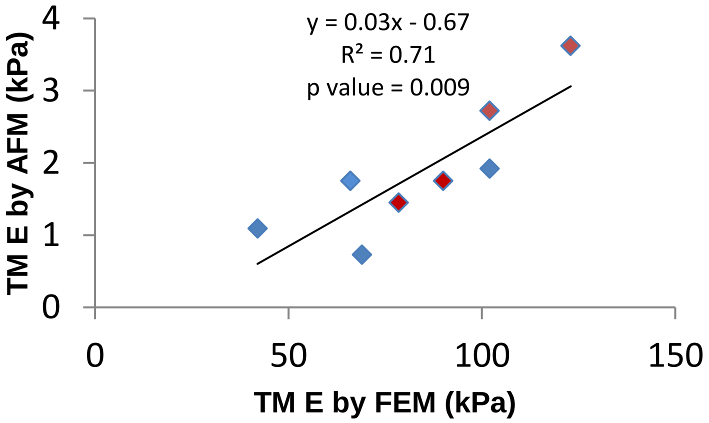

Figure 2.7: Cross-plot between TM stiffness measured by two approaches for 4 normal (blue symbols) and 4 glaucomatous (red symbols) eyes. Only eyes where TM stiffness was measured by both AFM and inverse FEM were included. The solid line and equation represent the linear regression of the pooled data.

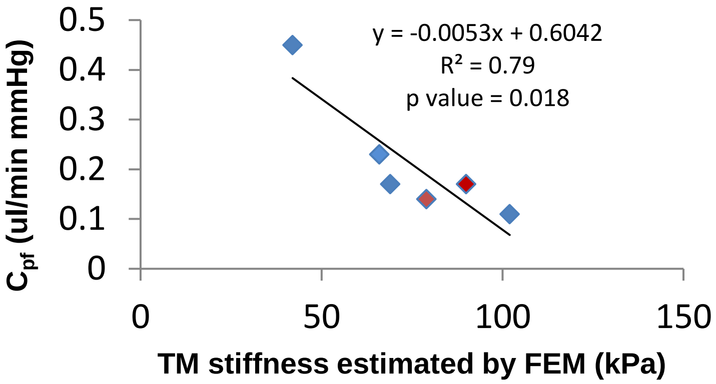

Figure 2.8: Cross-plot between TM stiffness (estimated by inverse FEM) and Cpf from normal (n=4, blue symbols) and glaucomatous (n=2, red symbols) human eyes. Only eyes where both Cpf and TM stiffness were measured were included. The solid line and equation represent the linear regression of the pooled data.

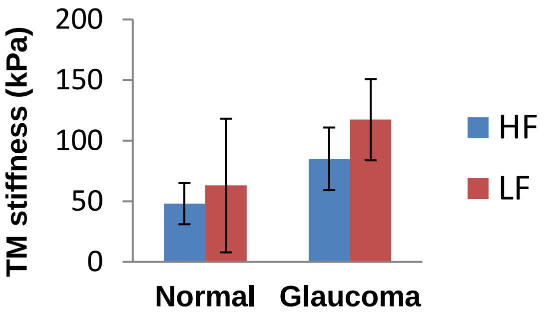

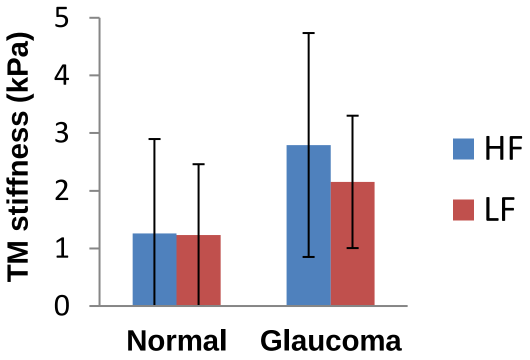

Figure 2.9: Regional heterogeneity in normal and glaucomatous eyes. The TM stiffness in HF (blue bar) and LF (red bar) wedges obtained by inverse FEM (upper) or AFM (bottom) are shown. Mean values from FEM: Normal eyes: mean±SD=48±17 kPa for HF and 63±55 kPa for LF; Glaucomatous eyes: 85±26 kPa for HF and 117±34 kPa) Mean values from AFM: Normal eyes: 1.60±1.50 kPa for HF and 1.15±1.15 kPa for LF; Glaucomatous eyes: 2.95±1.39 kPa for HF and 2.55±1.14 kPa. Error bars: are standard deviation. HF = high flow; LF = low flow.

2.5 Discussion

This study estimated the stiffness of hTM in normal and glaucomatous eyes using an inverse FEM approach, while also performing AFM on the same tissues. Our results indicated that TM stiffness is slightly greater in glaucomatous eyes compared to that in normal eyes, which is qualitatively consistent with the previous study of Last et al. [30]. However, it is extremely important to note that stiffness differences that we observed did not reach statistical significance, and the TM stiffnesses of glaucomatous eyes measured by AFM were of much smaller magnitude than those observed by Last et al. Thus, our results were not quantitatively consistent with those of Last et al [30]. This is most likely due to methodological differences: Last et al. dissected the TM and measured the stiffness of the outermost part of the tissue (the JCT), while we used intact wedges and measured the stiffness of the innermost aspects of the tissue. This methodological difference may also explain, at least partially, why our AFM results on HF/LF wedges (uveal side) contradict those of a previous study, which measured the stiffness of the JCT side of the meshwork, and demonstrated that LF regions of the TM were more rigid than HF regions in both normal and glaucomatous TMs [120]. This suggests that any stiffness differences in HF vs. LF regions of TM occur closer to the inner wall of SC.

It is also important to point out that differences in Cpf between the normal and glaucomatous eyes did not reach statistical significance. In fact, some of the 'glaucomatous' eyes had facilities that were much higher than that in 'normal' eyes. This may indicate an inaccurate classification of the donated eyes; all patients that the eye bank reported as having glaucoma were included in our study as glaucomatous eyes. Some "glaucoma" eyes may have been from patients with normal-tension glaucoma without an outflow system abnormality, and/or facility may have been affected by long-term use of anti-glaucoma medication (e.g. prostaglandin analogs) [49, 71, 73, 121, 122]. However, it is of interest that we did observe a statistically significant correlation between Cpf and hTM stiffness when the data was pooled from all eyes. This suggests that these factors are highly associated in both normal and glaucomatous eyes, although perhaps to a lesser extent than originally suggested by the study of Last et al [30].

We also point out that the hTM stiffness determined by the inverse FEM method cannot be directly quantitatively compared with that measured by AFM, even though the two were correlated. This is because several factors differ between the two methods, including how the load is applied to the tissue. In the OCT experiments the TM was primarily in tension, while in the AFM studies the TM was primarily in compression. Soft tissues, such as the TM, can be orders of magnitude softer when loaded in compression vs. when they are loaded in tension. Thus, in our study, the Young's modulus deduced by inverse FEM can be interpreted as a general indication of the TM tensile stiffness, while the modulus obtained by AFM tends to reveal the local compressive stiffness of the inner uveal meshwork. However, comparison of differences between normal and glaucoma hTM stiffness within a measurement method should remain valid.

Compared with other data in the literature for hTM (**Table 2.2**), our estimated FEM mean hTM stiffness value is close to that measured by Johnson et al [65]. Instead of direct measurement on TM, Johnson et al. used a beam-bending model to predict TM stiffness based on in vivo changes in TM and SC thickness which were visualized by OCT as IOP was elevated [65]. In that study, the pressure load was applied from the anterior chamber side, not the SC side in our FEM approach. However, in both studies, the TM was in tension along a direction which is perpendicular to SC lumen. For AFM results, our measured hTM stiffness of normal eyes was on the same scale but slightly lower than that measured by Last et al. [30], and much less than that measured by Camras et al. [52, 59]. In Camras' study, the whole dissected TM were stretched in a direction parallel to SC with elastic connections disrupted, while in Last's and our studies, the TM was compressed locally from different side of TM. However, our measurements were done on an intact wedge where elastic connections to scleral spur should be well preserved, as well as any interactions with cornea and to the outer all of SC.

There are several limitations of our study. First, steady state IOP is usually greater than steady state SC luminal pressure, i.e. IOP normally ranges from 10-20 mmHg [123] and episcleral venous pressure (EVP) is 7.6 – 11.4 mmHg. The experimental pressurization of SC lumen created a pressure gradient in the opposite direction. However, it must be recalled that EVP and SC pressure are both highly dynamic. For example, activities such as gymnastics and yoga frequently involve body inversion and a spectrum of partial inversions is present in many activities. With full inversion, EVP rises with a resultant increase in SC pressure [124, 125] and entry of blood into SC [126]. An IOP increase occurs within seconds with IOP increasing to as much as 43 mmHg [125]. Syndromes that cause persistent EVP and SC pressure increases are associated with IOP elevation that can result in an intractable glaucoma [127, 128]. Our SC inflation test is therefore not inconsistent with physiological situations. To be conservative, we only analyzed OCT scans with reservoir pressures limited to 30 mmHg, assuring luminal pressures well below the 43 mmHg documented in clinical studies.

Table 2.2: Comparison of TM stiffness with other studies in human eyes

Data Source	Methods	TM Modulus (kPa)
Our data (normal)	Inverse FEM	62 ± 13[a]
Our data (glaucoma)	Inverse FEM	84.5 ± 8[a]
Our data (normal)	AFM	1.64 ± 0.21[a]
Our data (glaucoma)	AFM	2.47 ± 1.52[a]
Johnson et al. (normal) [65]	Beam-bending	128[n]
Last et al. (normal) [30]	AFM	4 ± 2.2[a]
Last et al. (glaucoma) [30]	AFM	80.8 ± 32.5[a]
Camras et al. (normal) [52, 59]	Uniaxial test	51500 ± 13600[b]
Camras et al. (glaucoma) [53]	Uniaxial test	12500 ± 1400[b]

a: mean ± SD; b: geometric mean ± geometric SE; n: not specified

Second, a potential confounding factor arises in the OCT experiment because the pressure at the OCT scan location was not precisely known. We attempted to account for this (see Methods) and used our best estimate of the local pressure for FEM simulations. Interestingly, in a few specimens we observed SC collapse at the free (non-cannulated) end of SC (**Figure A.10**). This could be due to anatomic factors, or curvature of SC out of the imaging plane. Another interpretation is that SC was acting like a Starling resistor, a well-known phenomenon in which the exit pressure in a collapsible tube adjusts itself to match the surrounding bath pressure while luminal pressure is relatively spatially uniform, with a steep pressure gradient in the immediate vicinity of the outlet. If this were to occur, it would make the calculation of the pressure at the scan location very difficult and our estimated pressure at the scan location, as described above, would be incorrect. Because we did not consistently see collapse at the distal end of SC, we reasoned that in most, perhaps all, cases, it was not appropriate to treat SC as a Starling resistor. Ideally, future studies would have a better way of determining SC luminal pressure at the scan location, although this would be very technically challenging.

Third, although the neo-Hookean material model that we used is not ideal at large strains [48], it is possible to use it for hyperelastic materials in the initial linear range, where strains are less than 20%. In our simulations, the maximum first principal strain in the deformed configuration was usually less than 20%, justifying the use of the neo-Hookean model.

Fourth, in most OCT images, transluminal structures (TLS) can be observed spanning SC [129]. TLS include endothelial lining (ET) and septa. It has been suggested that these structures attach to the TM and corneoscleral wall and undergo motion [104, 130-136]. To better address the above issue, a 3D model containing TLS was built to investigate the effect of TLS on estimated TM stiffness (see Appendix A for more details). When compared TM stiffness between the 2D and 3D model, there was not a major difference. Thus, we decided not to pursue the 3D model because it was very time-consuming to construct such models.

Fifth, we found large disagreements between simulated and experimental SC contours for some of the samples. One possible reason for such deviations might be tissue movement induced by factors other than the applied luminal SC pressure. Factors like loose attachment to the petri dish, cannula movement and/or changes of tissue curvature resulting from segment straightening in response to SC pressure changes might have induced a small amount of tissue translation or rotation, leading to errors in the OCT images. Further investigation of such types of displacement errors is warranted.

Finally, as mentioned above, there was uncertainty in AFM measurement locations due to different focus planes of the cantilever and tissue when the sample was observed from the bottom. We estimated that the distance between cantilever tip before and after the refocusing was about 20 µm. Although the deviation between the desired and actual measurement locations is much less than width of defined the TM band, it may still cause small variations in the resultant TM stiffness. These deviations suggest the method of defining the start location of the AFM measurements may need to be improved.

There are two potential issues with use of post mortem human eyes. The first is the freshness of the eye. In our study, the time lag from donation to OCT and AFM measurements could be as long as 15 days, although for much of this time the eyes were being perfused in anterior segment organ culture. The relation between freshness of outflow tissue and its mechanical properties has not been fully characterized, although outflow tissues are well preserved for several weeks in organ culture as assessed by TM ultrastructure and glycosaminoglycan profiles [112]. The second issue is specific to eyes with a reported history of glaucoma. We could not obtain full medical histories for such eyes. It has been reported that there is a clear need to improve access to well-documented human eye tissue [137]. For example, there may be eyes with normal-tension glaucoma which simply appear with the diagnosis of ‘glaucoma’ on medical records. Such patients have normal IOPs and thus ostensibly normal TM function, and thus should not be included in the glaucoma group in our study.

In conclusion, our data suggest that differences in perfusion outflow facility in both normal and glaucomatous human eyes are correlated with differences in TM stiffness. These data provide a motivation for initiating further studies to identify mechanisms responsible for varying TM stiffness, particularly the altered stiffness in glaucomatous eyes.

CHAPTER 3. THE RELATIONSHIPS BETWEEN TM STIFFNESS AND OUTFLOW RESISTANCE IN MICE

This chapter forms part of a submitted journal paper to Scientific Reports: Wang K, Li G, Read AT, Navarro I, Mitra AK, Stamer WD, Sulchek T, Ethier CR. The relationship between outflow resistance and trabecular meshwork stiffness in mice.

3.1 Abstract

Purpose: There are naturally-occurring differences in intraocular pressure (IOP) and outflow facility among genetically distinct mouse strains (e.g. C57BL/6J vs. CBA/J). The purpose of this study is to test the hypothesis that this inherent variation in outflow facility may be related to inherent differences in trabecular meshwork (TM) stiffness in those two wild-type mouse stains.

Methods: Using wild-type C57BL/6J (n=18) and CBA/J (n=10) mice, valid outflow facilities (C) were measured in 22/28 mice by ocular perfusion. TM stiffness (E) was measured using a cryosection-based atomic force microscopy technique as previously described.

Results: C was slightly lower in CBA/J vs. C57BL/6J mice (mean±SD: 6.17±2.91 vs. 6.28±2.18 nl/min/mmHg) while TM was stiffer in CBA/J mice (3.09±3.55 kPa) than in C57BL/6J mice (2.20±1.12 kPa). However, none of the above differences were statistically significant. Importantly, TM stiffness was significantly correlated with outflow resistance (1/C; R^2=0.35, P=0.006).

Conclusions: Aqueous outflow resistance, which shows natural variation across wild-type mouse strains, is correlated with TM stiffness in two strains. This suggests that TM stiffness is intimately involved in establishing outflow resistance, motivating further studies to investigate factors underlying TM biomechanical property regulation. Those factors may play a role in the pathophysiology of primary open-angle glaucoma (POAG).

3.2 Introduction

Increased intraocular pressure (IOP) is present in many cases of glaucoma and is considered to be the most significant risk factor for glaucoma, although other risk factors such as age, race, family history and comorbidity are also important. The cause of elevated IOP in glaucoma patients is increased resistance (decreased outflow facility) to aqueous humor outflow. However, the mechanisms underlying this increased outflow resistance are still not well understood.

Previous studies have suggested that the bulk of outflow resistance is generated near the inner wall of Schlemm's canal (SC), including the juxtacanalicular connective tissue (JCT) layer of the trabecular meshwork (TM) [2, 3]. In addition, the stiffness of TM, as measured on the JCT side, was dramatically increased in glaucomatous eyes compared to that in normal eyes [30]. This motivated us to further study the correlation between mechanical properties of the TM and outflow resistance.

There are a number of drawbacks to using human eyes for such studies. Most notably, it is near-impossible to obtain untreated glaucomatous human eyes. Thus, it is possible that the stiffness difference we measured may not be directly related to the pathogenesis of glaucoma and instead could be caused by glaucoma medications. Thus, it is important to repeat TM stiffness measurement in eyes that have not been exposed to glaucoma medications and whose pressure history is known.

Mice are widely-used animal models for studying aqueous humor outflow, in part because they are convenient to use, and in part, because TM anatomy and conventional outflow pathway function in mice are generally similar to those in human eyes [7]. For example, outflow facility in mice responds to compounds that similarly affect outflow facility in human eyes [11]. Although mice do not tend to spontaneously develop POAG themselves as humans do, genetically distinct mouse strains have different IOPs, and different conventional outflow facilities [138]. A previous study has shown that there was a correlation between IOP and outflow facility across three mouse strains (CBA/J, C57BL/6J, and BALB/CJ), with 70% of the variation in IOP being attributable to variation in outflow resistance (1/C) [97]. Thus, using different strains of mice may provide one way to study the relation of TM stiffness to IOP and outflow facility.

Given these facts, we were motivated to perform studies using those same mouse strains to further investigate the correlation between TM stiffness and outflow resistance. If those two parameters were closely related, it would open new paradigms for IOP control and/or provide new insights to glaucoma pathophysiology.

3.3 Methods

All experiments were done in compliance with the ARVO Statement for the Use of Animals in Ophthalmic and Vision Research. All mice were purchased from the Jackson Laboratory.

We chose strains that had previously been characterized and which covered a range of IOPs and facilities, namely CBA/J, C57BL/6J and BALB/CJ mice. Unfortunately, it proved impossible to measure TM stiffness in BALB/CJ mice, since our technique required the presence of pigmented tissues to identify the location of the TM during stiffness measurements (see below). Thus, a total of 10 CBA/J and 18 C57BL/6J wild-type mice were used in this study. For each eye, outflow facility was measured ex vivo using the iPerfusion system [139], after which TM stiffness was measured using our previously developed cryosection-based AFM technique [140].

3.3.1 Ex vivo Mouse Eye Perfusion

Mice were sacrificed using CO_2. Eyes were enucleated using forceps within 5 minutes of death and stored in Dulbecco's phosphate buffered saline (DPBS, Mediatech Inc, Manassas, VA) at room temperature until use (<10 minutes). Eye perfusion was performed using the previously described iPerfusion system [139]. Briefly, eyes were cannulated with a glass micropipette (outer diameter 70-75 µm, Clunbury Scientific LLC, Bloomfield Hills, MI) under a stereomicroscope using a micromanipulator. LabVIEW software controlling the hardware automatically varied the pressure by adjusting the height of a reservoir connected to the micropipette. Both IOP and flow were recorded in real time. Eyes were perfused at sequential pressures of 4.5, 6, 7.5, 9, 10.5, 12, 13.5, 15, 16.5 and 18 mmHg. Typically, 10 minutes was required at each pressure step to obtain 6 minutes of stable perfusion flow data. During perfusion, the entire eye was submerged in a PBS bath maintained at a temperature of 35 °C. Eyes were perfused with DPBS plus 5.5mM glucose.

3.3.2 Outflow Facility Analysis

We calculated the pressure-dependent outflow facility by fitting pressure-flow rate data to the following empirical equation:

$$\boldsymbol{Q}(\boldsymbol{P}) = \boldsymbol{C}\left(\frac{\boldsymbol{P}}{\boldsymbol{P_r}}\right)^{\boldsymbol{\beta}}\boldsymbol{P} \tag{5}$$

where $\boldsymbol{Q}$ is flow rate (nl/min) measured by the flow sensor, $\boldsymbol{C}$ is outflow facility (nl/min · mmHg), $\boldsymbol{\beta}$ is a parameter characterizing the nonlinearity of the pressure-flow relationship, $\boldsymbol{P}$ is IOP, and $\boldsymbol{P_r}$ is a reference pressure, taken as 8 mmHg. Using equation 5, values for $\boldsymbol{C}$ and $\boldsymbol{\beta}$ are obtained as fitting outcomes. The reported outflow resistance is the reciprocal of facility.

3.3.3 AFM Measurement of TM Stiffness using Cryosections

After perfusion, TM stiffnesses were measured using a previously developed AFM technique on cryosections [140]. Briefly, immediately after the glass micropipette was removed from the anterior chamber, a small dab of glue (Superglue, Loctite, Germany) was placed onto the cornea to seal the resulting hole. This ensured that IOP was maintained at a value close to the last perfusion value, so that an open SC lumen was more likely to be found, aiding in TM localization (**Figure 3.1**). Eyes coated with optimal cutting temperature compound (O.C.T.; Tissue-Tek) were then frozen by immersion in 2-methylbutane (Sigma-Aldrich, St. Louis, MI) cooled by liquid nitrogen [141, 142]. For each eye, a few 10 µm thick sagittal cryosections from 3 different quadrants were cut on a Microm Cryostar NX70 cryostat (Dreieich, Germany), collected on adhesive slides (Plus gold slide, Electron Microscopy Sciences, Hatfield, PA) and stored in ice-cold PBS for AFM analysis (**Figure 3.1**).

TM stiffnesses were measured following the same protocol we used previously. Specifically, for each cryosection, the TM was first localized as the region between the pigmented ciliary body and the inner wall endothelium of SC (**Figure 3.1**). Multiple locations in the TM region (typically 3-9) were probed by the cantilever and three repeated measurements were conducted at each location. The average from the three measurements was taken as the TM stiffness at that location. TM stiffnesses from all locations within a cryosection were then averaged to obtain the TM stiffness of that cryosection. We typically made AFM measurements on 9 cryosections (collected from 3 different quadrants) from each individual eye, since TM stiffness may be location-dependent. Finally, the mean stiffness of all cryosections was taken as the TM stiffness of the eye.

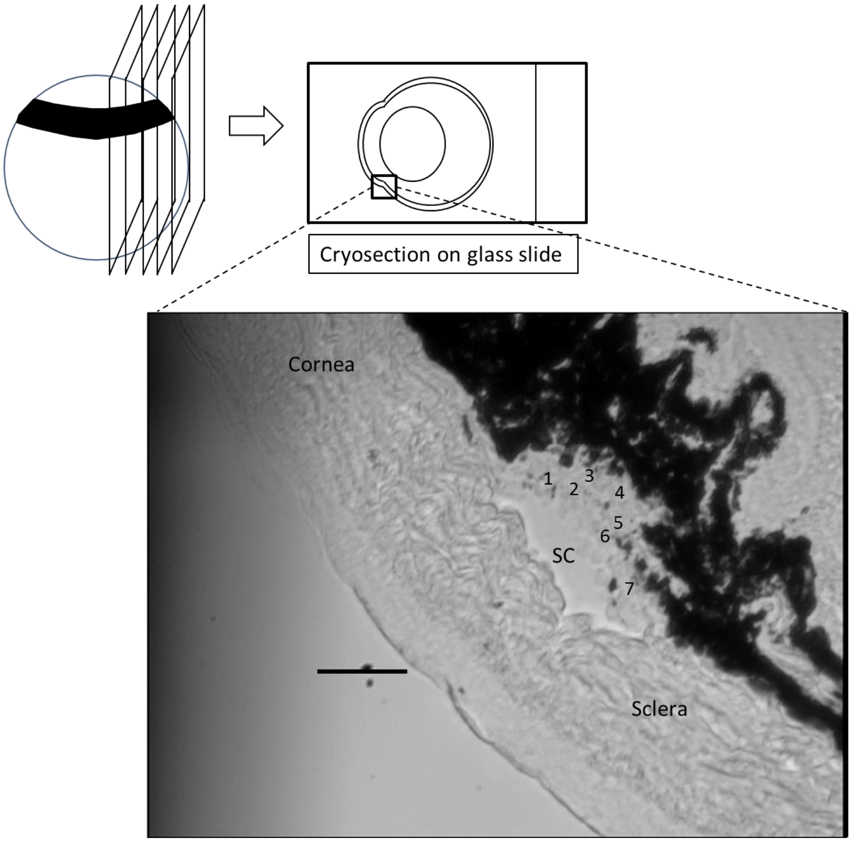

Figure 3.1: Schematic diagram of the cryosection-based AFM technique. Sagittal cryosections were cut from a frozen eye and mounted to an adhesive glass slide without glue. The bottom figure shows the limbal region of a representative cryosection observed from the AFM bottom camera (SC=Schlemm's canal). Numbers within the TM region indicate individual locations indented by the AFM probe. Scale bar: 50 µm. Section thickness: 10 µm.

3.4 Statistical Analysis

For each mouse, only the data from the OD eye was used to avoid non-independence effects between the two eyes from one animal [143]. The exception was in animals for which measurements on the right eye yielded invalid facility data due to technical issues, in which case the left eye was used. The Wilcoxon rank-sum test was used to compare differences outflow facility and TM stiffness between groups (C57BL/6J vs. CBA/J wild-type mice). The above comparisons were also performed where the data of a mouse was taken as the mean values from the two eyes (See details in Appendix B), using the same statistical methods. Linear regression was used to test the correlation between outflow resistance and TM stiffness. The significance threshold was defined to be 0.05 for all statistical tests.

3.5 Results

The facility of C57BL/6J mice was slightly higher than that of CBA/J mice (6.28 ± 2.18 vs. 6.17 ± 2.91 nl/min mmHg; p = 0.692, **Figure 3.2**). This trend is consistent with a previous study [97] but the difference we observed was not statistically significant. Similarly, average TM stiffness in C57BL/6J mice was less than in CBA/J mice, but this difference was also not significantly different (2.20 ± 1.12 vs. 3.08 ± 3.55 kPa; p=0.719, **Figure 3.2**).

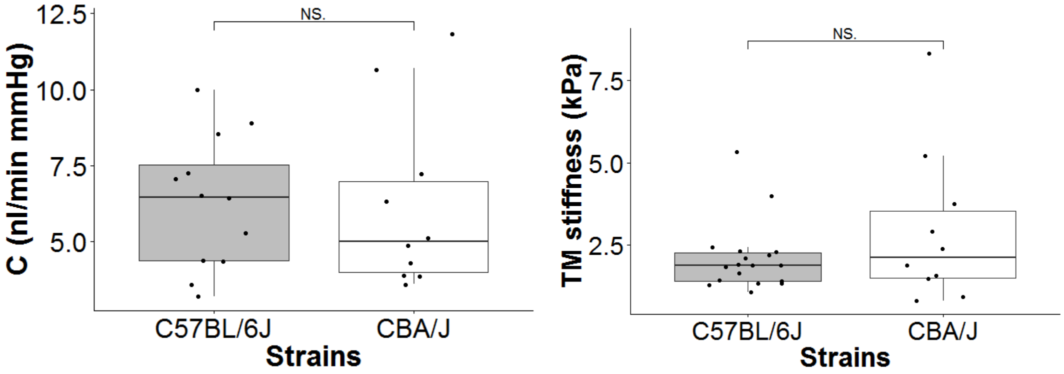

Figure 3.2: Facility (C; left) and TM stiffness (right) for two mouse strains. For each box, the central line represents the median, and the edges of the box are the 25th and 75th percentiles, and whiskers extend to the most extreme data points not considered outliers. Each dot represents the data from one eye per mouse, as described in more detail in the Statistical Analysis section. Due to technical issues, not all measurements in all mice were successful; number of eyes shown for facility plot are n=12 for C57BL/6J and n=10 for CBA/J. For the stiffness plot, the respective values are n=18 and n=10. NS: Not Significant.

Surprisingly, we observed a significant correlation between outflow resistance (1/C) and TM stiffness when pooling data from two strains, although the correlations for each strain individually were not significant (**Figure 3.3**). This indicates that there is an inherent relationship between the mechanical properties of TM and outflow resistance in these mice, independent of strain.

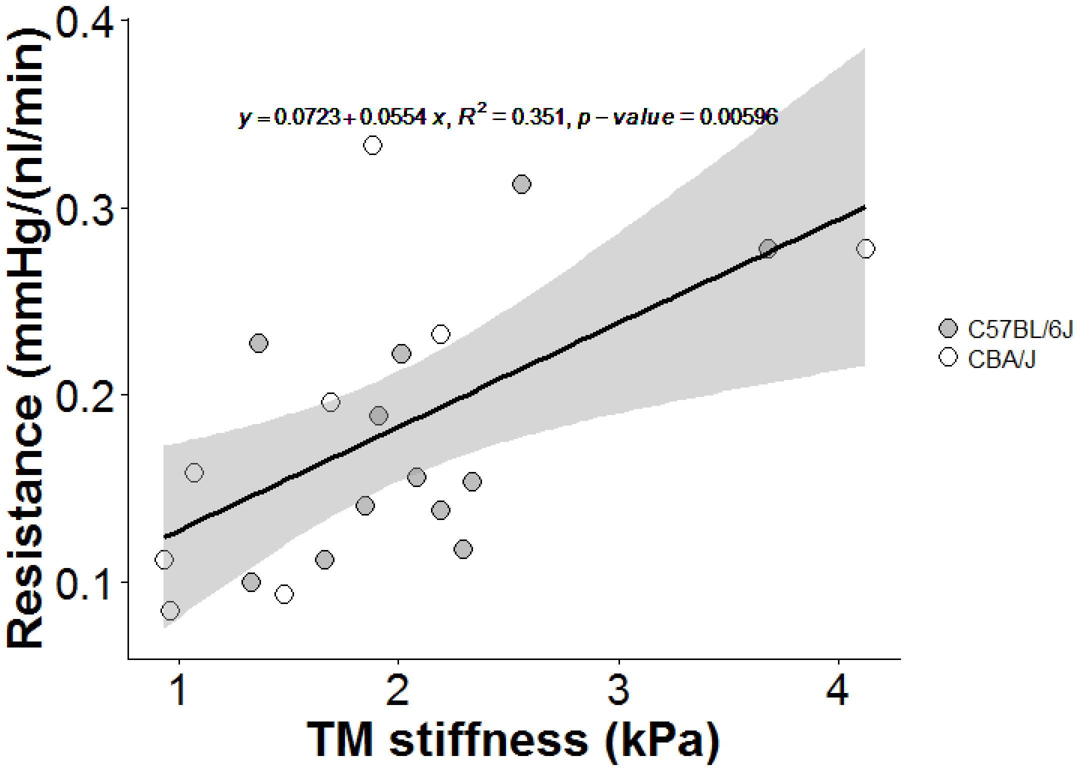

Figure 3.3: Cross-plot between outflow resistance and TM stiffness, with each data point representing one mouse. The black solid line and equation represent the linear regression of the pooled data. The gray-shaded region shows 95% confidence bounds for the regression. For each mouse, only the data from the OD eye was used, except in cases where the OD eye yielded invalid facility data due to technical issues, in which case data from the OS eye was used. Only mice where both outflow resistance and TM stiffness were measured in the same eyes were included. Number of data points: n=12 for C57BL/6J, n=8 for CBA/J.

3.6 Discussion

The major finding of this work is that there is a significant correlation between aqueous outflow resistance and TM stiffness across two strains of pigmented wild-type mice. This suggests that an intrinsic link between the mechanical properties of the TM and aqueous humor outflow dynamics exists. This finding is consistent with evidence that Rho-associated protein kinase (ROCK) inhibitors, known to reduce TM actomyosin contractile tone, decrease outflow resistance. Interestingly, we have also observed a statistically significant inverse correlation between outflow facility and TM stiffness in a previous study using human tissue from both normal and glaucomatous eyes [144], consistent with the above results. This further suggests commonalities between humans and mice in the TM stiffness-outflow resistance relationship.

We also found that neither facility nor TM stiffness showed significant differences between C57BL/6J and CBA/J mice. From the boxplot in Figure 3.2, it appears that several data points were outliers, since they were outside the whiskers. We investigated this further, defining outliers as values lying more than three scaled median absolute deviations (MAD) away from the median. In facility comparisons, we detected 2 outliers for CBA/J mice, while in TM stiffness comparisons, we detected 2 and 1 outliers for C57BL/6J and CBA/J mice, respectively. However, conclusions about statistical significance were unchanged for all statistical comparisons when tests were rerun with outliers removed.

In view of the lack of statistical significance, we asked how many samples would have been needed to observe statistically significant results. Power analyses performed with

G*Power software (α = 0.05, power = 0.8) using the means and standard deviations in Section 3.5 indicated that, in order to show statistically significant inter-strain differences in outflow facility and TM stiffness, more than 6000 (effect size: 0.043) and 100 (effect size: 0.334) animals for each group would be needed, respectively. Thus, we hypothesize that it is unlikely that the facility and TM stiffness are different between the two strains. This is inconsistent with the results of a previous study, which detected a significant difference in outflow facility between the same two strains [97]. Despite the same trend of facility difference, the actual values from their study were about twofold higher than ours, probably due to different ocular perfusion methodologies and fitting of the flow-pressure curve.

This study has several limitations. First, we obtained the TM stiffness by performing measurements on nine distinct locations for each eye. Although those locations come from three quadrants, the average of their TM stiffness may not represent the properties of the entire TM, while by definition, the outflow resistance is a measurement of outflow characteristics of the entire TM. Additionally, outflow resistance can be affected by other factors such as the cross-sectional area of the outflow tissue and length of the TM from anterior chamber to SC. All the above factors could potentially add variance to the correlation. Another limitation is that the effects of the freeze-thaw procedure, inherent in making measurements on thawed cryosections, was not evaluated on TM mechanical properties. However, no significant ice crystals were observed on the cryosections and previous studies have concluded that the mechanical properties of cryopreserved human arteries and sclera were similar to that obtained in fresh samples [145, 146]. Therefore, we expect the effects of freezing on TM mechanical behavior to be small.

CHAPTER 4. THE EFFECT OF DEXAMETHASONE ON TM STIFFNESS IN MICE

This chapter, together with Chapter 3, forms the basis of a submitted journal paper: Wang K, Li G, Read AT, Navarro I, Mitra AK, Stamer WD, Sulchek T, Ethier CR. The relationship between outflow resistance and trabecular meshwork stiffness in mice.

4.1 Abstract

Purpose: Dexamethasone (DEX) treatment can increase intraocular pressure (IOP) which may lead to the development of steroid-induced glaucoma. It has been reported that the stiffnesses of cultured trabecular meshwork (TM) cells and of their extracellular matrix were elevated when treated with DEX. However, whether the increased TM stiffness contributes to altered IOP homeostasis after DEX treatment remains unknown. Thus, we studied how IOP, outflow facility (C), and TM stiffness changed in DEX-treated mice.

Methods: 41 C57BL/6J mice received DEX (n=25) or vehicle (n=16) delivered by custom nano-sized polymers incorporating either DEX or vehicle and injected into the subconjunctival space. IOP was recorded approximately twice a week using tonometry. Valid outflow facilities (C) were measured by ocular perfusion. TM stiffness (E) was measured using a cryosection-based atomic force microscopy technique as previously described.

Results: All DEX mice had significantly elevated IOP vs. control mice on the day of sacrifice (27.1 ± 2.7 vs 20.5 ± 3.2 mmHg; $P<0.001$). C of DEX mice was lower than

control mice (3.05±1.47 vs. 4.09±1.71 nl/min/mmHg; P=0.192). The TM in DEX-treated mice was stiffer than that in vehicle-treated mice, but this difference was not statistically significant (2.38±1.31 vs. 1.99±0.91 kPa; P=0.357). Importantly, TM stiffness was significantly correlated with outflow resistance (1/C) (R^2=0.41, P=0.002).

Conclusions: DEX treatment caused a significant elevation in IOP, but only a slight increase in outflow resistance and TM stiffness on average. The significant correlation between TM stiffness and outflow resistance suggests that about 40% of the change in outflow resistance is associated with changed TM stiffness. This motivates further studies to investigate molecular or genetic factors contributing to the mechanical property changes we observed in the outflow tissue.

4.2 Introduction

Previous studies have indicated that trabecular meshwork (TM) stiffness may be related to aqueous humor outflow resistance [30, 52, 59, 144]. Specifically, using atomic force microscopy (AFM), TM stiffness was found to be dramatically increased in human glaucomatous eyes compared to that in normal eyes, which may be associated with dysregulation of the extracellular matrix (ECM) observed in glaucoma [30]. Further, in normal and glaucomatous human eyes, we have recently reported an association between facility and TM stiffness as deduced by OCT imaging and numerical modeling [144]. In addition, increased stiffness of TM cells and TM ECM has been reported after exposure to the glucocorticoid dexamethasone (DEX) in cultured human TM cells or in rabbit eyes [60]. Clinically, glucocorticoid exposure can lead to steroid-induced glaucoma (SIG) that has commonalities with primary open-angle glaucoma, and thus an understanding of TM changes in SIG may shed light on TM dysfunction in glaucoma in general.

DEX-treated animals have been used in several previous studies to examine the effect of glucocorticoids on IOP, outflow facility (C), or TM stiffness. Raghunathan et al. reported that 3 weeks of topically-administered DEX resulted in a 3.5-fold increase in TM stiffness in rabbit eyes [60]. However, no statically significant changes in IOP were observed between the DEX-treated eyes and control eyes. Whitlock et al. observed a significant IOP increase after systemic DEX treatment using minipump implantation in mice [61] which can sustain DEX delivery for up to 30 days. Similarly, Overby et al. [147] demonstrated that DEX-induced ocular hypertension (OHT) in mice mimicked hallmarks of human SIG, and that reduced outflow facility was correlated with newly formed ECM in the TM (e.g. increased fibrillar material, basement membrane material, etc.). However, systemic delivery of DEX is undesirable and thus alternative DEX delivery methods are preferred. Agrahari et al. [148] have recently developed a method to deliver DEX to human TM cells using DEX-encapsulated pentablock copolymer-based nanoparticles (DEX-PB-NPs). They showed that DEX was released continuously from the PB-NPs over 3 months, with 50% released within the first 6 weeks. This provides the possibility to deliver DEX locally by injecting the DEX-PB-NPs into or adjacent to mouse eyes, as a mouse model to study the pathophysiology of steroid-induced OHT.

In view of the above, we were motivated to use mice to further investigate the correlation between TM stiffness and outflow resistance. If those two parameters were closely related, it would open new paradigms for IOP control and possibly provide new insights into the pathophysiology of POAG and SIG.

4.3 Methods

4.3.1 Animals and Overview of Experimental Design

All procedures on living mice were conducted in compliance with the ARVO Statement for the Use of Animals in Ophthalmic and Vision Research. All mice were purchased from the Jackson Laboratory.

To study changes in TM stiffness induced by DEX treatment, 41 C57BL/6J mice (separated into five cohorts; 25 DEX-treated and 16 vehicle-treated mice; **Table 4.1**) were used. IOP was recorded before and during DEX treatment. Both outflow facility and TM stiffness were measured in post mortem eyes as described above. All the DEX/vehicle treatments, and IOP and facility measurements for the DEX treatment study were done in the Stamer lab.

Table 4.1: Number of mice, number of valid measurements (i.e. IOP, facility, and TM stiffness) and treated eyes in each cohort for DEX study.

Cohort	**DEX-treated mice**	**Vehicle-treated mice**	**IOP**	**C**	**E**	**Treated eye**
1	6	3	9	0	9	OD
2	4	0	4	0	4	
3	6	5	11	5	11	OU
4	5	4	9	9	9	
5	4	4	8	7	8	
Total	25	16	41	21	41	

OD: right eye; OU: both eyes. IOP: intraocular pressure; C: facility; E: TM stiffness.

4.3.2 DEX Treatment

DEX-PB-NPs were formulated by an oil-in-water single emulsion solvent evaporation method as described previously [148] and stored at -20°C until further use. The particle size was in the range of 109 ± 3.77 nm [148]. Control PB-NPs (Con-PB-NPs) were prepared with the same approach except that no DEX was added. Nanoparticles were loaded such that 1 mg of DEX-PB-NPs contained 23 µg of DEX, while 1mg of Con-PB-NPs contained no DEX.

On a typical injection day, DEX-PB-NPs or Con-PB-NPs were dissolved in phosphate buffered saline (PBS) to obtain a DEX-PB-NPs solution or Con-PB-NPs solution at a concentration of 1 mg/20 µl (1mg DEX-PB-NPs or 1mg Con-PB-NPs in 20 µl PBS). For each injection, 20 µl of DEX-PB-NPs solution or Con-PB-NPs solution was injected into the subconjunctival/periocular space using 30-gauge needles in DEX and control mice, respectively. The injection location was consistent between DEX-treated and control eyes. Typically, three injections at days 0, 7 and 14 were administered. Importantly, in the first two cohorts of mice, DEX or vehicle was delivered into only the right eyes on days 0 and 14, while the left eyes served as a control. However, we observed a bilateral IOP increase in these animals. Thus, for cohorts 3-5, injections were performed bilaterally, with a subset of mice acting as controls (bilateral Con-PB-NP injection) and the remaining mice acting as experimental animals (bilateral DEX-PB-NP injection). Details of mouse numbers in each cohort and the injected eyes are listed in **Table 4.1**. A previous in vitro study showed that DEX release from the particles typically lasted for 3 months, with about 20% of DEX released in the first 2 days [148].

4.3.3 IOP Measurements

IOPs were recorded non-invasively using a commercially available tonometer (TonoLab, TV02, Icare, Finland) in anaesthetized mice. Briefly, mice were anesthetized with ketamine (60 mg/kg) and xylazine (6 mg/kg). IOP was measured just as the mice stopped moving (light sleep). Each recorded IOP was the average of six measurements from the same eye. IOPs were obtained right before each injection and on the day when mice were euthanized. All IOP measurements were performed between 10 am to 1 pm.

We were concerned that the DEX treatment could possibly have affected corneal stiffness, leading to an artifactual “change” in measured IOP. Thus, the tonometer was calibrated in six eyes of three mice (one control mouse and two DEX-treated mice). Calibration was performed on live, anesthetized animals secured on a platform. The anterior chamber was cannulated with a glass needle (opening ~70 µm × 80 µm) filled with filtered D-glucose in phosphate-buffered saline (DBG, 5.5mM) connected to a PowerLab system (ML870/P PowerLab 8/30, ADInstruments, Colorado Springs, Colorado, USA) and then an adjustable height reservoir containing filtered ddH_2O. IOP was set to either 10, 15, 20, 25, or 30 mmHg by adjusting reservoir height, and confirmed using the PowerLab system zeroed to tear film, with the needle tip placed at the same level as its eventual position inside the eye, before the micropipette was inserted in to the anterior chamber. Tonometer measurements were performed under a microscope to ensure that probe rebounded against the central cornea perpendicularly. Five readings from the tonometer were recorded for each pressure level. For each eye, a linear correlation (Equation 6) between the tonometer-measured pressure *(IOPtono*) and the true IOP (*IOPtrue*) was determined from:

$$\boldsymbol{IOPtono = a \cdot IOPtrue + b} \qquad \textbf{(6)}$$

with slope $\boldsymbol{a}$, intercept $\boldsymbol{b}$ and R^2 given in **Table 4.2**. Since there was no significant difference in the parameters of the linear regression between treatments (p=0.70, ANCOVA), all data were pooled together to yield a single regression (**Figure 4.1**). We conclude that DEX treatment did not affect the accuracy of the IOP measurements using the TonoLab tonometer. All IOP value reported in this manuscript were IOPtrue, i.e. IOPs corrected by a single calibration curve as follows (Equation 7; note that IOPs are expressed in mmHg in this equation):

$$\boldsymbol{IOPtrue = \frac{IOPtono + 0.096}{1.002}} \qquad \textbf{(7)}$$

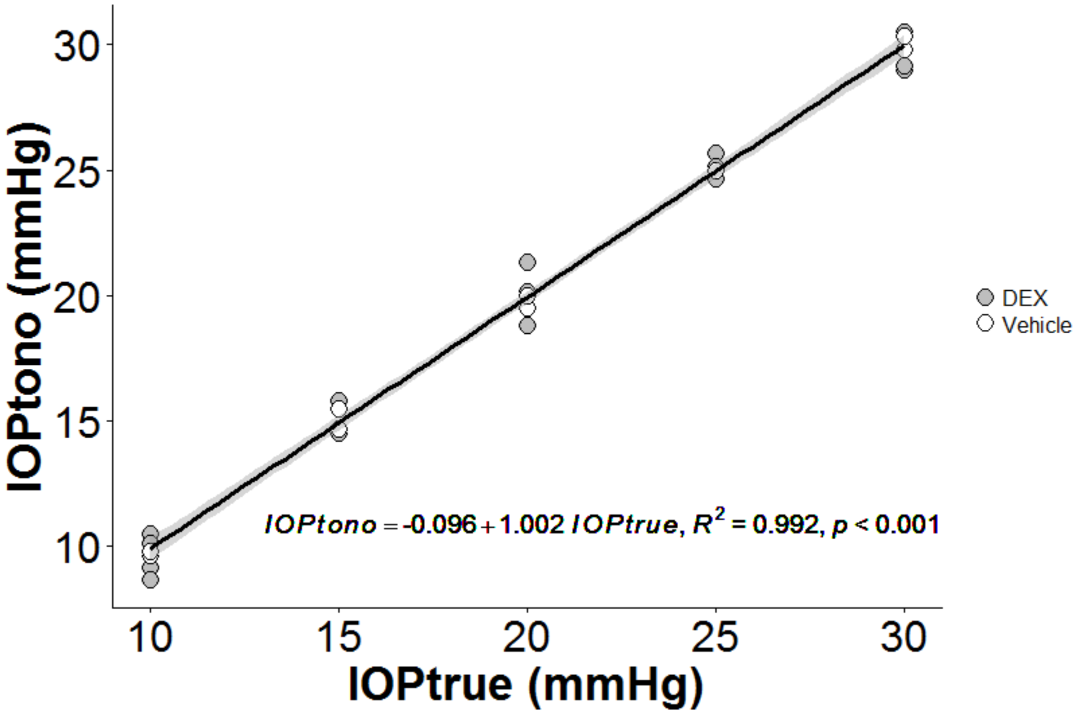

Figure 4.1: Correlation between IOP measured by tonometer (IOPtono) and set by reservoir (IOPtrue) in mouse eyes. Each data point refers to a single eye. Grey is for DEX-treated eyes and white is for vehicle-treated eyes. The line is the best fit using linear least squares regression. The gray-shaded region shows 95% confidence bounds to the regression.

Table 4.2: Results of the tonometer calibration. a: slope; b: intercept and R: correlation coefficient.

Groups	Mouse	Eye	a	b (mmHg)	R^2
Vehicle	1	OD	0.9967	-0.0333	0.9976
		OS	1.0267	-0.5667	0.9997
DEX	2	OD	1.0433	-0.4000	0.9921
		OS	0.9233	1.2333	0.9951
	3	OD	1.0224	1.1524	0.9980
		OS	1.001	0.3429	0.9985

4.3.4 Outflow Facility Measurement

Both OD and OS eyes were enucleated after mice were sacrificed and outflow facility was measured ex vivo using the standard iPerfusion system [139]. On a typical experimental day, 2-3 pairs of eyes were perfused, with each pair of eyes being perfused simultaneously to eliminate any errors caused by post mortem time differences. The detailed perfusion procedures can be found in Chapter 3, Section 3.3.1-3.3.2.

4.3.5 TM Stiffness Measurement

After facility measurement, the eyes were snap-frozen in the Stamer lab and sent to Atlanta for TM stiffness measurement. The detailed procedures can be found in Chapter 3, Section 3.3.3.

4.3.6 Statistical Analysis

For each mouse, only the data from the OD eye was used to avoid non-independence effects between the two eyes from one animal. The exception was in animals for which measurements on the right eye yielded invalid facility data due to technical issues, in which case the left eye was used. The Wilcoxon rank-sum test was used to compare differences in IOP, outflow facility and TM stiffness between groups (DEX-treated vs. Vehicle-treated mice). For completeness, and for consistency with other studies, we also repeated our analyses by averaging data from both eyes of each mouse, using the same statistical methods (See details in Appendix B). Linear regression was used to test the correlation between IOP and outflow resistance, and the correlation between outflow resistance and TM stiffness. Further, ANCOVA was used to investigate whether other factors (e.g. treatment conditions, cohorts) were significant contributors to the changes in outflow resistance (R; version 3.4.1; R Core Team). In those models, the TM stiffness was the independent variable and outflow resistance was the dependent variable. Other factors were treated as covariates. The significance threshold was defined to be 0.05 for all statistical tests.

4.4 Results

Local DEX delivery resulted in significant IOP elevation compared to vehicle-treated animals on day 14 and on the day when mice were sacrificed (n: 25 DEX and 16 control mice; **Figure 4.2**). IOP remained near the baseline level (day 0) in control mice (**Figure 4.2**). On the day mice were sacrificed (day 20-40), IOP was 27.12±2.72 mmHg (mean ± SD) in DEX-treated mice and 20.53±3.16 mmHg in vehicle-treated mice ($p<0.001$, **Figure 4.3**A). Further, all DEX-treated mice had increased IOP on the day of sacrifice compared to that on day 0.

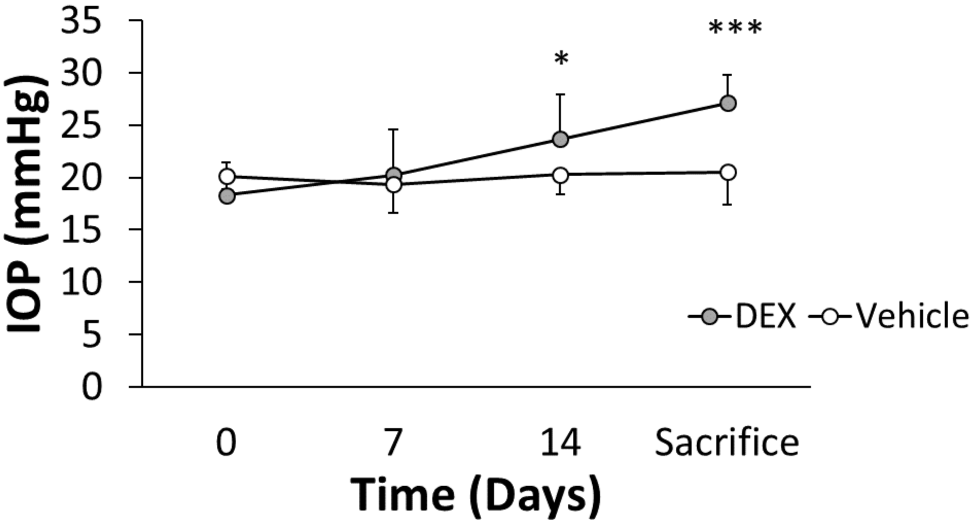

Figure 4.2: IOP as a function of time for DEX-treated (grey) and vehicle-treated (white) mice averaged over five cohorts. For cohort 1 and 2, DEX or vehicle were injected on day 0 and 7. For cohort 3-5, injections were performed on day 0, 7 and 14. All IOPs were measured immediately before injections. Bars are standard deviation. *p<0.05, ***p<0.001. p-values were Benjamini-Hochberg corrected.

The mean facility of DEX mice was lower than that of control mice (**Figure 4.3**B), but the difference did not reach statistical significance (DEX: 3.05 ± 1.47 nl/min mmHg; Control: 4.09 ± 1.71 nl/min mmHg; p= 0.192). The IOP measured before death tended to be negatively correlated with 1/C in the same eye. However, the low R^2 indicated that only about 15% of the IOP elevation was attributable to the variation in facility, and the relationship was not statistically significant (p=0.0788; R^2: 0.154; **Figure 4.3**C).

The TM was stiffer in some of the DEX mice, although not all (**Figure 4.4**). The average TM stiffness in DEX-treated mice was about 20% higher than that in vehicle-treated mice, but this difference did not reach statistical significance (2.38±1.31 vs. 1.99±0.91 kPa; p=0.357). Interestingly, despite the modest differences in facility and TM stiffness between the DEX-treated and control mice, there was a positive correlation between outflow resistance and TM stiffness for pooled data which reached statistical significance ($p=0.002$; $R^2 = 0.41$; **Figure 4.5**). Mouse cohort, as a covariant, did not have a significant effect on the above correlation (ANCOVA, $p=0.54$). Further, the same correlation within each group was also statistically significant (DEX group: $R^2=0.483$, $p=0.0176$; Control group: $R^2=0.421$, $p=0.0425$, **Figure 4.6**). ANCOVA showed that neither the slopes nor the intercepts were significantly different between the two correlations (p for slope=0.78; p for intercept=0.09, **Figure 4.6**), justifying performing a single correlation between resistance and TM stiffness using pooled data in **Figure 4.5**.

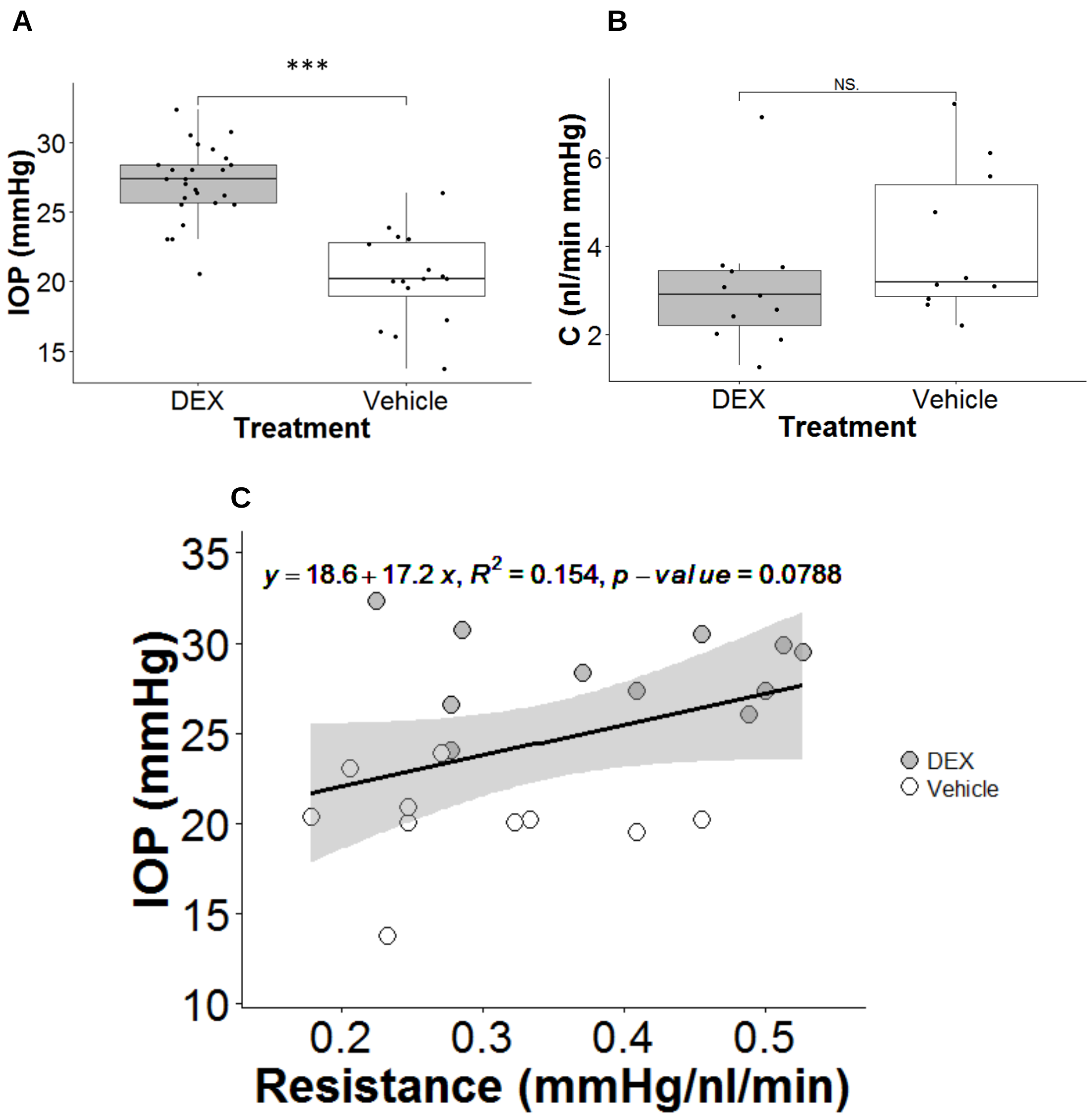

Figure 4.3: DEX treatment affected IOP and facility. (A) Boxplot of IOP for DEX-treated (n=25) and vehicle-treated mice (n=16). (B) Boxplot of facility (C) for DEX-treated (n=11) and vehicle-treated mice (n=10). For each box, the central mark is the median, the edges of the box are the 25th and 75th percentiles, and whiskers extend to the most extreme data points not considered outliers. Each dot represents the data from one eye. (C) IOP measured on the day mice were sacrificed plotted as a function of resistance for DEX-treated (grey dots, n=11) and vehicle-treated (white dots, n=10) mice. The black solid line is the best fit using linear least squares regression. The gray-shaded region shows 95% confidence bounds for the regression. ***p-value<0.001. NS.: Not Significant. Data in panels B and C are from cohorts 3-5.

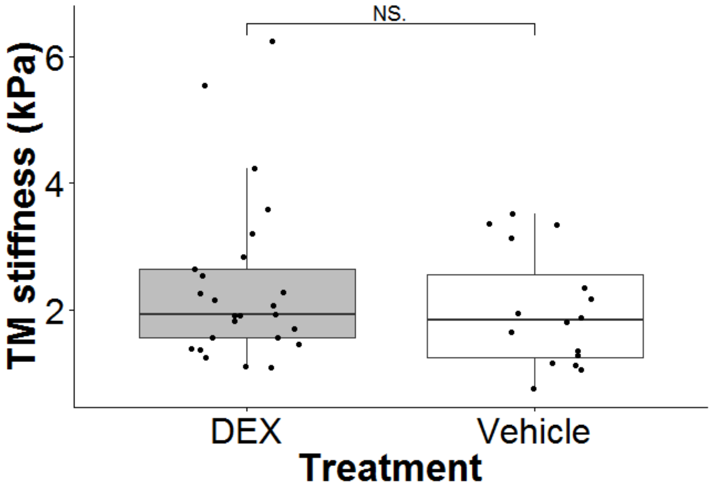

Figure 4.4: Boxplot of TM stiffness for DEX-treated (n=25) and vehicle-treated mice (n=16). For each box, the central mark is the median, the edges of the box are the 25th and 75th percentiles, and whiskers extend to the most extreme data points not considered outliers. Each dot represents the data from one eye. NS: Not Significant.

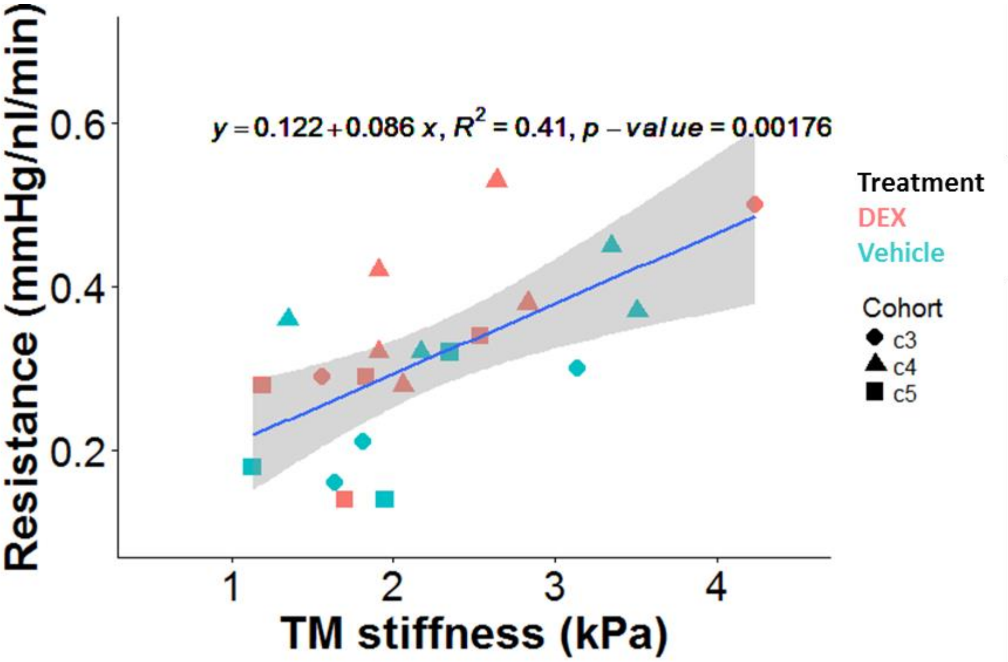

Figure 4.5: Cross-plot between outflow resistance and TM stiffness for DEX-treated (n=11) and vehicle-treated mice (n=10). The blue line and equation represent the linear regression of the pooled data. The gray-shaded region shows 95% confidence bounds for the regression. Different shapes represent different cohorts.

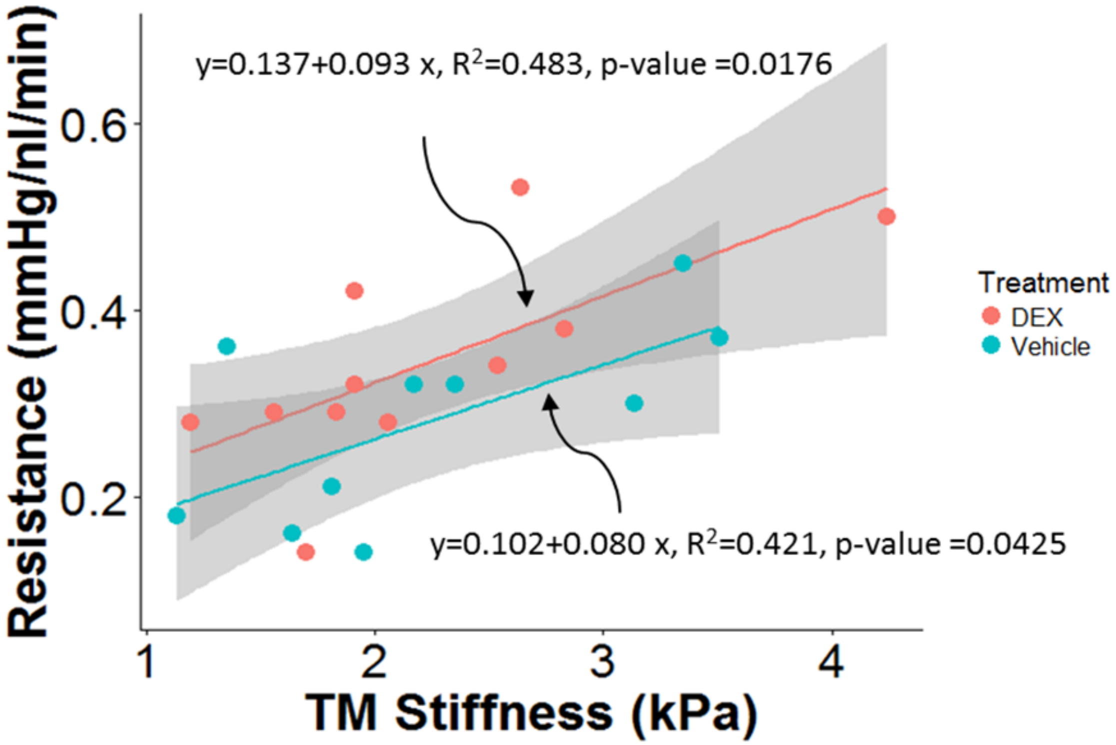

Figure 4.6: Cross-plot between outflow resistance and TM stiffness within each group of mice, with DEX mice shown in red (n=11) and control mice shown in green (n=10). The gray-shaded regions show 95% confidence bounds for the regressions.

4.5 Discussion

The major finding of this work is that there is a significant correlation between aqueous outflow resistance and TM stiffness in DEX-treated and control mice. The mechanism(s) behind the trend towards higher TM stiffness in DEX-treated eyes remain unclear. It is important to recall that we interrogated the stiffness of histologic 10-micron sections, so that most cells within the section had likely been cut during section preparation. It is difficult to unambiguously assign measured stiffness values to a specific TM component in our experiments, but in view of inevitable cell damage sustained during the sample preparation technique, it seems probable that our measurements primarily reflected ECM stiffness. This supposition is consistent with the observations of

Overby et al., who found that systemic treatment with DEX led to increased ECM in the JCT, including fibrillar material and basement membrane material under the inner wall of Schlemm's canal [149]. Of course, in situ, overall TM stiffness depends on TM cells, the ECM and the interaction between the two [39-43, 150]. It is important to recall that there is a constant mechanobiologic interplay between cells and ECM in soft tissues, so that, for example, TM cell tone can induce ECM reorganization/deposition which may in turn affect TM stiffness [42, 44, 45]. Thus, the variations in TM stiffness that we observe could have arisen due to cellular-level variations that led to matrix alteration, due to primary variations in ECM composition or density, or both. Better understanding these mechanistic details will be very important for developing novel therapies that act on TM stiffness to modulate IOP.

Within some of the cryosections with relatively large TM regions, it was possible to reliably make measurements closer to the SC ("Outer" TM, likely involving the JCT and part of the corneoscleral TM) and further from SC ("Inner" TM, likely including uveal meshwork and part of the corneoscleral TM, Figure 4.7). It was consistently observed that the measurements in the outer TM region were stiffer than those in the inner region in both DEX and vehicle-treated mice (Figure 4.8), with the difference reaching statistical significance in DEX mice ($P<0.001$; Paired Wilcoxon test; $N=12$). This emphasizes the heterogeneity of the TM and is consistent with the hypothesis we proposed in Section 2.5, where we suggested that any stiffness differences in HF vs. LF regions of TM may occur closer to the inner wall of SC.

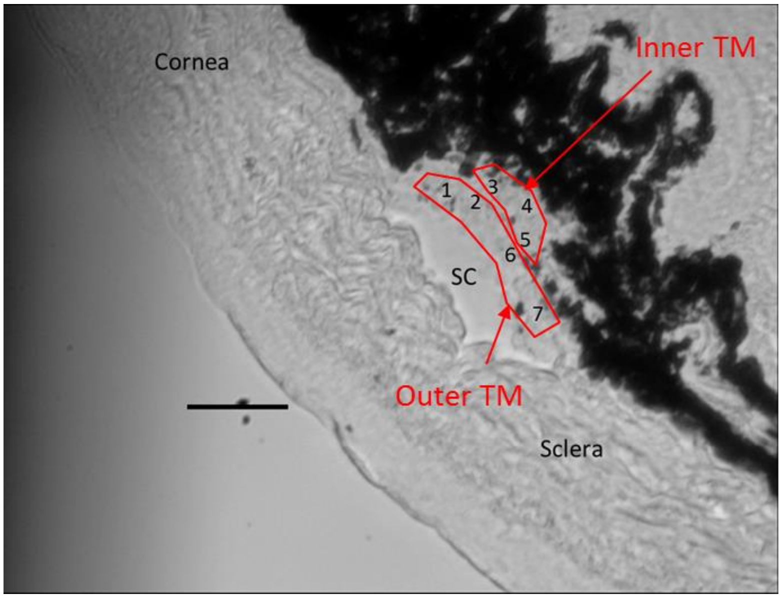

Figure 4.7: A representative cryosection with a relatively large TM. Numbers within the TM region indicate individual locations indented by the AFM probe. "Outer" TM and "inner" TM were labeled. Scale bar: 50 µm. Section thickness: 10 µm.

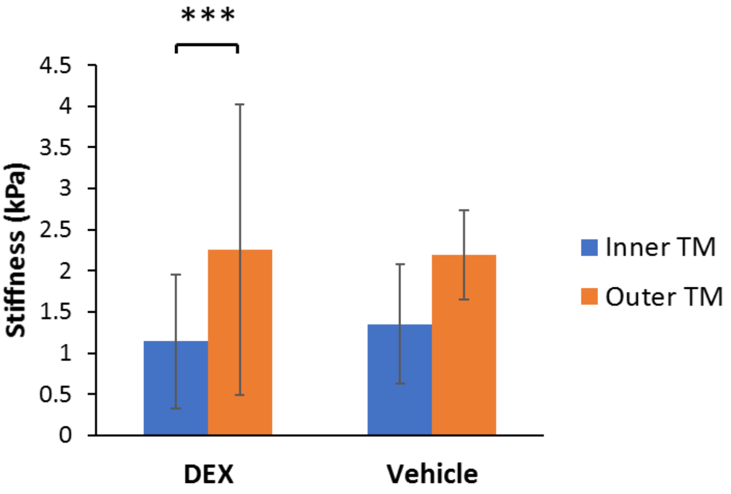

Figure 4.8: Regional heterogeneity of TM in DEX- (N=12) or vehicle- (N=5) treated mice. The outer TM (orange bar) tended to be stiffer than the inner TM (blue bar) in both groups (DEX mice: mean±SD=2.26±1.76 kPa for outer TM and 1.14±0.82 kPa for inner TM; Vehicle mice: 2.19±0.55 kPa for outer TM and 1.35±0.73 kPa for inner TM). Error bars: standard deviation. ***p < 0.001.

An unexpected observation in our study was that outflow resistance was not significantly related to IOP ($R^2 = 0.154$), in the DEX treatment study. There are several possible explanations of this observation, besides the relatively small sample size. Consider Goldmann’s equation (Equation 8):

$$\boldsymbol{Q} = \boldsymbol{C}\,(\boldsymbol{IOP} - \boldsymbol{EVP}) + \boldsymbol{Q_u} \tag{8}$$

where $\boldsymbol{Q}$ is total outflow rate, $\boldsymbol{Q_u}$ is the unconventional outflow rate, EVP is episcleral venous pressure and $\boldsymbol{C}$ is the conventional outflow facility. The linear relationship between IOP and outflow resistance (1/C) only holds when three other factors (aqueous humor production rate, episcleral venous pressure and any pressure-independent flow) are constant. However, all three factors can differ from animal to animal. Thus, the mathematical correlation between outflow resistance and IOP can vary from mouse to mouse. The lack of a correlation between facility and IOP within our cohort of mice may suggest that the TM adapts to “external” factors such as EVP and inflow rate to try to reach a target IOP level.

As discussed in Section 3.6, outlier detection procedures were performed, and again, statistical testing outcomes remained the same for all the statistical tests when outliers were excluded. In the facility comparison, we detected 1 outlier for DEX mice and 1 outlier for vehicle mice; in the TM stiffness comparison, we detected 2 outliers for the DEX group.

One limitation of this study is that the clearance mechanisms of nanoparticles from the subconjunctival space after injections were not investigated. Further studies may need to test the degradation rate of the particles and better understand their clearance route over time after injection. It would also be worthwhile to determine whether their presence alone can affect tissue mechanical properties and IOP, which could be done by comparing eyes with ghost NP injection to naïve eyes.

In summary, this project investigated the role of mechanical properties of TM in outflow resistance in mouse eyes, showing that outflow resistance is positively and significantly associated with TM stiffness in DEX-treated mice. These data demonstrate that mechanical properties of TM are closely involved in the function of the outflow and this finding has interesting implications. Importantly, manipulating TM stiffness via mechanisms beyond ROCK inhibition may be a fruitful approach to restore normal outflow dynamics in SIG. Further, TM stiffness might be a surrogate marker for conventional outflow pathway function in general. Novel technologies are being developed to measure ocular tissue stiffness in situ [151-154], and could thus hold promise for future diagnostic benefit in SIG if they could be adapted to the TM.

CHAPTER 5. CONCLUSIONS AND FUTURE DIRECTIONS

5.1 Summary of the Main Findings and Contributions

5.1.1 Development of a Method to Directly Measure Trabecular Meshwork (TM) Stiffness in Mice

By combining the techniques of cryosectioning and AFM, we were able to develop a technique to measure compressive Young's modulus of TM in the mouse eye. This is the first time that the stiffness of mouse TM has been measured. In this approach, the mouse TM can be clearly identified in cross-section by using the pigmented ciliary body and the open lumen of Schlemm's canal (SC) as landmarks. We expect that this approach will be used in future work, for example to identify molecular factors and associated genes involved in TM stiffness regulation. Progress in this area may lead to further understanding of the role of TM stiffness in ocular hypertension, which may help guide the design of future glaucoma therapies. In addition, this approach could potentially be applied to measurement of other tissues that are not easily accessible or inappropriate for measurements with conventional mechanical testing instruments due to size limitations.

5.1.2 Development of a Method to Estimate Human TM Stiffness in situ

By combining numerical modeling and advanced optical coherence tomography (OCT), we were able to estimate human TM (hTM) stiffness without excision of the TM. Our results showed that:

1. The elastic modulus of normal hTM ranged from 42 to 102 kPa (mean, 70 ± 20 kPa), which was lower than glaucomatous hTM samples, ranging from 79 to 123 kPa (mean, 98 ± 19 kPa).
2. TM stiffness measured by AFM was approximately 1/40 of that estimated by inverse FEM. This difference was almost certainly due, at least in part, to different modes of testing (compressive in AFM versus primarily tensile by SC luminal pressurization).
3. Outflow facility and TM stiffness were significantly correlated. For consistency with mouse studies, we here replot our data to show the correlation between outflow resistance and TM stiffness. The correlation reached statistical significance (Figure 5.1, R^2= 0.85, p=0.0086), suggesting that more than 80% of the variation in outflow resistance was associated with variation in TM stiffness in human eyes.

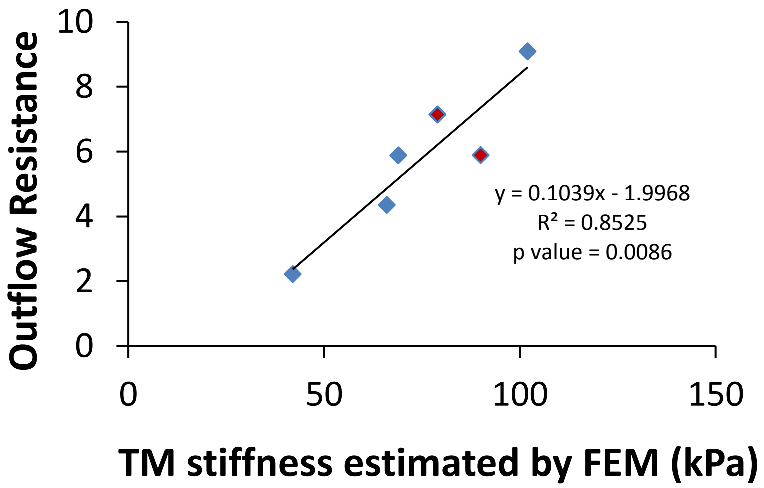

Figure 5.1: Cross-plot between TM stiffness (estimated by inverse FEM method) and outflow resistance (1/C) from normal (blue symbols) and glaucomatous (red symbols) human eyes. The solid line and equation represent the linear regression of the pooled data.

This percentage is larger than we observed in mice, where approximately 40% of the variation in outflow resistance was attributable to changes in TM stiffness. This discrepancy might reflect the difference in sensitivity of outflow resistance to the variation in TM stiffness between species.

4. Additionally, this approach can be extended to 3D to predict the stiffness of other outflow structures/tissues, such as transluminal structures across SC and septae at collector channels (CC), which may also play a role in influencing aqueous humor drainage.

5.1.3 The TM stiffness in Mice across a Range of Conditions

With a cryosection-based AFM technique, we were able to measure TM stiffness in mice across a range of conditions, including natural variation across wild-type strains and in DEX treatment. Our main findings are:

1. Some DEX-treated mice had much stiffer TMs than control mice, despite the non-significant difference on average between the DEX and control groups.
2. There was a significant correlation between aqueous outflow resistance and TM stiffness in both wild-type strains of mice and DEX-treated mice. This suggests that an intrinsic link between the mechanical properties of the TM and aqueous humor outflow dynamics exists.
3. The correlation between TM stiffness and outflow resistance for the wild-type C57BL/6J mice in the strain study was not significantly different from the same correlation for the control C57BL/6J mice in the DEX study (p=0.66). We noted that the latter reached statistical significance (p=0.043) while the former did not

(p=0.064). This discrepancy might be due to the difference in gender (strain study: mixed genders; DEX project: all males) and/or age (average age of C57BL/6J mice in the strain study: 12 weeks; DEX study: 18 weeks).

4. Our data strongly suggest that modulating TM stiffness may be a novel approach to restore normal outflow dynamics in glaucoma patients.
5. Our results have implications for the diagnosis of glaucoma, specifically motivating the adaption of in vivo tissue stiffness measurement techniques to the TM.

Overall, the five questions raised from the three objectives at the beginning of this dissertation have been answered. Here are the brief answers to those questions:

1. Can we measure human TM stiffness without excising the TM from its physiological environment?

Answer: Yes. In the inverse FEM approach, the TM remains intact within each anterior segment wedge, with the anterior TM connected to the cornea and the posterior TM attached to the ciliary muscle and sclera spur.

2. Is there a significant correlation between outflow resistance and TM stiffness in human eyes?

Answer: Yes, those two parameters were positively and significantly correlated in human eyes.

1. Can we measure TM stiffness in mice?

Answer: Yes, by using the cryosection-based AFM technique, TM in mouse eyes can be clearly identified and TM stiffness can be directly measured through a compression test.

3. Is there a significant correlation between outflow resistance and TM stiffness in wild-type mice?

Answer: Yes, there is.

4. Is there a significant correlation between outflow resistance and TM stiffness in a single mouse strain after DEX treatment?

Answer: Yes, there is. Further, such a correlation exists even within each group, i.e. when considering DEX-treated mice or control mice.

5.2 Future Work

5.2.1 Refinement of Research Methods

For the inverse finite element modeling approach, we used the neo-Hookean material model for all the tissue components (sclera, TM, cornea and transluminal structures). This model works well for hyperelastic materials in the initial linear range where the strains are less than 20%. However, it is known that the neo-Hookean material model is not ideal at large strains. In our simulations, the maximum first principal strain in the deformed state was usually less than 20% for most samples, but only if the pressure difference across TM was less than 20 mmHg. This limited the estimation of mechanical properties of TM to relatively low strain situations, while higher deformations could occur in abnormal conditions such as glaucoma. Therefore, adopting a more complex material model (e.g. the Mooney-Rivlin material model) could potentially allow us to examine TM stiffness at higher stress level as well as the nonlinear mechanical properties of the TM. However, implementing such a model would come at the cost of greater complexity in stiffness calculation and potentially more uncertainty in model parameter estimation.

Another factor not considered in the current inverse FEM study was the anisotropy of the TM. Previous studies have shown a large discrepancy in TM stiffness measured circumferentially (parallel to the surface of the limbus) and transversely (along the outflow direction) [30, 52, 53, 59]. Further, histological images either published in the literature or obtained in our lab suggest that the collagen fiber orientations in the uveal and corneoscleral meshwork may be quite different. In human TM, the beams in the uveal meshwork closest to the anterior chamber are more cord-like and oriented predominantly in a net-like fashion, as shown in Gong's paper (**Figure 5.2**) [9]. In contrast to the uveal meshwork, the corneoscleral TM is composed of flattened sheets. Most of the collagen fibers in the beam cores in this region appear to be oriented circumferentially in human eyes [155] but a significant portion are also oriented transversely. From the above evidence, it would be interesting to include the effects of structural anisotropy in models of the corneoscleral meshwork, with the main collagen fibers being oriented circumferentially, and to investigate the stiffness in different layers of the TM. This approach might allow us to better compare estimated TM stiffnesses to a variety of experimentally measured values that use a range of measurement approaches. Such a model would require advanced imaging and image processing to identify different layers of the TM from the OCT images, which is extremely difficult using current imaging techniques.

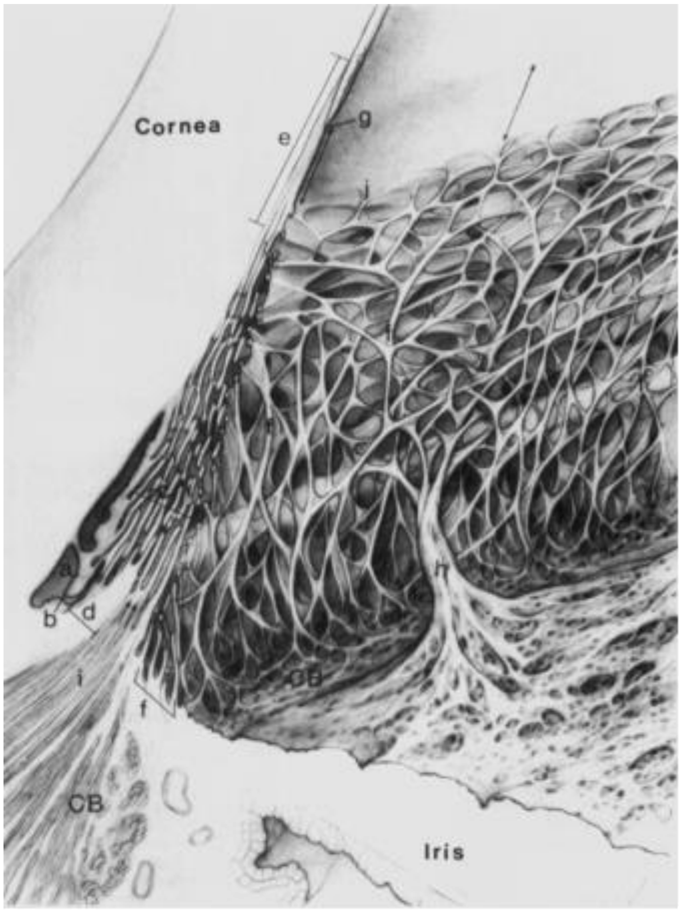

Figure 5.2: Diagrammatic representation of the anterior chamber angle. Schlemm's canal (a) is divided into two portions at various points along its length. An internal collector channel (Sondermann) (b) opens into the posterior part of the canal. The sheets of the corneoscleral meshwork (c) extend from the corneolimbus (e) to the scleral spur (d). The beamlike components of the uveal meshwork (f) occupy the inner portion of the trabecular meshwork; they arise in the ciliary body (CB) near the angle recess and end just posterior to the termination of Descemet's membrane, called Schwalbel's line (g). An iris process (h) extends from the root of the iris to merge with the uveal meshwork at about the level of the anterior part of the scleral spur. The longitudinal ciliary muscle (i) is attached to the scleral spur but has a portion which joins the corneoscleral meshwork (double-headed arrows). (Reproduced from Hogan et al., 1971)

In the inverse FEM approach, only one stiffness value was obtained for the entire TM region under investigation. However, we expect that TM stiffness can vary from location to location within a single cross-section since the microstructures and ECM/cell densities are different for the three layers of TM (**Figure 5.2**). Thus, it would be better to estimate local TM stiffness and study the change of stiffness as a pattern instead of a single value which represents the bulk TM stiffness in a cross-section. This would require some sort of an advanced imaging and tracking technique to determine local deformation of the TM in a cross-sectional plane. Moreover, such an approach would add considerable computing time to the inverse FEM process because the deduction process involves multiple TM stiffness representing multiple locations.

All our AFM measurements used the bottom camera, which means that we looked at the sample from its bottom while the AFM tip probed the upper tissue surface. This configuration added uncertainty about the AFM measurement locations due to the cantilever tip and tissue having different focus planes. We estimated that the difference between the location of the cantilever tip as observed from the bottom camera and the actual indentation location was approximately 20 µm for 1mm thick samples. Samples with different thickness or tissue compositions (thereby with different coefficients of refraction) might result in larger deviations. Although the deviation between the desired and actual measurement locations was much less than the typical width of the TM band in human eyes, this uncertainly in location may introduce errors into the measured TM stiffness, especially when combined with errors in TM boundary definitions. Therefore, an improved method to track the measurement locations would be desirable. Two possible approaches may be worth trying in this regard. First, instead of using the bottom camera, using a new upper camera with much higher resolution would allow us to view both the sample and the cantilever from the top. In that case, the focus plane of the cantilever tip and the measurement location would be the same and any deviation induced by the sample thickness could be avoided. Another possible solution could be to use very fine markers to replace the Sharpie markers we used to draw on the back of the glass slide. For example, a transmission electron microscopy grid (**Figure 5.3**) with different numbers of grids and diameter could serve as a set of fine markers when adhered to the back of the slide, overlapping with the target measurement locations of the tissue. In this way, it would be possible for users to track each individual measurement location more accurately and to allow for repetitive measurements on the same spot before and after certain treatment or experimental conditions.

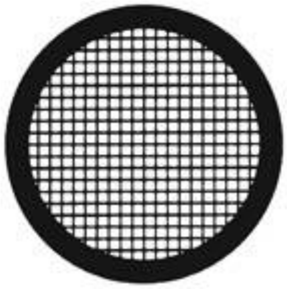

Figure 5.3: Transmission Electron Microscopy grids with 200 mesh, 3.05 mm O.D. Image source: https://www.tedpella.com/grids_html/maxtafrm.htm

5.2.2 Additional Experiments

One limitation we mentioned for the cryosection-based AFM technique is that it is possible the freeze-thaw procedure may alter tissue stiffness. Additional validation tests could be performed to test whether this is indeed the case. Ideally, we need to compare tissue stiffness at the same location on a cutting surface before and after freezing since in the AFM technique we used, the TM stiffness was measured on a cutting surface of the cryosections. For such a study, the cornea could be considered as a surrogate tissue for the TM, since it would be nearly impossible to cut cross-sections from fresh TM in mouse eyes. The simplified method we propose is as follows:

1. Cut a strip of fresh cornea from the anterior segment and fix it to a glass slide by putting glue dots on the edge, with the corneal endothelium facing upward;
2. Make an oblique cut on the surface using micro-scissors or a sharp razor blade;
3. Fix a grid (Figure 5.3) with a suitable size to the back of the slide;
4. Make AFM measurements on selected locations which fall onto the cutting surface region on the fresh cornea, with the aid of the grid;
5. Snap-freeze the whole slide with the cornea strip covered by O.C.T., and stored the slide in the freezer;
6. After a few days, make AFM measurements on the same locations on the thawed sample;
7. Compare the differences in cornea stiffness in steps 4 and 6 using Wilcoxon rank-sum test.

One aspect not considered is whether DEX affects other anterior segment tissues, including the cornea. Although in Chapter 4 we found that the IOP readings obtained from the tonometer were nearly identical to the actual IOP, there could be more subtle effects of DEX on the stiffness of the cornea or other anterior segments tissues. It is possible that the DEX injected into the subconjunctival space may diffuse into the aqueous humor and therefore may have access to the cornea when aqueous humor flows through the anterior chamber. Thus, another experiment for future studies would be to measure corneal stiffness. We suggest using the MicroSquisher device (CellScale, Waterloo, Canada) rather than AFM for this experiment because the Microsquisher is able to test the overall stiffness of the sample on a much larger scale. We propose the following simplified experimental protocol:

1. For each frozen eye, the cornea is removed and then thawed at 4 ºC. A 1 mm biopsy punch is used to obtain a small round cornea sample from the flat mount piece of cornea and stored in 4 ºC PBS until used.
2. Each sample is tested in a parallel-plate compression configuration using a CellScale MicroSquisher and accompanying SquisherJoy software program. The area of the stainless-steel compression plate is about 5 mm^2. All samples are tested in a PBS fluid bath warmed to 37 °C.
3. Prior to compression, the compression plate of the cantilever is lowered toward the sample surface until gentle contact occurs. Preliminary studies have shown that when the compression plate applies 100 nN to the cornea surface, the sample curvature is barely seen and the entire sample surface contacts the compression plate. Samples are compressed to at least 25% engineering strain at a rate of 2.5 um/second, held at a constant deformation for 10 seconds, and then released at a rate of 2.5um/sec to record any hysteresis. The above measurement parameters reference the parameters used for measuring stiffness of stem cell spheroids [156] and may need to be adjusted for cornea measurement.
4. The resulting force-deformation curves are converted to engineering stress vs. engineering strain relationships. The effective Young's modulus is calculated by fitting the 0-20% strain range with a linear regression line. The resulting slope of the regression line is taken as the effective modulus of the sample [157, 158].

5. Compare cornea stiffness from DEX mice and control mice using Wilcoxon rank-sum test.

Another aspect not included in our mouse studies which needs further investigation is the mechanism behind TM stiffness variation. It has been suggested that TM cells, TM ECM and the interactions between the two can contribute to the overall TM stiffness supported by evidence such as increased basement membrane materials, increased cell-cell junction complexity, and increased fibrillar material under the inner wall of Schlemm's canal [147] in DEX-treated mice. Additional experiments could be done to quantify the levels of protein expression in the TM, such as α-SMA (overexpression of α-SMA has been detected in primary human TM cells treated with DEX [60]), and then correlating protein expression levels with TM stiffness.

5.2.3 Long-term Goals

One of the long-term translational goals of the research in this dissertation is to find novel treatments to restore normal outflow resistance in glaucoma patients by better understanding the pathophysiology of altered mechanical properties in outflow tissues. Currently, the only treatment for POAG is to reduce IOP through a variety of approaches. However, lowering IOP does not cure the disease since glaucoma symptoms are often noticed by patients in late stage when damage to the optic nerve is permanent. Thus, early diagnosis of glaucoma and timely treatment would be greatly benefit patients' quality of life.

Since we have shown that outflow function (described by outflow facility or outflow resistance) is closely correlated with TM stiffness in both human eyes (Chapter 2) and mouse eyes (Chapter 3 and 4), it has become clear that measuring TM stiffness in vivo could be clinically useful. For example, TM stiffness could be another testable risk factor for glaucoma and could provide guidance for potential treatment. Longitudinal studies of TM stiffness in glaucoma patients could also help understand whether stiffening precedes ocular hypertension, or vice versa. For example, if the TM became significantly stiffer in a person who did not receive any glaucoma medication, it might indicate that the person was a candidate for “TM softening”. A recent study published by the Amini lab [159] has shown an example of estimating TM stiffness in vivo using an inverse finite element approach. However, although this technique is exciting and promising, improvements are needed in several aspects before clinical application can be envisioned, e.g. increasing resolution of the OCT images, quantifying the actual incompressibility of the TM, etc.

How could we manipulate TM stiffness? To answer this question, we need to identify the underlying signaling pathways which regulate protein expression, ECM reorganization/turnover and TM contractility by TM cells or surrounding tissue structures, such as ciliary muscle and endothelium of Schlemm’s canal. Further, it may worth trying to map genes that are responsible for those molecular factors which could be another whole research area for diagnosis and treatment (i.e. gene therapy). Such studies are beyond the scope of this thesis.

5.3 Author Contributions to Each of the Studies

For clarity, the contributions of the author to each of the collaborative studies reported in this thesis are summarized here.

- FEM study (Chapter 2): Model creation, TM stiffness estimation, AFM measurements and data analysis, primary writing.
- Strain Study (Chapter 3): TM stiffness and outflow facility collection and data analysis, primary writing.
- DEX Study (Chapter 4): TM stiffness value collection and data analysis, primary writing.
- All studies described in the Appendices were done by the author.

5.4 Associated Publications and Abstracts

5.4.1 Journal Publications

K. Wang, G. Li, A. T. Read, I. Navarro, A. K. Mitra, W. D. Stamer, T. Sulchek, C. R. Ethier. The relationship between outflow resistance and trabecular meshwork stiffness in mice. Submitted

K. Wang, M.A. Johnstone, C. Xin, S. Song, S. Padilla, J. A. Vranka, T.S. Acott, K. Zhou, S. A. Schwaner, R. K. Wang, T. Sulchek, C. R. Ethier. Estimating human trabecular meshwork stiffness by numerical modeling and advanced OCT imaging. IOVS. 2017 Sep 1;58(11):4809-4817

K. Wang, A.T. Read, T. Sulchek and C.R. Ethier. Trabecular Meshwork Stiffness in Glaucoma. Experimental Eye Research. Jul 19, 2016. PubMed PMID: 27448987

B. Chiang, **K. Wang**, C.R. Ethier and M.R. Prausnitz. Clearance Kinetics and Clearance Routes of Molecules from the Suprachoroidal Space after Microneedle Injection. IOVS.

2017 Jan; 58(1): 545–554. (This publication is not directly related to the dissertation topic.)

5.4.2 Conference Abstracts

K. Wang, A.T. Read, G. Li, W.D. Stamer and C.R. Ethier. Changes in IOP, Outflow Facility and Trabecular Meshwork Stiffness in Dexamethasone-Treated Mice. ISER Poster 59, 2017.

K. Wang, A.T. Read, G. Li, W.D. Stamer and C.R. Ethier. Effects of dexamethasone on Trabecular Meshwork Stiffness in Mice. IOVS 2017; 58: ARVO E-Abstract 3146.

K. Wang, M.A. Johnstone, C. Xin, S. Padilla, R.K. Wang, A.T. Read, T. Sulchek and C.R. Ethier. Estimates of Trabecular Meshwork Stiffness using Novel Approaches. ISER Oral Presentation, 2016.

K. Wang, M.A. Johnstone, C. Xin, S. Padilla, R.K. Wang and C.R. Ethier. Estimating human trabecular meshwork stiffness by numerical modeling and advanced OCT imaging. IOVS 2016; 57: ARVO E-Abstract 3543.

K. Wang, T. Sulchek and C.R. Ethier. Determining the Compressive Modulus of Mouse Trabecular Meshwork with Atomic Force Microscopy. SB^{3}C, 2015 E-Abstract 1047.

APPENDIX A. SUPPLEMENTARY MATERIALS FOR CHAPTER 2

A.1 Mesh Refinement Study

A.1.1 Methods

For the 2D modelling approach, it was important to ensure that any finite element mesh was sufficiently refined so that the numerical simulations based on that mesh were not prone to significant numerical error, while also minimizing the required computing time. To test this, we carried out a mesh refinement study on the finite element model created from quadrant 77R-IN. All parameters including boundary conditions, loading pressure, and tissue stiffness remained the same. TM stiffness was set at 114 kPa. Simulations were run for a series of different element sizes which were characterized by edge length.

A.1.2 Results

The predicted SC perimeter and area both converged to asymptotic values as the mesh element size was reduced (**Figure A.1**). Based on these results, an edge length of c. 7 μm was judged suitable to balance accuracy and computational cost, which was approximately the average element size we used for our models (5 – 10 μm).

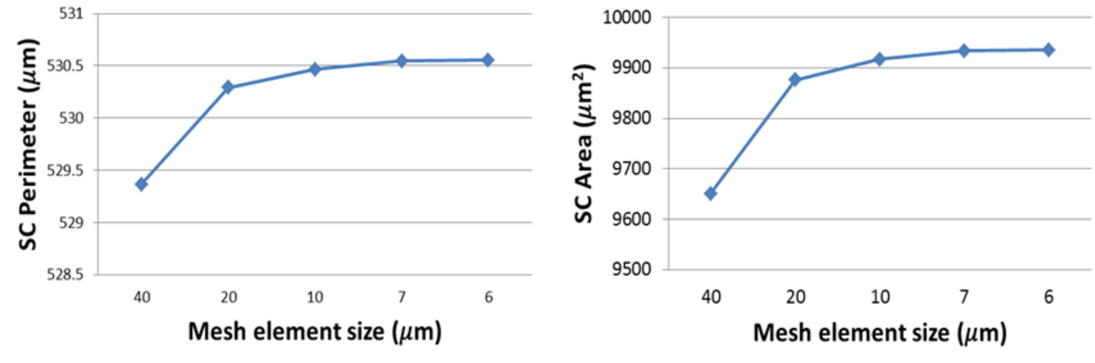

Figure A.1: Mesh refinement test for FEM simulation. Y axes: SC lumen perimeter (µm) and area (µm2). X axis: average edge length of hexahedral element (µm). Note inverted scale for x-axis. Sample: inferior nasal quadrant of Eye 77R

A.2 3D Model

A.2.1 Methods

With the pseudo-2D modelling approach, the model geometry was created based only on tissue structures observed from a single 2D OCT slice. The tissue regions modeled in 2D at a single location were unable to adequately characterize the TLS oriented circumferentially in SC and therefore, it was impossible to depict those tissue structures which spanned several slices. Thus, a 3D model, including tissue structures such as TLS, collector channel and septae, was built and the estimated TM stiffnesses were compared between the 2D and 3D approaches. Specifically, a 3D model was built for the superior temporal quadrant of eye 80R to compare against the 2D approach. The geometry for the 3D model was based on 9 adjacent OCT images, instead of a single image as for the pseudo-2D models. The central OCT image used in the 3D model was the same as that in pseudo-2D model for eye 80R, giving a 3D model thickness of 80 µm thus allowing us to include potentially relevant outflow tissue structures such as transluminal structures (TLS), septa and a collector channel (CC) (**Figure A.2**). Cornea/Sclera and CB were given the same stiffness values as those in pseudo-2D model. In the absence of any specific data, septae were assigned a stiffness which was close to that of TM. A pressure load was applied to all inner surfaces of the open SC and CC lumens, with a magnitude identical to that applied in the pseudo-2D model of the same quadrant. This did not precisely replicate the experimental situation, but allowed a direct comparison between results of the pseudo-2D model and the 3D model. As with the pseudo-2D models, the SC lumen configuration was compared between simulated and experimentally measured results. Specifically, the difference in SC area at the higher pressure (in this case 30 mmHg) of the 3D model was computed as

$$\Delta\text{Area} = \sqrt{\sum_{\boldsymbol{n=1}}^{\boldsymbol{9}} (\boldsymbol{Area_{OCT\_layer\_n}} - \boldsymbol{Area_{FEM\_layer\_n}})^{\boldsymbol{2}}} \qquad (9)$$

where the index n refers to summation over the OCT cross-sections that the model was constructed from. This quantity was computed for different TM stiffnesses. The best match between computed and experimentally measured SC area was achieved at a TM stiffness of 48 kPa, which can be compared to 60 kPa obtained from the pseudo-2D model.

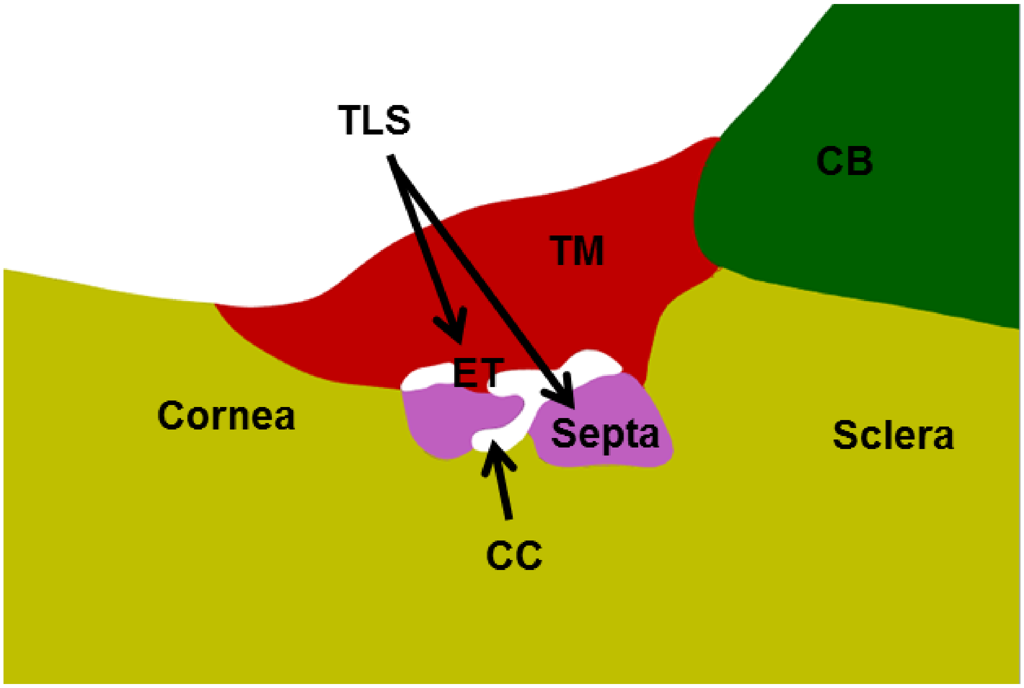

Figure A.2: One cross-section of the 3D model for superior quadrant of eye 80R. TM = trabecular meshwork, CB = ciliary body, TLS = Trans Luminal Structure, ET = Endothelial lining, CC = collector channel.

A.2.2 Results

The best match between computed and experimentally measured SC area was achieved at a TM stiffness of 48 kPa (**Figure A.3**), which can be compared to the value of 60 kPa obtained from the pseudo-2D model.

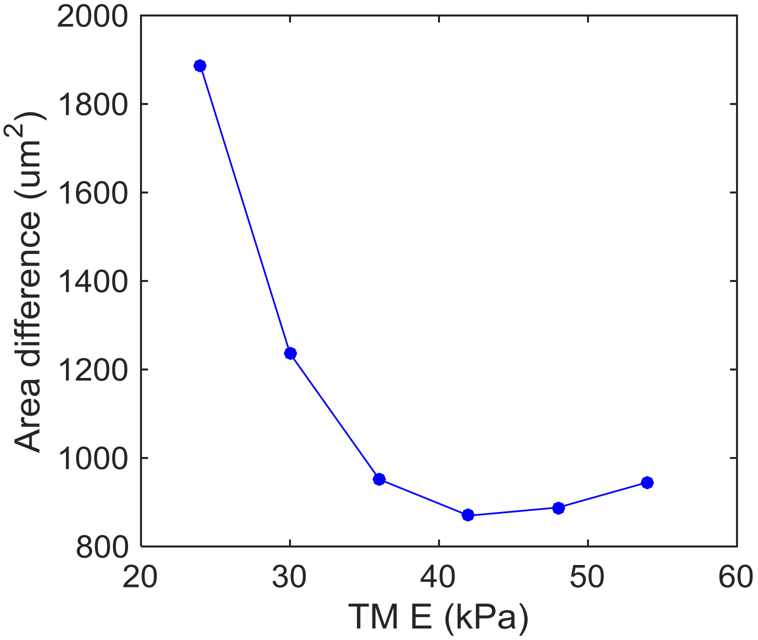

Figure A.3: Quantification of SC lumen area difference at a reservoir pressure of 30 mmHg in the 3D model. The X-axis is Young's modulus of TM. Blue curve is the difference between observed and computed SC lumen area. The minimum difference was observed at 48 kPa. Sample: superior temple quadrant of Eye 80R.

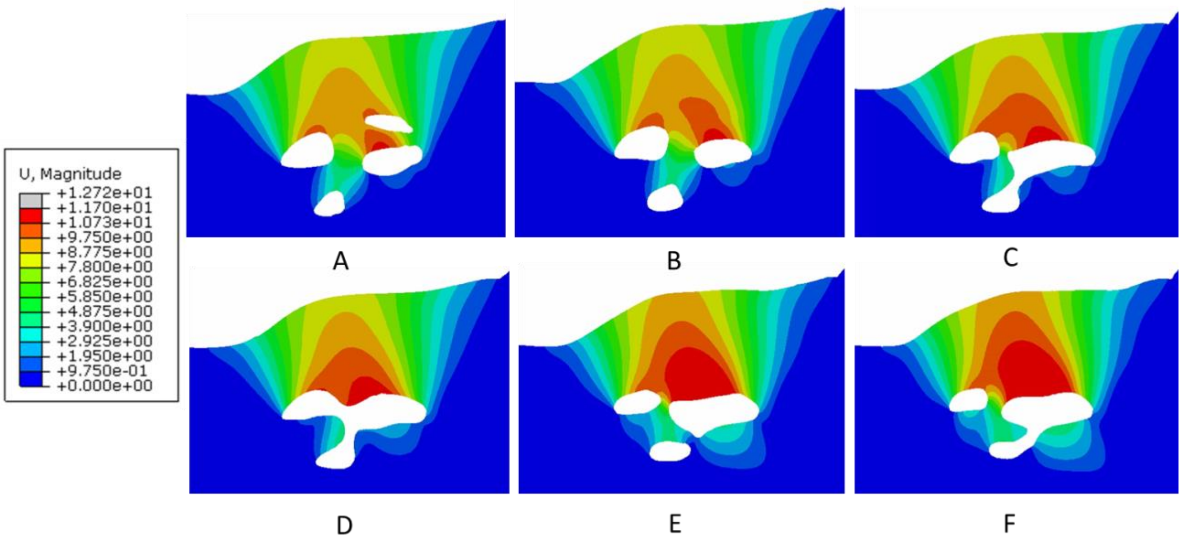

Figure A.4: Distribution of the total displacement of the 3D model at 6 different locations (A-F) along the SC lumen. Reservoir pressure = 30 mmHg. Unit of color bar is µm. Sample: superior temple quadrant of Eye 80R.

In addition, our 3D model predicted that, in general, the largest TM displacement occurred in the area around the inner wall of SC and center of the TM (**Figure A.4**). Interestingly, relatively large deformations also appeared in the TLS region which divided the canal into compartments at the entrance of CC (**Figure A.4**, A-C, E-F).

When comparing deformation patterns between the pseudo-2D and 3D models at the same scanning location, the deformation of the outflow tissues looked very similar (**Figure A.5**), except that there was more deformation experienced in the septa region in the 3D model. The slightly lower TM stiffness predicted by the 3D model (48 kPa vs. 60 kPa) might be partially explained by these TLS, since the deformation of those structures suggested that they are in tension and therefore resisted SC lumen distention.

The 3D model had several advantages over the pseudo-2D model. It provided a more realistic tissue geometry which included multiple OCT slices. However, it suffered from some limitations. For example, the exact boundaries of TLS were not entirely clear and the stiffness used for TLS was somewhat arbitrary. In view of the very significant time commitment needed to create such 3D models, and the relatively small difference in predicted TM stiffness between the 3D and pseudo-2D models, we chose to simply use pseudo-2D models in this work.

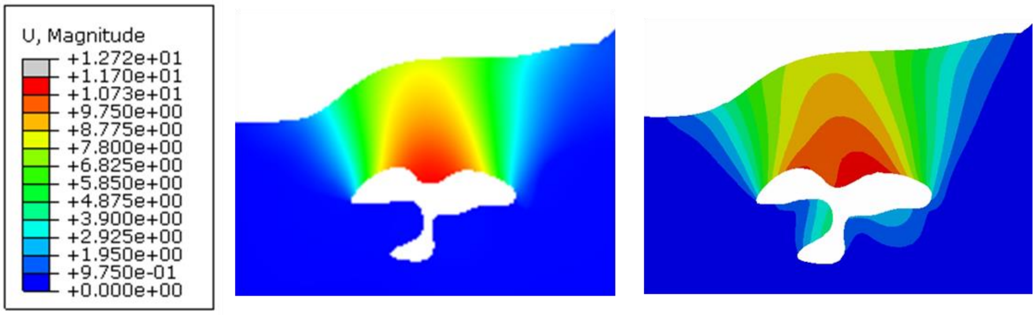

Figure A.5: Color map of the total displacement at the same location in 2D (left) and 3D (right) model. Sample: superior temple quadrant of Eye 80R.

A.3 Sensitivity Analysis

A.3.1 Methods

In practice, the biomechanical properties of outflow tissue other than the TM can vary from sample to sample. In addition, manual tissue boundary delineation may differ from reality and is somewhat subjective. We thus performed a sensitivity analysis on these aspects of the simulations in the 2D modelling approach.

First, the effects of sclera/cornea and ciliary body stiffnesses on predicted TM stiffness were evaluated using Latin Hypercube Sampling (LHS). LHS is an efficient stratified sampling technique where each input variable in a simulation is described by a probability distribution which is decomposed into equi-probable intervals [160]. For each simulation, a value for each variable is randomly selected from one equi-probable interval, without replacement. These input variables are used to drive a numerical simulation, and this process is repeated for many combinations of input variable values. An advantage of LHS is that it efficiently provides sensitivity information, which in this case was used to determine how changes in two variables (sclera/cornea stiffness and CB stiffness) impacted on estimated TM stiffness. The minimum number of required simulations, $\mathbf{N}$, for a LHS study has been empirically established as $\mathbf{N > 4k/3}$, where $\mathbf{k}$ is the number of input variables [160, 161]. In this study, fifteen random combinations of sclera/cornea and CB stiffnesses were generated by LHS, which satisfied the above criterion.

A key step in the LHS process is specifying the probability distributions of the input variables. We took mean stiffnesses for sclera/cornea and CB to be 3000 kPa and 100 kPa, respectively, as in the preliminary simulations. The stiffness range for normal human sclera/cornea was taken as 1000 – 5000 kPa [116, 162]. CB stiffness varied from 30 – 170 kPa. The lower and upper bounds for the CB stiffness were assumed to be mean ± 0.7*mean, to match the proportional range for sclera/cornea. Values in both ranges were assumed to be uniformly distributed.

Next, the effect of boundary delineation on estimated TM stiffness was tested using three different TM/CB delineations, where the boundary between the two tissue structures was most ambiguous and indistinguishable as observed in OCT images (**Figure A.6**). Three different plausible CB delineations were established (**Figure A.6**) and the analysis was repeated for each delineation.

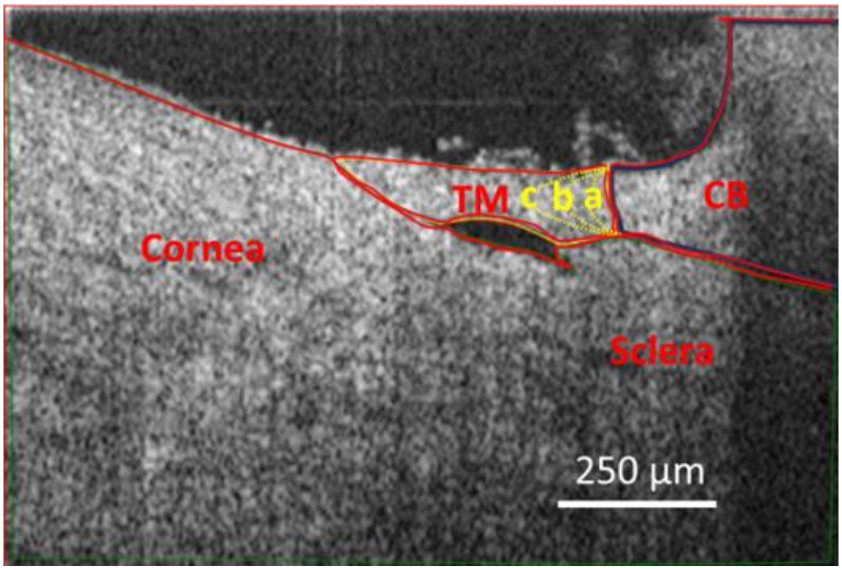

Figure A.6: Different TM/CB boundary delineations. Three possible TM/CB boundaries (a - c) are indicated by yellow dashed lines overlain on an OCT image. Sample: inferior nasal quadrant of Eye 77R.

A.3.2 Results

We found that estimated TM stiffnesses were relatively insensitive to variations in input parameters (mean±SD: 122 ± 8.7 kPa for the quadrant considered). In fact, the estimated TM stiffness were between 114-120 kPa for more than 65% of the LHS combinations (**Figure A.7**). Even though statistical analysis suggested that there was a significant partial correlation between two factors (stiffness of sclera/cornea and CB) and the estimated TM stiffness ($p < 0.05$), the squared partial rank correlation coefficients, which is a nonparametric measure of statistical dependence between the ranking of two variables, showed moderate correlations (< 0.5) between CB stiffness and estimated TM stiffness (**Table A.1**). Overall, this analysis indicated that the estimated TM stiffness was insensitive to variation of CB stiffness, which we judged as the major source of material property uncertainty in our simulations.

For the sensitivity analysis on TM/CB boundary delineation, the estimated TM stiffness (120 kPa) was identical for all three delineations.

In summary, the sensitivity analyses indicated that estimates of TM stiffness were relatively insensitive to both surrounding tissue stiffnesses and boundary delineation between the CB and TM.

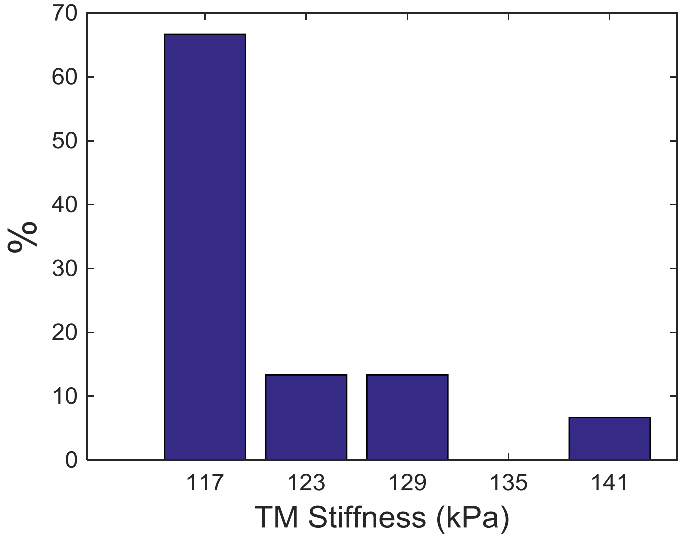

Figure A.7: Histogram of estimated TM stiffnesses arising from LHS analysis.

Table A.1: Partial correlation between stiffness of two tissue components (sclera/cornea and CB) and TM*

	Sclera/Cornea	**CB**
prcc^2	0.89	0.45
p-value	< 0.05	< 0.05

*$prcc^2$: squared partial rank correlation coefficient (or Spearman rank correlation coefficient), computed as $prcc = 1 - 6\sum_{i=1}^{N}\frac{D_i}{N(N^2-1)}$, where D_i is the difference between the ranks assigned to the corresponding pairs and N is the sample size. Ties are assigned average ranks [163, 164].

A.4 Corrected Loading Pressure

A.4.1 Methods

We realized that the pressure within the SC lumen is not necessarily the same as the reservoir pressure because of flow resistance in the system. For FEM, we must apply a pressure load that is consistent with the real situation in order to accurately simulate tissue deformation. The following shows how we estimated the relevant flow resistances and thus luminal SC pressures, using quadrant 77R-IN as an example.

Resistance Calculation in the OCT-based Inflation Test System:

(1) Resistance of tubing: There were 6 sections of tubing with known inner diameters (ID) and lengths (**Figure A.8**) in the system. We assumed the tubing to be cylindrical and thus used Poiseuille flow (Equation 10) to calculate the hydrodynamic flow resistance to flow

$$\boldsymbol{R_{cylinder}} = \frac{\mathbf{128}\boldsymbol{\mu L}}{\boldsymbol{\pi D^4}} \tag{10}$$

where μ is the viscosity of saline, taken as 1 cP; $\boldsymbol{L}$ is the length of the tubing; and $\boldsymbol{D}$ is the inner diameter of the tubing.

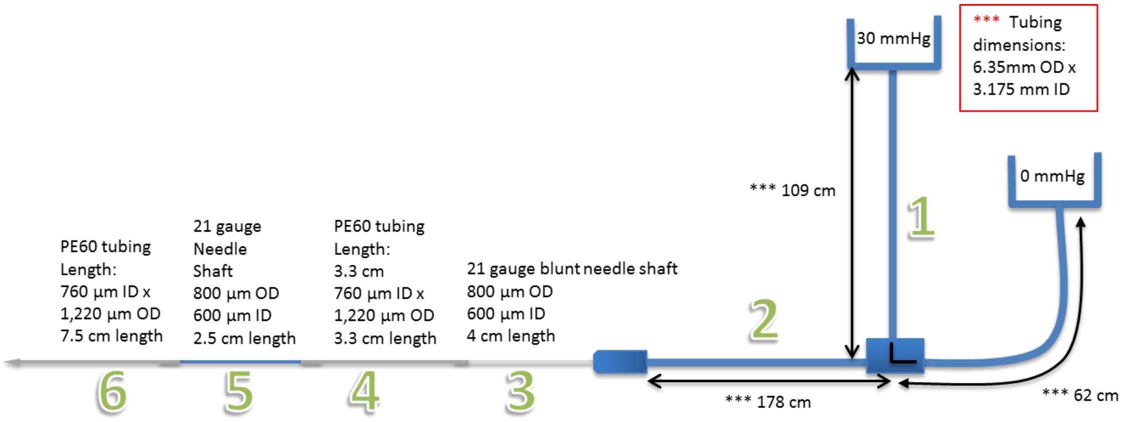

Figure A.8: Schematic diagram of tubing system upstream of cannula. All tubing segments are numbered and labeled with inner and outer diameters.

(2) Resistance of cannula: The dimensions of the cannula were measured on several 3D OCT images using Fiji software and are shown in **Figure A.9**. The cross-sections of the cannula were taken to be ellipses. Since both semi-major and semi-minor axes of the ellipses are functions of the distance from cannula tip, the resistance of cannula could be calculated by treating the flow as locally Poiseuille and integrating along the length of the cannula [18], as follows:

$$\boldsymbol{R_{cannula}} = \int_0^L \frac{4\mu\left(b^2(x)+c^2(x)\right)}{\pi b^3(x)c^3(x)}\,dx \qquad (11)$$

where *b(L)* and *c(L)* are the local semi-major and –minor axes of the ellipse; μ is the viscosity of saline; L is the length of the cannula and $R_{cannula}$ is the cannula resistance.

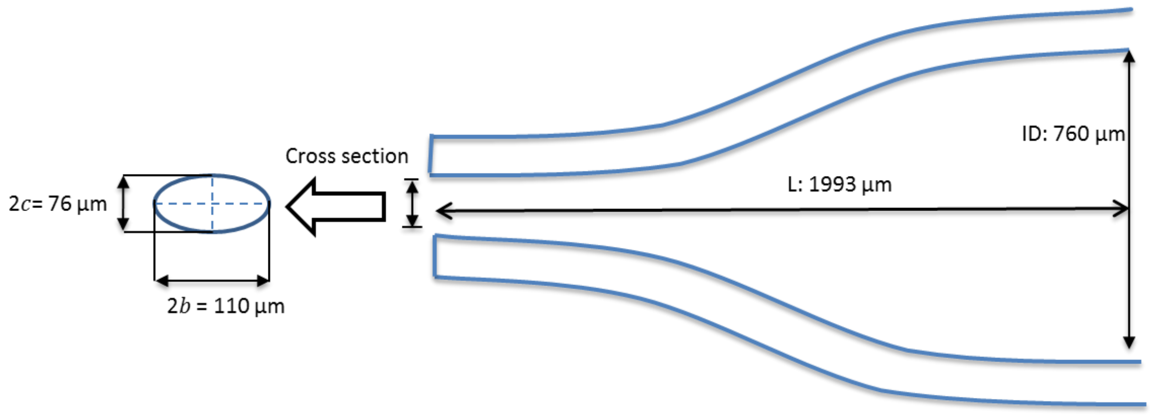

Figure A.9: Schematic view of the cannula. b: semi-major axis of ellipse; c: semi-minor axis of ellipse

(3) Resistance of SC: We assume the SC lumen to be a cylinder with elliptic cross section. The SC lumen resistance R_{SC} can be calculated as follows:

$$\boldsymbol{R_{SC}} = \frac{\boldsymbol{4\mu L_{SC}(b_{SC}^2+c_{SC}^2)}}{\boldsymbol{\pi b_{SC}^3 b_{SC}^3}} \tag{12}$$

where b_{SC} and c_{SC} are the semi-major and –minor axes of the elliptic SC cross section measured by ImageJ (Version 1.5, National Institutes of Health, Bethesda MD) from OCT scans; μ is the viscosity of saline; and L_{SC} is the length of SC. L_{SC} was approximated as 8 mm since each quadrant is one fourth of the anterior eye, which made it about 9 mm, and one millimeter was taken off for wastage from cutting and trimming, etc.

The distance from the tip of the cannula to the scan location was about 2 mm. Thus, the pressure at the scan location $\boldsymbol{P_{scan}}$ was equal to the pressure drop from scan location to the free end of the SC, which had a length of three fourths of the total SC length for this specific quadrant:

$$\boldsymbol{P_{scan} = \frac{3}{4} R_{SC} \times Q} \tag{13}$$

where Q is the flow rate along the SC (see equation 14). We assumed the pressure on the free end of SC (**Figure A.10**) was zero referenced to the bath pressure.

$$\boldsymbol{Q = \frac{P_{reservoir}}{R_{tubing}+R_{cannula}+R_{SC}}} \tag{14}$$

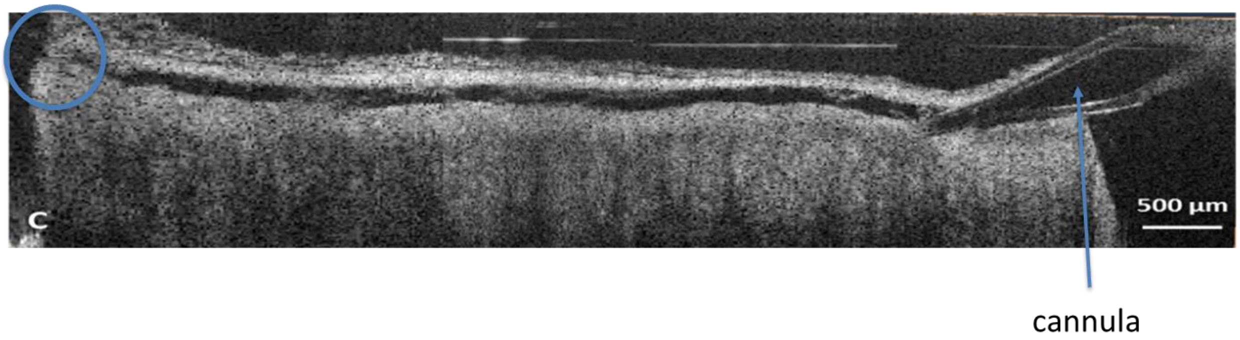

Figure A.10: Representative cross-sectional OCT image containing the entire SC lumen. Cannula was inserted into the right side of the SC. The region inside the blue circle shows apparent SC collapse, which was occasionally seen in some samples.

A.4.2 Results

For quadrant 77R-IN, the total tubing resistance $\boldsymbol{R_{tubing}}$ and cannula resistance were estimated to be 0.26 and 1.53 mmHg/(μL·s) (**Table A.2**). The resistance of SC was 107.42 mmHg/(μL·s).

Table A.2: Resistance of tubing segments

Tubing segment	Resistance (mmHg/μL·s)
1	0.0033
2	0.0054
3	0.0943
4	0.0302
5	0.0598
6	0.0687

P_{scan} values at different $P_{reservoir}$ values are summarized in **Table A.3**. The difference between P_{scan} and $P_{reservoir}$ is greater when $P_{reservoir}$ is higher.

Table A.3: Flow rate and pressure in the experimental system*

	$P_{reservoir}$ = 5 mmHg (undeformed)	$P_{reservoir}$ = 20 mmHg (deformed)
Q	0.05	0.18
P_{scan}	3.69	14.75

*Q: flow rate, unit: μL/s; P: pressure, unit: mmHg

A.5 Shear Stress Applied to the Endothelial Cells in the SC

It is important to note that the SC endothelial cells (SCE) cells may also play an important role in glaucoma. In vivo, these cells are subjected to a shear stress due to the flow of aqueous humor within SC. It has been suggested that the shear stresses acting on SCE could reach levels comparable to those in the arterial system and play a signaling role through nitric oxide release [165]. Thus, we asked what the shear stress acting on SCE was during our experiments, since there was a non-zero flow along the SC (Table A.3) during the OCT experiment. The following shows an example calculation using quadrant 77R-IN.

A.4.1 Methods

We used the same theoretical model previously developed by Ethier et al. [165]. Briefly, we used the same value for the viscosity of aqueous humor (0.75 cP), and used the following values specific to the 77R-IN quadrant:

- Anterior-posterior dimension of SC (2a) = 186 µm;
- Inner-outer wall separation of the SC, 2b, of 40 or 52 µm at reservoir pressures of 5 and 20 mmHg, respectively; and

- Total flow rate in SC of 3.0 or 10.8 µl/min at reservoir pressures of 5 and 20 mmHg, respectively (**Table A.3**).

We assumed that all the flow delivered by the cannula passed circumferentially within SC and exited the cut end of the canal, neglecting drainage from collector channels. Thus, the estimates given below are upper bounds.

A.4.2 Results

For quadrant 77R-IN, the circumferentially averaged shear stress was 10.0 dynes/cm^2 at a reservoir pressure of 5 mmHg and 21.4 dynes/cm^2 at 20 mmHg. These values were larger than those previous reported except at extreme canal collapse [165], due primarily to the large flow rate passing within SC. It is likely that these shear stress levels would trigger nitric oxide release [166], which could lead to a softening of the TM, depending on the viability of the resident cells.

APPENDIX B. SUPPLEMENTARY MATERIALS FOR CHAPTER 3 AND 4

B.1 Statistical Analysis

It is common in the literature to average values from two eyes of an animal to get a single "per animal" value. This avoids the statistical pitfall of treating the two eyes as independent. We chose not to follow this approach in the main body of the thesis, because such averaging can possibly obscure correlations, e.g. if the two eyes of an animal had very different values for measured outcomes and the two outcomes being correlated were related in a nonlinear manner.

For completeness, and to enable comparisons with existing data, we present here the statistical analysis and results following the "average two eyes to get a single value per animal" approach. All comparisons between groups were performed with the same statistical test (Wilcoxon rank-sum test) as used in the main body of the thesis, with the data for each mouse being taken as the mean values from the two eyes. The exceptions were as follows

- Mice in cohorts 1 and 2 from the DEX study had only one treated eye.
- Some mice had a valid facility measurement for only one of the eyes.

In both cases, only the data (facility, TM stiffness or IOP) from the treated or "successful" eye was used for that mouse.

B.2 Results

The main conclusions were unchanged when the data were analyzed in this way, except that correlation between outflow resistance and TM stiffness was significant only within the control group, but not within the DEX group.

B.2.1 Effect of Genetic Background on Facility and TM Stiffness

The facility of C57BL/6J (n=12) mice was slightly higher than that of CBA/J (n=10) mice (6.33 ± 2.28 vs. 5.97 ± 2.43 nl/min mmHg; p = 0.717, **Figure B.1**). The average TM stiffness in C57BL/6J (n=18) mice was less than in CBA/J mice (n=10), but this difference was not significantly different (2.10 ± 1.04 vs. 2.92 ± 2.33 nl/min mmHg; p=0.581, **Figure B.1**). Similarly, we observed a significant correlation between outflow resistance (1/C) and TM stiffness when pooling data from the two strains.

B.2.2 Effects of DEX treatment

IOP remained near the baseline level (day 0) in control mice (**Figure B.2**). On the day mice were sacrificed (day 20-40), IOP was 26.91±2.39 mmHg (mean ± SD) in DEX-treated mice and 20.51±3.03 mmHg in control mice (p<0.001, **Figure B.2, B.3**).

The mean facility of DEX mice was significantly lower than that of control mice (**Figure B.4**; DEX: 2.76 ± 0.88 nl/min mmHg; Control: 3.73 ± 1.06 nl/min mmHg; p= 0.032). The IOP measured before death tended to be negatively correlated with 1/C in the same eye (**Figure B.4**).

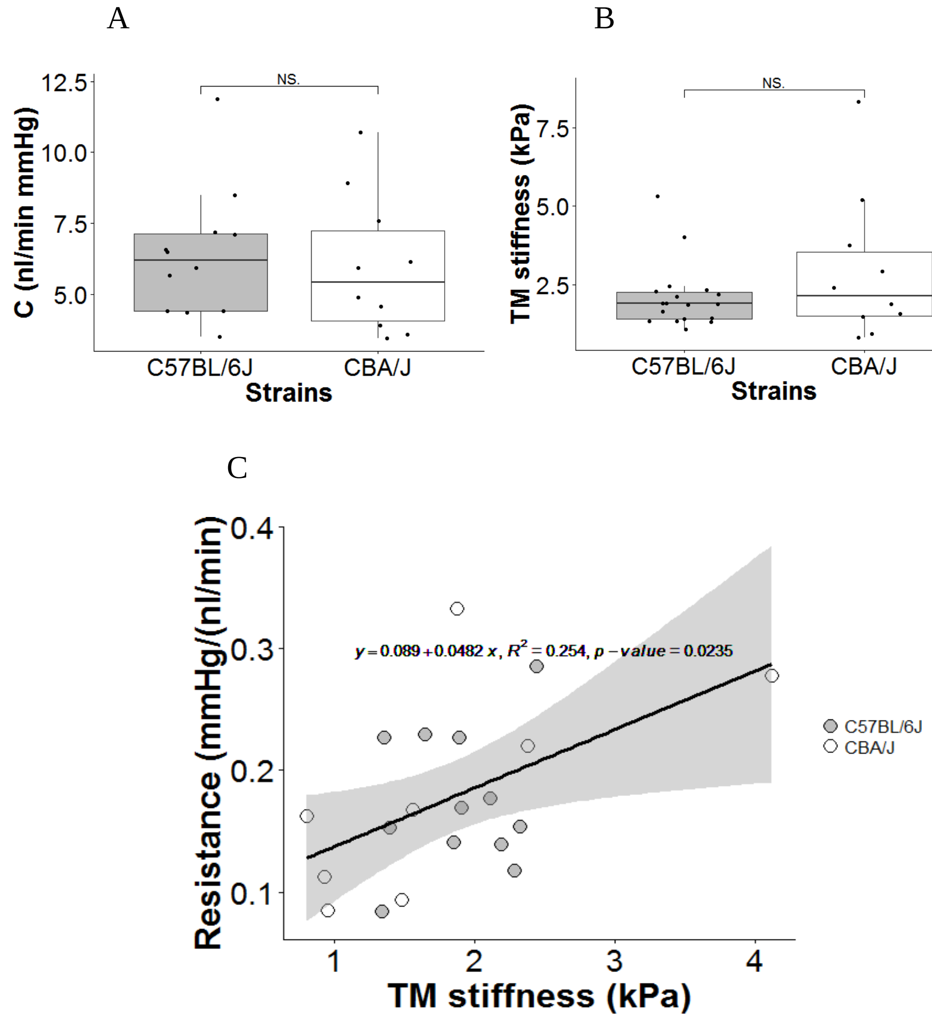

Figure B.1: (A) Outflow facility (C) and (B) TM stiffness for two mouse strains. For each box, the central line represents the median, and the edges of the box are the 25th and 75th percentiles, and whiskers extend to the most extreme data points not considered outliers. Each dot represents the average of two eyes per mouse. Number of eyes shown for facility plot are n=12 for C57BL/6J and n=10 for CBA/J. For stiffness plot, the respective values are n=18 and n=10. NS: Not Significant. (C) Cross-plot between outflow resistance (1/C) and TM stiffness, with each data point representing one mouse. The black solid line and equation represent the linear regression of the pooled data. The gray-shaded region shows 95% confidence bounds for the regression. For each mouse, data from both eyes was averaged, except in cases where the one of eyes yielded invalid facility data due to technical issues, in which case data from the one eye was used. Only mice where both outflow resistance and TM stiffness were measured were included. Number of data points: n=12 for C57BL/6J, n=8 for CBA/J.

The average TM stiffness in DEX-treated mice was about 27% higher than that in vehicle-treated mice, but this difference did not reach statistical significance (2.38±1.34

vs. 1.79±0.58 kPa; p=0.25; **Figure B.5**). Again, there was a positive correlation between resistance and TM stiffness for pooled data which reached statistical significance (p=0.017; $R^2 = 0.27$; **Figure B.5**). Further, the same correlation was also statistically significant within control group, but not in DEX group (DEX group: R^2=0.258, p=0.1106; Control group: R^2=0.40, p=0.0499, **Figure B.6**).

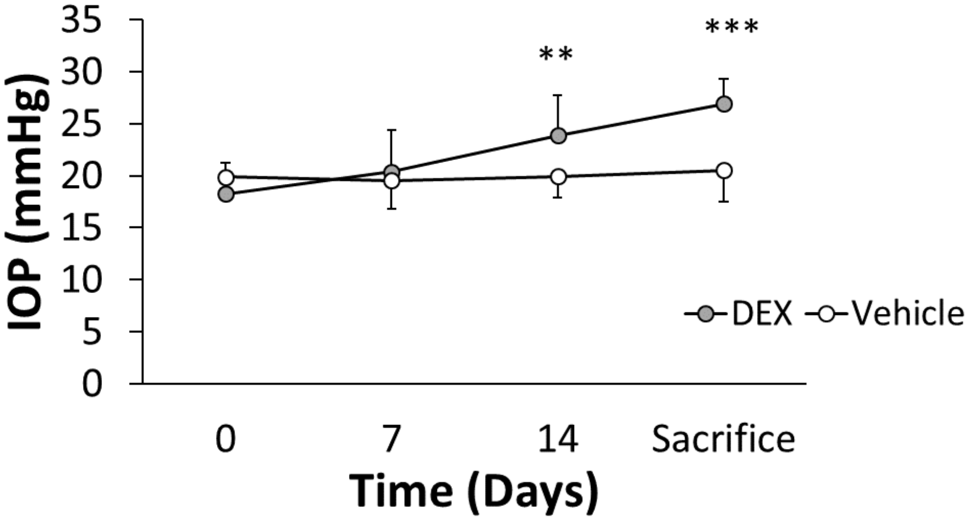

Figure B.2: IOP as a function of time for DEX-treated (grey) and control (white) mice averaged over five cohorts. For cohort 1 and 2, DEX or vehicle were injected on day 0 and 14. For cohort 3-5, injections were performed on day 0, 7 and 14. All IOPs were measured immediately before injections. Bars are standard deviation. **p<0.01, ***p<0.001. p-values were Benjamini-Hochberg corrected. For each mouse, the average IOP from both eyes was used. At day 0, 7 and 14, n=25 DEX-treated mice and n=16 vehicle-treated mice. At the day of sacrifice (day 20-40 depending on cohort), n=24 DEX-treated mice and n=15 vehicle-treated mice. Two mice were injured during fighting and were euthanized at day 14.

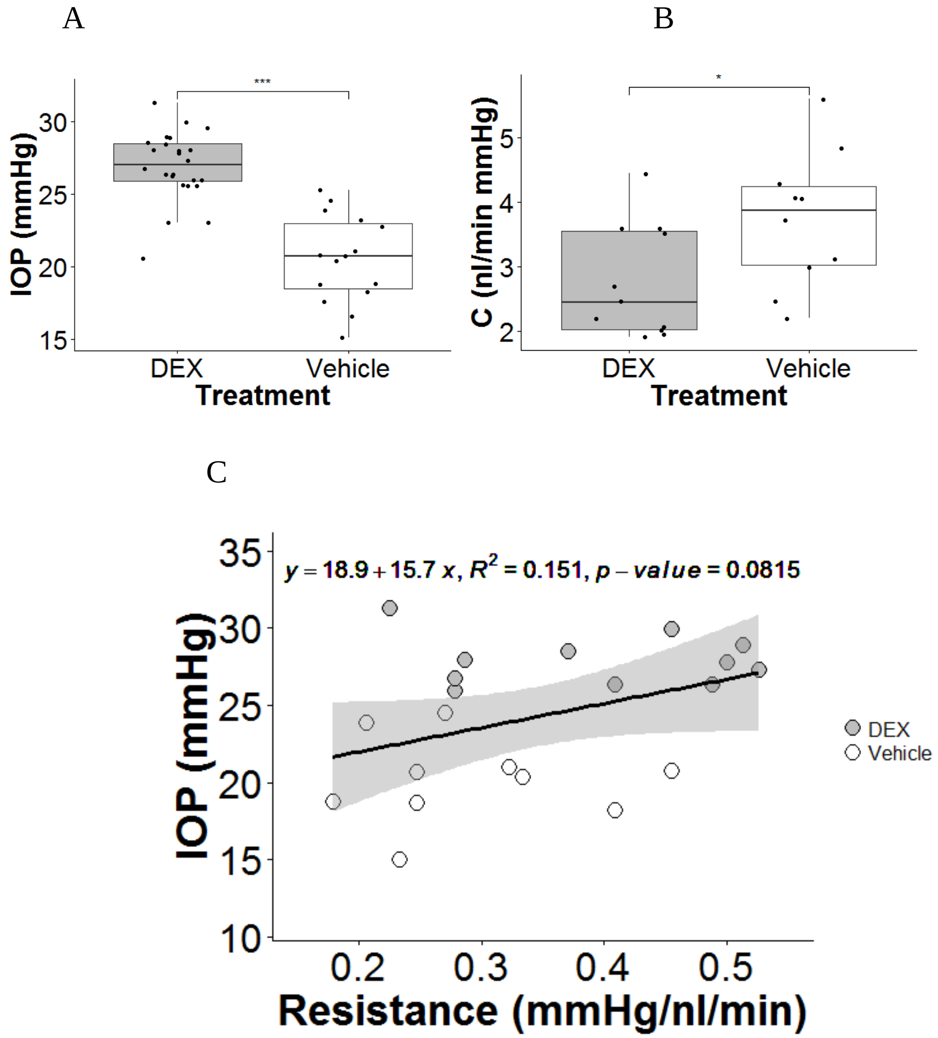

Figure B.3: DEX treatment affected IOP and outflow facility. (A) Boxplot of IOP for DEX-treated (n=24) and vehicle-treated mice (n=15). (B) Boxplot of outflow facility (C) for DEX-treated (n=11) and vehicle-treated mice (n=10). For each box, the central mark is the median, the edges of the box are the 25th and 75th percentiles, and whiskers extend to the most extreme data points not considered outliers. Each dot represents the data from one eye. (C) IOP measured on the day mice were sacrificed plotted as a function of outflow resistance (1/C) for DEX-treated (grey dots, n=11) and vehicle-treated (white dots, n=10) mice. The black solid line is the best fit using linear least squares regression. The gray-shaded region shows 95% confidence bounds for the regression. *p-value<0.05; ***p-value<0.001. NS.: Not Significant. Data in panels B and C are from cohort 3-5.

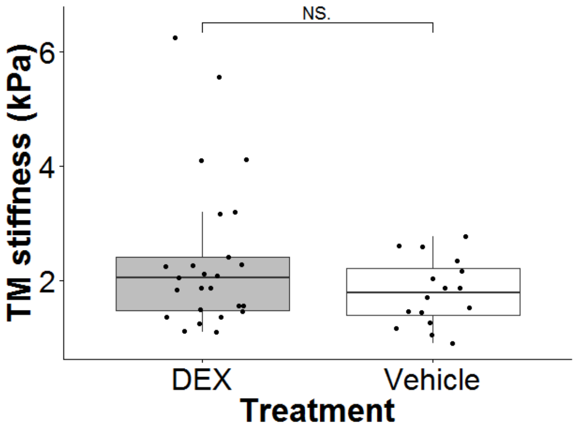

Figure B.4: Boxplot of TM stiffness for DEX-treated (n=25) and vehicle-treated mice (n=16). For each box, the central mark is the median, the edges of the box are the 25th and 75th percentiles, and whiskers extend to the most extreme data points not considered outliers. Each dot represents the data from one eye. NS: Not Significant.

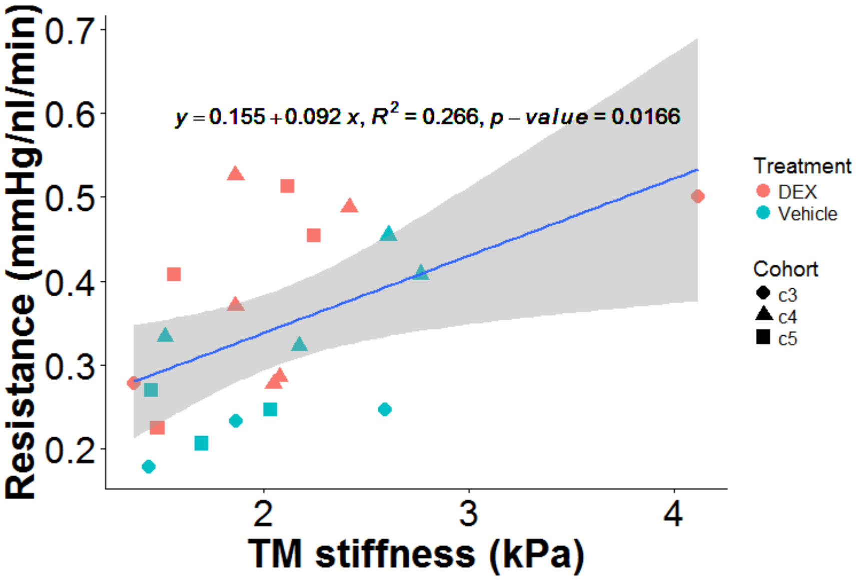

Figure B.5: Cross-plot between outflow resistance (1/C) and TM stiffness for DEX-treated (n=11) and vehicle-treated mice (n=10). The blue line and equation represent the linear regression of the pooled data. The gray-shaded region shows 95% confidence bounds for the regression. Different shapes represent different cohorts.

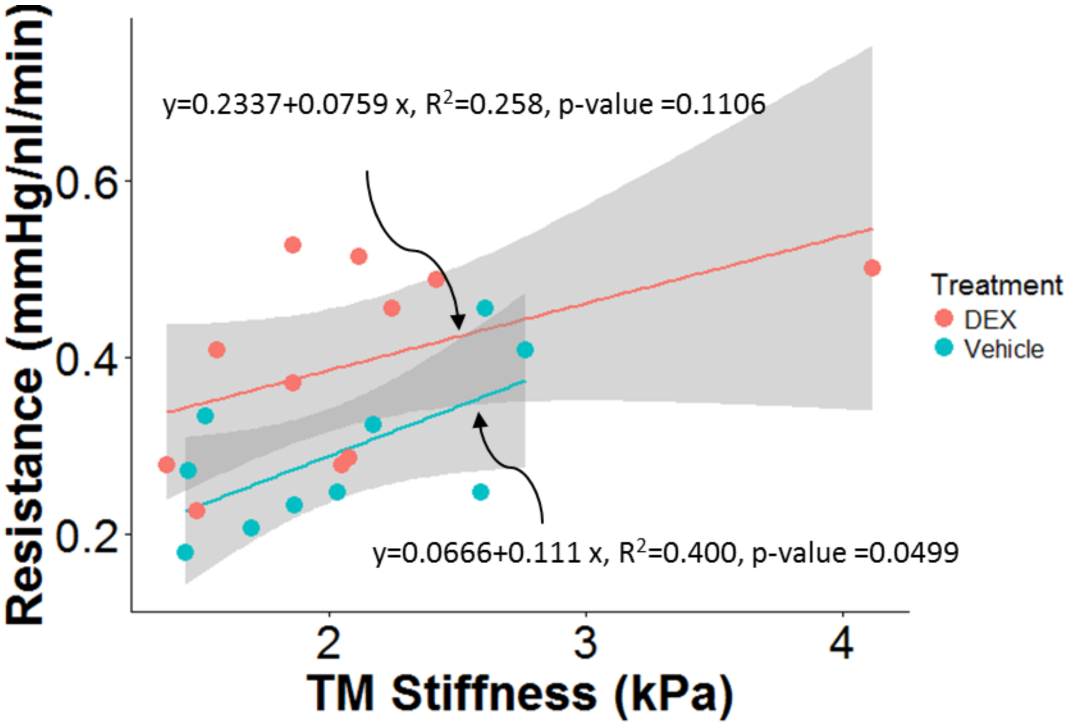

Figure B.6: Cross-plot between outflow resistance (1/C) and TM stiffness within each group of mice, with DEX mice shown in red (n=11) and control mice shown in green (n=10). The gray-shaded regions show 95% confidence bounds for the regressions.

APPENDIX C. UNSUCCESFUL TM STIFFNESS MEASUREMENT APPROACHES

The techniques used to measure TM stiffness in this thesis were arrived at after several unsuccessful alternative approaches were tried. For completeness, these methods and their results are described here. We specifically explored two unsuccessful approaches to try to measure TM stiffness in mice. The first used whole tissue wedges, where the AFM tip approached the TM in an en face orientation. The second used sagittal cryosectioning of outflow tissues, similar to the approach described in the main body of the thesis, except that the TM was localized by using fluorescent tracers. This chapter based in part on the author's PhD thesis proposal.

C.1 Methods

C.1.1 AFM Measurement using en face Wedges

Mouse eyes were dissected using microscissors by making a circumferential cut in the posterior sclera centered on the optic nerve. The lens was expelled and the iris removed by traction. The anterior eye was divided into four quadrants, and the choroid and remaining vitreous were removed by gently scraping the sclera with forceps or a swab. One of the quadrants was attached to a Plus gold slide (Electron Microscopy Sciences, Hatfield, PA), oriented so that the inner (uveal) TM faced upwards (**Figure C.1**). No glue was needed since the sample was secured by the permanent positive charges on the slide surface. AFM measurements were performed at room temperature within 24 hours of enucleation. A series of forcemaps were obtained in regions located along a line starting on the cornea and ending on the pigmented region, representing the sclera. The starting location for this line was determined visually, and thus it was impossible to ensure that the starting points were identical between samples. Each forcemap region consisted of 4 × 4 force curves over a lateral scan size of 10 µm x 10 µm. The center-to-center distance between adjacent forecemap regions was 10 µm. Each force curve was taken at a rate of 8 µm/s. The average modulus from the valid measurements points within a forcemap region was taken as the compressive modulus of that region. These moduli from all forcemap regions in one sample were then plotted as a function of region location along the measurement line (cornea to sclera). The anterior border of the TM was putatively defined as the anterior-most location that: (i) was adjacent to a modulus peak, and (ii) had a compressive modulus less than 10 kPa. Moving posteriorly, the first location which had modulus larger than 10 kPa was treated as the posterior border of the TM.

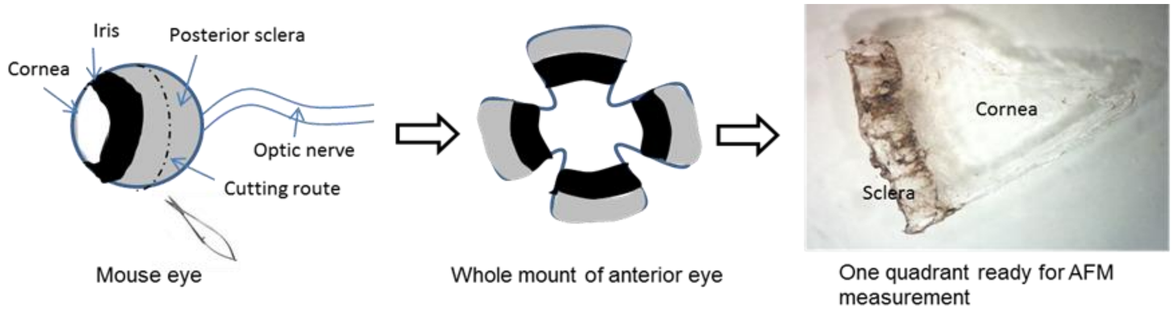

Figure C.1: Schematic view of the sample preparation procedure for AFM on en face anterior wedges.

To investigate whether the TM was well-preserved or damaged after preparation, since the TM could not be observed from the bottom camera on the AFM, we performed two types of post-measurement check: conventional histology, and scanning electron microscopy (SEM). For conventional histology, anterior wedges of the eye were immersion fixed in 4% paraformaldehyde and embedded in epoxy resin using standard protocols. Semi-thin plastic sections were cut and stained with toluidine blue. For SEM, tissue was fixed in Universal Fixative, incubated in Ta/Gu-HCL solution, rinsed thoroughly in PBS and post fixed in 1% osmium tetroxide in PBS for 1 hour. Tissue was dehydrated in an ethanol series (25%-100%), incubated in Hexamethyldislazane for 20 minutes, air dried in a fume hood and sputter coated with gold-palladium. The samples were then examined with a Hitachi SU8230 SEM. All SEM was done by Dr. A. Thomas Read in our lab and conventional histology was done by M.D. Guorong at Duke University.

C.1.2 AFM Measurement using Cryosections

Cryosectioning procedures were done in the same way as described in Chapter 3. To assist with TM localization, we perfused fluorescent microbead tracer into the eye to highlight the outflow pathway. Briefly, after facility measurement, eyes were perfused a second time with a solution containing fluorescent microbeads and cryoprotectant at 8 mmHg for 45 minutes. For perfusate preparation, 20 µL of fluorescent microbead tracer (carboxylate-modified 20 nm microspheres, 2% mass concentration, Life Technologies, Carlsbad, CA) was diluted (1:400) in 15% glycerol. 45 minutes was found to be the optimal perfusion time for tracer to strongly penetrate the TM and SC [15]. During AFM measurement, fluorescent areas at the limbal region were first identified under the fluorescent microscope attached to the AFM. Single force measurements were then performed in those areas.

C.2 Results

C.2.1 AFM Measurement of en face Wedges

The compressive modulus profiles of the samples tested showed several broadly similar features (**Figure C.2, C.3**). Specifically, tissue was stiff in the cornea and softened gradually as the measurement location moved posteriorly. Most eyes then showed a local peak in stiffness between the corneal region and a region with softer modulus. However, towards the posterior end of the measurement zone, the modulus increased again and showed large variations. Based on the criteria listed above, a putative TM location was identified in each sample (red brackets; **Figure C.3**); however, the anterior-posterior extent of the TM varied significantly from eye to eye. The compressive modulus of C57BL/6J mouse TM, as identified, ranged from 1.23 to 5.42 kPa (mean, 3.91 ± 1.73 kPa). In addition, the TM stiffness was positively correlated to the tissue freshness which was indicated by hours from enucleation to measurement ($R^2 = 0.78$, $p=0.019$), indicating that tissue freshness needs to be consistent when measuring the stiffness.

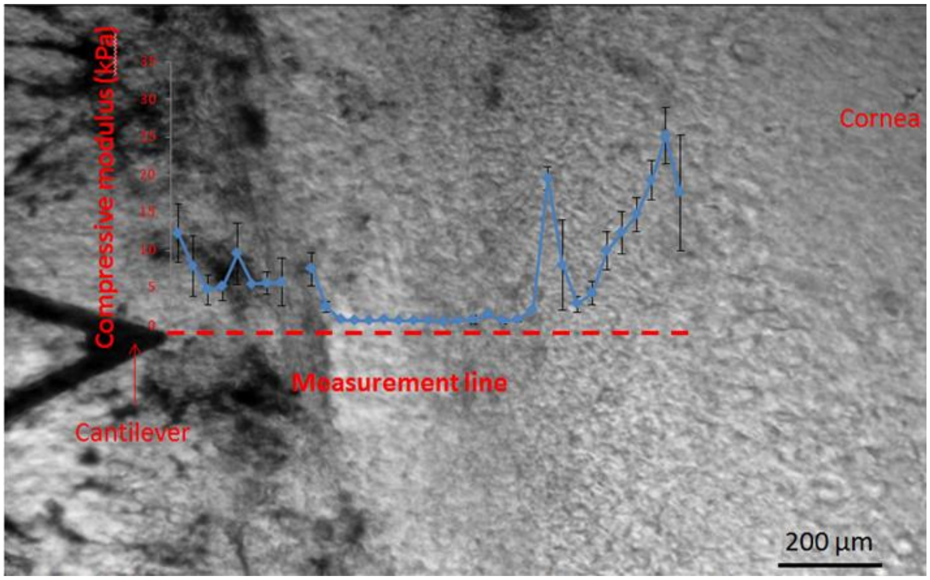

Figure C.2: A representative view of sample (sample 4 in Figure C.3) and cantilever from the bottom camera on the AFM. Measurements started in the cornea on the right side (labeled), along the measurement line (red dashed line) and towards to the pigmented region. The measured compressive modulus of each location along the measurement line is indicated in blue dots. Error bar: standard deviation.

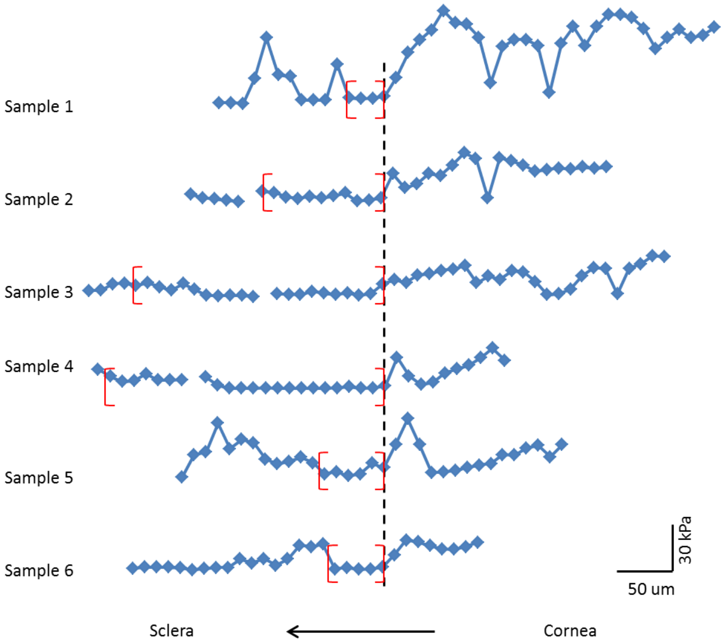

Figure C.3: Compressive modulus values measured in mouse TM by AFM. Measurements were made from right to left (cornea to sclera) as described in the text. All curves have been aligned at the putative anterior border of TM (dashed line). The regions inside red brackets are considered as the TM region.

As observed, stiffness varied significantly as a function of measurement position, which was expected based on known mechanical properties of the relevant tissues in other species, e.g. cornea is stiffer than TM in human eyes [167, 168]. We also observed stiffness peaks between stiff and soft regions. At the putative anterior edge of the TM, this peak may have been due to a transition zone between corneal endothelium and TM, known to exist in both human and bovine eyes [169]. Although the exact composition of this zone remained unknown, it was very likely the place where Descemet's membrane terminates. Given the fact that Descemet's membrane was stiffer than corneal endothelium in rabbits [170], we speculated that, in the mouse eye, there was a similar (stiffer) transition zone, which may account for the modulus peak at the putative anterior edge of the TM.

The large variation in modulus for regions on the posterior side of the curves may be due to residual iris root, ciliary body and/or choroid in the preparation. A modulus threshold of 10 kPa was chosen to help identify the TM, since 10 kPa was the maximum elastic modulus of normal human TM. However, it must be noted that the data reported on human TM was obtained from the Schlemm's canal side of TM, while in this study indentations were taken on the inner (uveal) side of the TM. Further, the anterior-posterior extents of the TM measured in this study were highly variable, which was unexpected. This suggests that this method of defining the anterior and posterior boundaries of the TM was insufficient and must be improved.

Histological images (**Figure C.4**) showed that TM integrity varied significantly from sample to sample. This may partially explain the significant variation in anterior-posterior extent of the TM in **Figure C.3**.

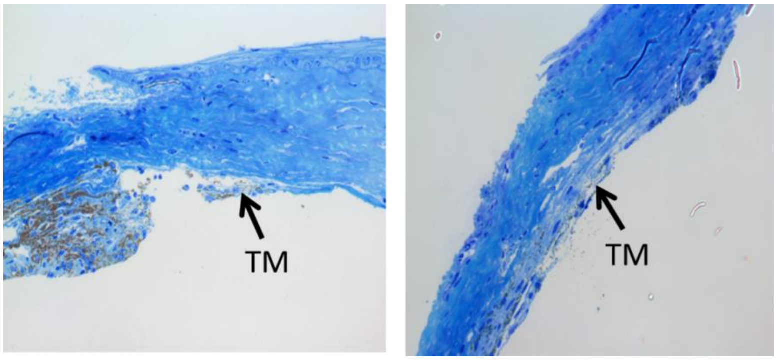

Figure C.4: Histological images of damaged (left) and intact (right) TM. Source: Guorong Li, M.D.

SEM images (**Figure C.5**) revealed a transition band between the cornea and CB/Iris. However, the putative TM region was not seen to be porous, as the TM is expected to be, and appeared possibly more similar to tendons or muscles of the CB. Thus, it seemed possible that the TM may have been located underneath this transition region and was not exposed to the AFM cantilever during measurement.

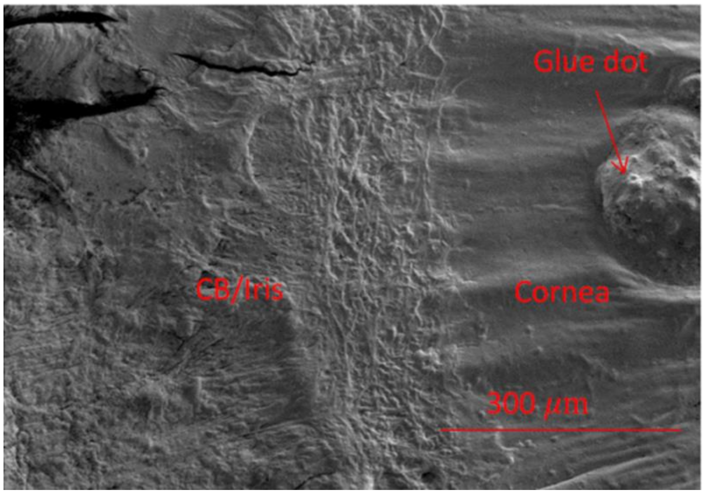

Figure C.5: Representative SEM image of one quadrant with inner (uveal) TM facing upward. Cornea and CB/iris are labeled. A glue dot was placed as a mark to indicate the starting point of the force curve measurements.

C.2.2 AFM Measurement on Cryosections

Figure C.6 shows a representative cryosection (mouse strain: C57BL/6J) observed from the fluorescent microscope of the AFM. A high concentration of fluorescent tracer was present around SC and mostly distributed near the outer wall of SC, possibly due to tracer diffusion. AFM measurements were performed on several tissue locations where high concentration of microbeads were present (marked with numbers).

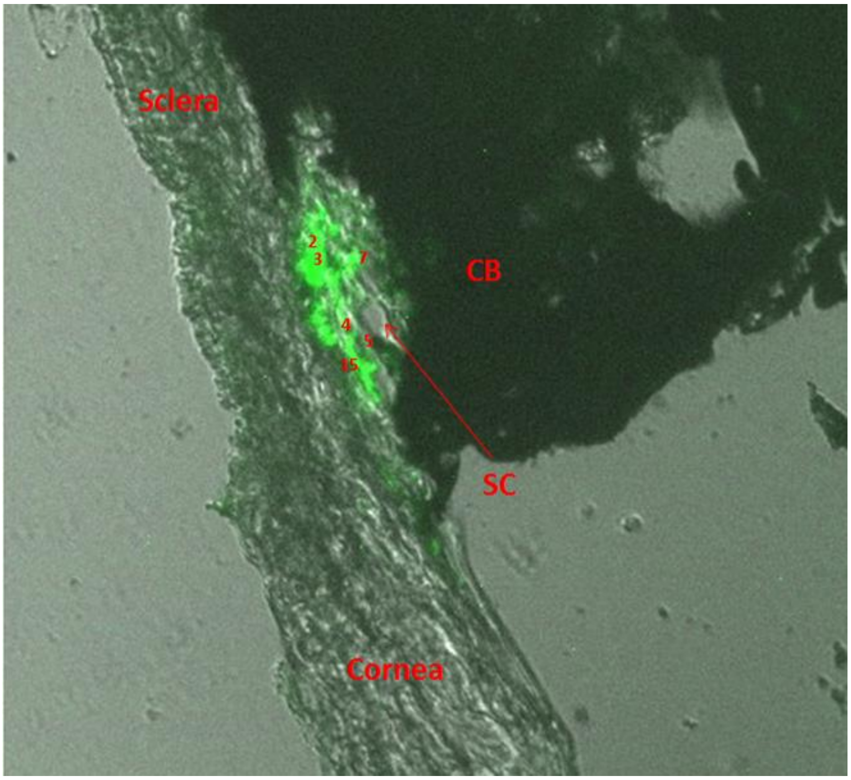

Figure C.6: Anterior angle in a representative cryosection (mouse strain: C57BL/6J) under the fluorescent microscope after microbead perfusion. Fluorescent microbead tracer appears green. TM, Trabecular Meshwork; CB, Ciliary Body; SC, Schlemm's canal. Small numbers are AFM measurement locations.

C.3 Summary

Overall, identification of the TM was very uncertain using the en face approach. Post-measurement checks (histology) using this approach indicated that TM integrity was not be guaranteed and that the TM might not even have been exposed to the cantilever during AFM measurements.

In the microbead-based approach, despite a relatively concentrated fluorescent signal at the iridocorneal angle, little tracer appeared between the inner wall of SC and the CB, where the TM most likely was located. The deviation between the actual TM location and the region of tracer accumulation may have been caused by tracer diffusion during sample preparation and measurement. Further, the effect of microbeads themselves on measured TM stiffness was uncertain. Therefore, we decided to abandon these two methods and use the open SC lumen-based method on cryosections for subsequent TM stiffness measurements, as described in detail in Chapter 3.

REFERENCES

1. Goel, M., R.G. Picciani, R.K. Lee, et al., *Aqueous humor dynamics: a review*. Open Ophthalmol J, 2010. **4**: p. 52-9.

2. Maepea, O. and A. Bill, *Pressures in the juxtacanalicular tissue and Schlemm's canal in monkeys.* Exp Eye Res, 1992. **54**(6): p. 879-83.

3. Overby, D.R., W.D. Stamer, and M. Johnson, *The changing paradigm of outflow resistance generation: Towards synergistic models of the JCT and inner wall endothelium.* Experimental Eye Research, 2009. **88**(4): p. 656-670.

4. Stamer, W.D. and T.S. Acott, *Current understanding of conventional outflow dysfunction in glaucoma.* Curr Opin Ophthalmol, 2012. **23**(2): p. 135-43.

5. Veleri, S., C.H. Lazar, B. Chang, et al., *Biology and therapy of inherited retinal degenerative disease: insights from mouse models.* Dis Model Mech, 2015. **8**(2): p. 109-29.

6. Llobet, A., X. Gasull, and A. Gual, *Understanding trabecular meshwork physiology: a key to the control of intraocular pressure?* News Physiol Sci, 2003. **18**: p. 205-9.

7. Overby, D.R., J. Bertrand, M. Schicht, et al., *The structure of the trabecular meshwork, its connections to the ciliary muscle, and the effect of pilocarpine on outflow facility in mice.* Invest Ophthalmol Vis Sci, 2014. **55**(6): p. 3727-36.

8. *Systematic Evaluation of the Mouse Eye: Anatomy, Pathology, and Biomethods*. 2002: CRC Press LLC.

9. Gong, H.Y., R.C. Tripathi, and B.J. Tripathi, *Morphology of the aqueous outflow pathway.* Microscopy Research and Technique, 1996. **33**(4): p. 336-367.

10. Lei, Y., D.R. Overby, A. Boussommier-Calleja, et al., *Outflow physiology of the mouse eye: pressure dependence and washout.* Invest Ophthalmol Vis Sci, 2011. **52**(3): p. 1865-71.

11. Boussommier-Calleja, A., J. Bertrand, D.F. Woodward, et al., *Pharmacologic manipulation of conventional outflow facility in ex vivo mouse eyes.* Invest Ophthalmol Vis Sci, 2012. **53**(9): p. 5838-45.

12. Stamer, W.D., A.T. Read, G.M. Sumida, et al., *Sphingosine-1-phosphate effects on the inner wall of Schlemm's canal and outflow facility in perfused human eyes.* Exp Eye Res, 2009. **89**(6): p. 980-8.

13. Millard, L.H., D.F. Woodward, and W.D. Stamer, *The role of the prostaglandin EP4 receptor in the regulation of human outflow facility*. Invest Ophthalmol Vis Sci, 2011. **52**(6): p. 3506-13.

14. Grant, W.M., *Clinical measurements of aqueous outflow*. Am J Ophthalmol, 1951. **34**(11): p. 1603-5.

15. Weinreb, R.N., T. Aung, and F.A. Medeiros, *The pathophysiology and treatment of glaucoma: a review*. JAMA, 2014. **311**(18): p. 1901-11.

16. Johnson, M., *'What controls aqueous humour outflow resistance?'*. Experimental Eye Research, 2006. **82**(4): p. 545-557.

17. Abu-Hassan, D.W., T.S. Acott, and M.J. Kelley, *The Trabecular Meshwork: A Basic Review of Form and Function*. J Ocul Biol, 2014. **2**(1).

18. Acott, T.S. and M.J. Kelley, *Extracellular matrix in the trabecular meshwork*. Exp Eye Res, 2008. **86**(4): p. 543-61.

19. Fuchshofer, R., U. Welge-Lussen, E. Lutjen-Drecoll, et al., *Biochemical and morphological analysis of basement membrane component expression in corneoscleral and cribriform human trabecular meshwork cells*. Invest Ophthalmol Vis Sci, 2006. **47**(3): p. 794-801.

20. Yue, B.Y., *The extracellular matrix and its modulation in the trabecular meshwork*. Surv Ophthalmol, 1996. **40**(5): p. 379-90.

21. Vittal, V., A. Rose, K.E. Gregory, et al., *Changes in gene expression by trabecular meshwork cells in response to mechanical stretching*. Invest Ophthalmol Vis Sci, 2005. **46**(8): p. 2857-68.

22. Marshall, G.E., A.G. Konstas, and W.R. Lee, *Immunogold localization of type IV collagen and laminin in the aging human outflow system*. Exp Eye Res, 1990. **51**(6): p. 691-9.

23. Malihi, M., J.W. McLaren, and A.J. Sit, *Effect of topical anesthesia on episcleral venous pressure in normal human subjects*. Invest Ophthalmol Vis Sci, 2015. **56**(5): p. 2968-70.

24. Toris, C.B., M.E. Yablonski, Y.L. Wang, et al., *Aqueous humor dynamics in the aging human eye*. Am J Ophthalmol, 1999. **127**(4): p. 407-12.

25. Brubaker, R.F., *Flow of aqueous humor in humans [The Friedenwald Lecture]*. Invest Ophthalmol Vis Sci, 1991. **32**(13): p. 3145-66.

26. Allingham, R.R., A.W. de Kater, and C.R. Ethier, *Schlemm's canal and primary open angle glaucoma: correlation between Schlemm's canal dimensions and outflow facility*. Exp Eye Res, 1996. **62**(1): p. 101-9.

27. Kupfer, C. and K. Ross, *The development of outflow facility in human eyes.* Invest Ophthalmol, 1971. **10**(7): p. 513-7.

28. Johnson, M., J.W. McLaren, and D.R. Overby, *Unconventional aqueous humor outflow: A review.* Exp Eye Res, 2017. **158**: p. 94-111.

29. Chen, J., S.A. Runyan, and M.R. Robinson, *Novel ocular antihypertensive compounds in clinical trials.* Clin Ophthalmol, 2011. **5**: p. 667-77.

30. Last, J.A., T. Pan, Y. Ding, et al., *Elastic modulus determination of normal and glaucomatous human trabecular meshwork.* Invest Ophthalmol Vis Sci, 2011. **52**(5): p. 2147-52.

31. Humphrey, J.D. and F.C. Yin, *A new constitutive formulation for characterizing the mechanical behavior of soft tissues.* Biophys J, 1987. **52**(4): p. 563-70.

32. Fung, Y.C., *Biomechanics*. Mechanical Properties of Living Tissues. 1993.

33. Russell, P., J.Z. Gasiorowski, P.F. Nealy, et al., *Response of human trabecular meshwork cells to topographic cues on the nanoscale level.* Invest Ophthalmol Vis Sci, 2008. **49**(2): p. 629-35.

34. Discher, D.E., P. Janmey, and Y.L. Wang, *Tissue cells feel and respond to the stiffness of their substrate.* Science, 2005. **310**(5751): p. 1139-43.

35. Engler, A., L. Bacakova, C. Newman, et al., *Substrate compliance versus ligand density in cell on gel responses.* Biophys J, 2004. **86**(1 Pt 1): p. 617-28.

36. Georges, P.C. and P.A. Janmey, *Cell type-specific response to growth on soft materials.* J Appl Physiol (1985), 2005. **98**(4): p. 1547-53.

37. Solon, J., I. Levental, K. Sengupta, et al., *Fibroblast adaptation and stiffness matching to soft elastic substrates.* Biophys J, 2007. **93**(12): p. 4453-61.

38. West, A.R., S. Connolly, J.D. Mih, et al., *Increased Extracellular Matrix Stiffness Enhances Airway Smooth Muscle Contractile Phenotype And Contractile Function.* American Journal of Respiratory and Critical Care Medicine, 2011. **183**.

39. Schlunck, G., H. Han, T. Wecker, et al., *Substrate rigidity modulates cell matrix interactions and protein expression in human trabecular meshwork cells.* Invest Ophthalmol Vis Sci, 2008. **49**(1): p. 262-9.

40. Thomasy, S.M., J.T. Morgan, J.A. Wood, et al., *Substratum stiffness and latrunculin B modulate the gene expression of the mechanotransducers YAP and TAZ in human trabecular meshwork cells.* Exp Eye Res, 2013. **113**: p. 66-73.

41. Tovar-Vidales, T., R. Roque, A.F. Clark, et al., *Tissue transglutaminase expression and activity in normal and glaucomatous human trabecular meshwork cells and tissues.* Invest Ophthalmol Vis Sci, 2008. **49**(2): p. 622-8.

42. Fuchshofer, R. and E.R. Tamm, *The role of TGF-beta in the pathogenesis of primary open-angle glaucoma.* Cell Tissue Res, 2012. **347**(1): p. 279-90.

43. Hoare, M.J., I. Grierson, D. Brotchie, et al., *Cross-linked actin networks (CLANs) in the trabecular meshwork of the normal and glaucomatous human eye in situ.* Invest Ophthalmol Vis Sci, 2009. **50**(3): p. 1255-63.

44. Lepple-Wienhues, A., F. Stahl, and M. Wiederholt, *Differential smooth muscle-like contractile properties of trabecular meshwork and ciliary muscle.* Exp Eye Res, 1991. **53**(1): p. 33-8.

45. Wiederholt, M., H. Thieme, and F. Stumpff, *The regulation of trabecular meshwork and ciliary muscle contractility.* Prog Retin Eye Res, 2000. **19**(3): p. 271-95.

46. Vargas-Pinto, R., H. Gong, A. Vahabikashi, et al., *The effect of the endothelial cell cortex on atomic force microscopy measurements.* Biophys J, 2013. **105**(2): p. 300-9.

47. Boudou, T., J. Ohayon, C. Picart, et al., *An extended relationship for the characterization of Young's modulus and Poisson's ratio of tunable polyacrylamide gels (vol 43, pg 721, 2006).* Biorheology, 2007. **44**(2): p. 139-139.

48. Kim, B., S.B. Lee, J. Lee, et al., *A Comparison Among Neo-Hookean Model, Mooney-Rivlin Model, and Ogden Model for Chloroprene Rubber.* International Journal of Precision Engineering and Manufacturing, 2012. **13**(5): p. 759-764.

49. Daneshvar, R. and N. Amini, *Rho-Associated Kinase Inhibitors: Potential Future Treatments for Glaucoma.* J Ophthalmic Vis Res, 2014. **9**(3): p. 395-8.

50. Nilsson, S.F., E. Drecoll, E. Lutjen-Drecoll, et al., *The prostanoid EP2 receptor agonist butaprost increases uveoscleral outflow in the cynomolgus monkey.* Invest Ophthalmol Vis Sci, 2006. **47**(9): p. 4042-9.

51. Lutjen-Drecoll, E. and P.L. Kaufman, *Long-term timolol and epinephrine in monkeys. II. Morphological alterations in trabecular meshwork and ciliary muscle.* Trans Ophthalmol Soc U K, 1986. **105 (Pt 2)**: p. 196-207.

52. Camras, L.J., W.D. Stamer, D. Epstein, et al., *Differential effects of trabecular meshwork stiffness on outflow facility in normal human and porcine eyes.* Invest Ophthalmol Vis Sci, 2012. **53**(9): p. 5242-50.

53. Camras, L.J., W.D. Stamer, D. Epstein, et al., *Circumferential tensile stiffness of glaucomatous trabecular meshwork.* Invest Ophthalmol Vis Sci, 2014. **55**(2): p. 814-23.

54. Chang, J., J. Huang, L. Li, et al., *Stiffness characterization of anisotropic trabecular meshwork.* J Biomech, 2017. **61**: p. 144-150.

55. Overby, D.R., E.H.H. Zhou, R. Vargas-Pinto, et al., *Altered mechanobiology of Schlemm's canal endothelial cells in glaucoma.* Proceedings of the National Academy of Sciences of the United States of America, 2014. **111**(38): p. 13876-13881.

56. Byfield, F.J., Q. Wen, I. Levental, et al., *Absence of filamin A prevents cells from responding to stiffness gradients on gels coated with collagen but not fibronectin.* Biophys J, 2009. **96**(12): p. 5095-102.

57. Raghunathan, V., J.S. Eaton, B.J. Christian, et al., *Biomechanical, ultrastructural, and electrophysiological characterization of the non-human primate experimental glaucoma model.* Sci Rep, 2017. **7**(1): p. 14329.

58. Yuan, F., L.J. Camras, and P. Gonzalez, *Trabecular Meshwork Stiffness in Ex Vivo Perfused Porcine Eyes.* Investigative Ophthalmology & Visual Science, 2011. **52**(14).

59. Camras LJ, S.W., Epstein D, Gonzalez P, Yuan F, *Erratum in: Differential effects of trabecular meshwork stiffness on outflow facility in normal human and porcine eyes.* Invest Ophthalmol Vis Sci, 2014. **55**(4).

60. Raghunathan, V.K., J.T. Morgan, S.A. Park, et al., *Dexamethasone Stiffens Trabecular Meshwork, Trabecular Meshwork Cells, and Matrix.* Invest Ophthalmol Vis Sci, 2015. **56**(8): p. 4447-59.

61. Whitlock, N.A., B. McKnight, K.N. Corcoran, et al., *Increased intraocular pressure in mice treated with dexamethasone.* Invest Ophthalmol Vis Sci, 2010. **51**(12): p. 6496-503.

62. Weinreb, R.N., J.R. Polansky, S.G. Kramer, et al., *Acute effects of dexamethasone on intraocular pressure in glaucoma.* Invest Ophthalmol Vis Sci, 1985. **26**(2): p. 170-5.

63. Huang, J., L.J. Camras, and F. Yuan, *Mechanical analysis of rat trabecular meshwork.* Soft Matter, 2015. **11**(14): p. 2857-65.

64. Li, G., S. Farsiu, J. Qiu, et al., *Disease progression in iridocorneal angle tissues of BMP2-induced ocular hypertensive mice with optical coherence tomography.* Mol Vis, 2014. **20**: p. 1695-709.

65. Johnson, M., J.S. Schuman, and L. Kagemann, *Trabecular Meshwork Stiffness in the Living Human Eye.* Investigative Ophthalmology & Visual Science, 2015. **56**(7).

66. Pattabiraman, P.P., R. Maddala, and P.V. Rao, *Regulation of plasticity and fibrogenic activity of trabecular meshwork cells by Rho GTPase signaling.* J Cell Physiol, 2014. **229**(7): p. 927-42.

67. Chudgar, S.M., P. Deng, R. Maddala, et al., *Regulation of connective tissue growth factor expression in the aqueous humor outflow pathway.* Mol Vis, 2006. **12**: p. 1117-26.

68. Rao, P.V., *Bioactive Lysophospholipids: Role in Regulation of Aqueous Humor Outflow and Intraocular Pressure in the Context of Pathobiology and Therapy of Glaucoma.* Journal of Ocular Pharmacology and Therapeutics, 2014. **30**(2-3): p. 181-190.

69. Zhou, E.H., R. Krishnan, W.D. Stamer, et al., *Mechanical responsiveness of the endothelial cell of Schlemm's canal: scope, variability and its potential role in controlling aqueous humour outflow.* J R Soc Interface, 2012. **9**(71): p. 1144-55.

70. Rao, *Modulation of aqueous humor outflow facility by the rho kinase-specific inhibitor Y-27632 (vol 42, pg 1029, 2001).* Investigative Ophthalmology & Visual Science, 2001. **42**(8): p. 1690-1690.

71. Honjo, M., M. Inatani, N. Kido, et al., *A myosin light chain kinase inhibitor, ML-9, lowers the intraocular pressure in rabbit eyes.* Exp Eye Res, 2002. **75**(2): p. 135-42.

72. Honjo, M., H. Tanihara, M. Inatani, et al., *Effects of rho-associated protein kinase inhibitor Y-27632 on intraocular pressure and outflow facility.* Invest Ophthalmol Vis Sci, 2001. **42**(1): p. 137-44.

73. Tamura, M., H. Nakao, H. Yoshizaki, et al., *Development of specific Rho-kinase inhibitors and their clinical application.* Biochimica Et Biophysica Acta-Proteins and Proteomics, 2005. **1754**(1-2): p. 245-252.

74. Williams, R.D., G.D. Novack, T. van Haarlem, et al., *Ocular hypotensive effect of the Rho kinase inhibitor AR-12286 in patients with glaucoma and ocular hypertension.* Am J Ophthalmol, 2011. **152**(5): p. 834-41 e1.

75. Gong, H. and C.Y. Yang, *Morphological and hydrodynamic correlations with increasing outflow facility by rho-kinase inhibitor Y-27632.* J Ocul Pharmacol Ther, 2014. **30**(2-3): p. 143-53.

76. Wang, S.K. and R.T. Chang, *An emerging treatment option for glaucoma: Rho kinase inhibitors.* Clin Ophthalmol, 2014. **8**: p. 883-90.

77. Ethier, C.R., A.T. Read, and D.W. Chan, *Effects of latrunculin-B on outflow facility and trabecular meshwork structure in human eyes.* Invest Ophthalmol Vis Sci, 2006. **47**(5): p. 1991-8.

78. Tian, B., B.T. Gabelt, J.A. Peterson, et al., *H-7 increases trabecular facility and facility after ciliary muscle disinsertion in monkeys.* Invest Ophthalmol Vis Sci, 1999. **40**(1): p. 239-42.

79. McKee, C.T., J.A. Wood, N.M. Shah, et al., *The effect of biophysical attributes of the ocular trabecular meshwork associated with glaucoma on the cell response to therapeutic agents.* Biomaterials, 2011. **32**(9): p. 2417-23.

80. Sabanay, I., B.T. Gabelt, B. Tian, et al., *H-7 effects on the structure and fluid conductance of monkey trabecular meshwork.* Arch Ophthalmol, 2000. **118**(7): p. 955-62.

81. Tripathi, R.C., J. Li, W.F. Chan, et al., *Aqueous humor in glaucomatous eyes contains an increased level of TGF-beta 2.* Exp Eye Res, 1994. **59**(6): p. 723-7.

82. Inatani, M., H. Tanihara, H. Katsuta, et al., *Transforming growth factor-beta 2 levels in aqueous humor of glaucomatous eyes.* Graefes Arch Clin Exp Ophthalmol, 2001. **239**(2): p. 109-13.

83. Trivedi, R.H., M. Nutaitis, D. Vroman, et al., *Influence of race and age on aqueous humor levels of transforming growth factor-beta 2 in glaucomatous and nonglaucomatous eyes.* J Ocul Pharmacol Ther, 2011. **27**(5): p. 477-80.

84. Li, J., B.J. Tripathi, and R.C. Tripathi, *Modulation of pre-mRNA splicing and protein production of fibronectin by TGF-beta2 in porcine trabecular cells.* Invest Ophthalmol Vis Sci, 2000. **41**(11): p. 3437-43.

85. Welge-Lussen, U., C.A. May, and E. Lutjen-Drecoll, *Induction of tissue transglutaminase in the trabecular meshwork by TGF-beta1 and TGF-beta2.* Invest Ophthalmol Vis Sci, 2000. **41**(8): p. 2229-38.

86. Flugel-Koch, C., A. Ohlmann, R. Fuchshofer, et al., *Thrombospondin-1 in the trabecular meshwork: localization in normal and glaucomatous eyes, and induction by TGF-beta1 and dexamethasone in vitro.* Exp Eye Res, 2004. **79**(5): p. 649-63.

87. Zhao, X., K.E. Ramsey, D.A. Stephan, et al., *Gene and protein expression changes in human trabecular meshwork cells treated with transforming growth factor-beta.* Invest Ophthalmol Vis Sci, 2004. **45**(11): p. 4023-34.

88. Zhao, X. and P. Russell, *Versican splice variants in human trabecular meshwork and ciliary muscle.* Mol Vis, 2005. **11**: p. 603-8.

89. Han, H., T. Wecker, F. Grehn, et al., *Elasticity-dependent modulation of TGF-beta responses in human trabecular meshwork cells.* Invest Ophthalmol Vis Sci, 2011. **52**(6): p. 2889-96.

90. Sethi, A., W. Mao, R.J. Wordinger, et al., *Transforming growth factor-beta induces extracellular matrix protein cross-linking lysyl oxidase (LOX) genes in human trabecular meshwork cells.* Invest Ophthalmol Vis Sci, 2011. **52**(8): p. 5240-50.

91. Wiederholt, M., A. Sturm, and A. Lepple-Wienhues, *Relaxation of trabecular meshwork and ciliary muscle by release of nitric oxide.* Invest Ophthalmol Vis Sci, 1994. **35**(5): p. 2515-20.

92. Dismuke, W.M., J. Liang, D.R. Overby, et al., *Concentration-related effects of nitric oxide and endothelin-1 on human trabecular meshwork cell contractility.* Exp Eye Res, 2014. **120**: p. 28-35.

93. Cavet, M.E., J.L. Vittitow, F. Impagnatiello, et al., *Nitric Oxide (NO): An Emerging Target for the Treatment of Glaucoma.* Investigative Ophthalmology & Visual Science, 2014. **55**(8): p. 5005-5015.

94. Morgan, J.T., V.K. Raghunathan, Y.R. Chang, et al., *The intrinsic stiffness of human trabecular meshwork cells increases with senescence.* Oncotarget, 2015. **6**(17): p. 15362-74.

95. Morgan, J.T., V.K. Raghunathan, Y.R. Chang, et al., *Wnt inhibition induces persistent increases in intrinsic stiffness of human trabecular meshwork cells.* Exp Eye Res, 2015. **132**: p. 174-8.

96. Raghunathan, V.K., J.T. Morgan, B. Dreier, et al., *Role of substratum stiffness in modulating genes associated with extracellular matrix and mechanotransducers YAP and TAZ.* Invest Ophthalmol Vis Sci, 2013. **54**(1): p. 378-86.

97. Boussommier-Calleja, A. and D.R. Overby, *The Influence of Genetic Background on Conventional Outflow Facility in Mice.* Investigative Ophthalmology & Visual Science, 2013. **54**(13): p. 8251-8258.

98. Raghunathan, V.K., J.T. Morgan, S.A. Park, et al., *Dexamethasone Stiffens Trabecular Meshwork, Trabecular Meshwork Cells, and Matrix.* Investigative Ophthalmology & Visual Science, 2015. **56**(8): p. 4447-4459.

99. Braunsmann, C., C.M. Hammer, J. Rheinlaender, et al., *Evaluation of lamina cribrosa and peripapillary sclera stiffness in pseudoexfoliation and normal eyes by atomic force microscopy.* Invest Ophthalmol Vis Sci, 2012. **53**(6): p. 2960-7.

100. Seifert, J., C.M. Hammer, J. Rheinlaender, et al., *Distribution of Young's modulus in porcine corneas after riboflavin/UVA-induced collagen cross-linking as measured by atomic force microscopy.* PLoS One, 2014. **9**(1): p. e88186.

101. Wilusz, R.E., L.E. DeFrate, and F. Guilak, *Immunofluorescence-guided atomic force microscopy to measure the micromechanical properties of the pericellular matrix of porcine articular cartilage.* J R Soc Interface, 2012. **9**(76): p. 2997-3007.

102. Wang, K., A.T. Read, T. Sulchek, et al., *Trabecular meshwork stiffness in glaucoma.* Exp Eye Res, 2016.

103. Tomlins, P.H. and R.K. Wang, *Theory, developments and applications of optical coherence tomography.* Journal of Physics D-Applied Physics, 2005. **38**(15): p. 2519-2535.

104. Hariri, S., M. Johnstone, Y. Jiang, et al., *Platform to investigate aqueous outflow system structure and pressure-dependent motion using high-resolution spectral domain optical coherence tomography.* Journal of Biomedical Optics, 2014. **19**(10).

105. Li, P., R. Reif, Z.W. Zhi, et al., *Phase-sensitive optical coherence tomography characterization of pulse-induced trabecular meshwork displacement in ex vivo nonhuman primate eyes.* Journal of Biomedical Optics, 2012. **17**(7).

106. Strouthidis, N.G., B. Fortune, H.L. Yang, et al., *Effect of Acute Intraocular Pressure Elevation on the Monkey Optic Nerve Head as Detected by Spectral Domain Optical Coherence Tomography.* Investigative Ophthalmology & Visual Science, 2011. **52**(13): p. 9431-9437.

107. Kagemann, L., B. Wang, G. Wollstein, et al., *IOP Elevation Reduces Schlemm's Canal Cross-Sectional Area.* Investigative Ophthalmology & Visual Science, 2014. **55**(3): p. 1805-1809.

108. Sigal, I.A., B. Wang, N.G. Strouthidis, et al., *Recent advances in OCT imaging of the lamina cribrosa.* British Journal of Ophthalmology, 2014. **98**: p. 34-39.

109. Nguyen, T.D. and B.L. Boyce, *An inverse finite element method for determining the anisotropic properties of the cornea.* Biomechanics and Modeling in Mechanobiology, 2011. **10**(3): p. 323-337.

110. Husain, A., D.K. Sehgal, and R.K. Pandey, *An inverse finite element procedure for the determination of constitutive tensile behavior of materials using miniature specimen.* Computational Materials Science, 2004. **31**(1-2): p. 84-92.

111. Zhang, K.Y., X.Q. Qian, X. Mei, et al., *An inverse method to determine the mechanical properties of the iris in vivo.* Biomedical Engineering Online, 2014. **13**.

112. Acott, T.S., P.D. Kingsley, J.R. Samples, et al., *Human Trabecular Meshwork Organ-Culture - Morphology and Glycosaminoglycan Synthesis.* Investigative Ophthalmology & Visual Science, 1988. **29**(1): p. 90-100.

113. Johnson, D.H. and R.C. Tschumper, *Human trabecular meshwork organ culture. A new method.* Invest Ophthalmol Vis Sci, 1987. **28**(6): p. 945-53.

114. Maas, S.A., B.J. Ellis, G.A. Ateshian, et al., *FEBio: Finite Elements for Biomechanics.* Journal of Biomechanical Engineering-Transactions of the Asme, 2012. **134**(1).

115. G.A., H., *Biomechanics of Soft Tissue*. 2000.

116. McKee, C.T., J.A. Last, P. Russell, et al., *Indentation versus tensile measurements of Young's modulus for soft biological tissues.* Tissue Eng Part B Rev, 2011. **17**(3): p. 155-64.

117. A., E.C.R.a.S.C., *Introductory Biomechanics: From Cells to Organisms.* 2013: Cambridge UP.

118. Akhtar, R., M.J. Sherratt, J.K. Cruickshank, et al., *Characterizing the elastic properties of tissues.* Mater Today (Kidlington), 2011. **14**(3): p. 96-105.

119. Allingham, R.R., A.W. deKater, and C.R. Ethier, *Schlemm's canal and primary open angle glaucoma: Correlation between Schlemm's canal dimensions and outflow facility.* Experimental Eye Research, 1996. **62**(1): p. 101-109.

120. Vranka, J.A., V. Raghunathan, P. Russell, et al., *Biomechanical Rigidity and Proteomics Analyses of Segmental Outflow Regions of the Trabecular Meshwork at Physiologic and Elevated Pressures.* Investigative Ophthalmology & Visual Science, 2016. **57**(12).

121. Linden, C. and A. Alm, *Prostaglandin analogues in the treatment of glaucoma.* Drugs Aging, 1999. **14**(5): p. 387-98.

122. Williams, R.D., G.D. Novack, T. van Haarlem, et al., *Ocular Hypotensive Effect of the Rho Kinase Inhibitor AR-12286 in Patients With Glaucoma and Ocular Hypertension.* American Journal of Ophthalmology, 2011. **152**(5): p. 834-841.

123. Bembridge, H.M.a.J., *Intraocular pressure.* Continuing Education in Anaesthesia, Critical Care & Pain, 2008. **8**(3): p. 100-103.

124. Weinreb, R.N., J. Cook, and T.R. Friberg, *Effect of Inverted Body Position on Intraocular-Pressure.* American Journal of Ophthalmology, 1984. **98**(6): p. 784-787.

125. Friberg, T.R. and R.N. Weinreb, *Ocular Manifestations of Gravity Inversion.* Jama-Journal of the American Medical Association, 1985. **253**(12): p. 1755-1757.

126. Friberg, T.R., G. Sanborn, and R.N. Weinreb, *Intraocular and Episcleral Venous-Pressure Increase during Inverted Posture.* American Journal of Ophthalmology, 1987. **103**(4): p. 523-526.

127. Phelps, C.D., *The pathogenesis of glaucoma in Sturge-Weber syndrome.* Ophthalmology, 1978. **85**(3): p. 276-86.

128. Phelps, C.D., H.S. Thompson, and K.C. Ossoinig, *The Diagnosis and Prognosis of Atypical Carotid-Cavernous Fistula (Red-Eyed Shunt Syndrome).* American Journal of Ophthalmology, 1982. **93**(4): p. 423-436.

129. Johnstone, M.A., *The aqueous outflow system as a mechanical pump - Evidence from examination of tissue and aqueous movement in human and non-human primates.* Journal of Glaucoma, 2004. **13**(5): p. 421-438.

130. Xin, C., M. Johnstone, N.L. Wang, et al., *OCT Study of Mechanical Properties Associated with Trabecular Meshwork and Collector Channel Motion in Human Eyes.* Plos One, 2016. **11**(9).

131. Xin, C., R.K. Wang, S. Song, et al., *Aqueous outflow regulation: Optical coherence tomography implicates pressure-dependent tissue motion.* Exp Eye Res, 2016.

132. Johnstone, M.A., *Pressure-dependent changes in configuration of the endothelial tubules of Schlemm's canal.* Am J Ophthalmol, 1974. **78**(4): p. 630-8.

133. Johnstone, M.A. and W.M. Grant, *Microsurgery of Schlemm's canal and the human aqueous outflow system.* Am J Ophthalmol, 1973. **76**(6): p. 906-17.

134. Van Buskirk, E.M., *Anatomic correlates of changing aqueous outflow facility in excised human eyes.* Invest Ophthalmol Vis Sci, 1982. **22**(5): p. 625-32.

135. Rohen, J.W. and F.J. Rentsch, *[Morphology of Schlemm's canal and related vessels in the human eye]*. Albrecht Von Graefes Arch Klin Exp Ophthalmol, 1968. **176**(4): p. 309-29.

136. Smit, B.A. and M.A. Johnstone, *Effects of viscoelastic injection into Schlemm's canal in primate and human eyes - Potential relevance to viscocanalostomy.* Ophthalmology, 2002. **109**(4): p. 786-792.

137. Williams, A.M., W.D. Stamer, and R.R. Allingham, *Increasing the Availability and Quality of Donor Eyes for Research.* Jama Ophthalmology, 2016. **134**(4): p. 351-352.

138. Savinova, O.V., F. Sugiyama, J.E. Martin, et al., *Intraocular pressure in genetically distinct mice: an update and strain survey.* BMC Genet, 2001. **2**: p. 12.

139. Sherwood, J.M., E. Reina-Torres, J.A. Bertrand, et al., *Measurement of Outflow Facility Using iPerfusion.* Plos One, 2016. **11**(3).

140. Wang, K., A.T. Read, T. Sulchek, et al., *Trabecular meshwork stiffness in glaucoma.* Experimental Eye Research, 2017. **158**: p. 3-12.

141. Erickson, Q.L., T. Clark, K. Larson, et al., *Flash freezing of Mohs micrographic surgery tissue can minimize freeze artifact and speed slide preparation.* Dermatol Surg, 2011. **37**(4): p. 503-9.

142. Steu, S., M. Baucamp, G. von Dach, et al., *A procedure for tissue freezing and processing applicable to both intra-operative frozen section diagnosis and tissue banking in surgical pathology.* Virchows Archiv, 2008. **452**(3): p. 305-312.

143. Sainani, K., *The Importance of Accounting for Correlated Observations.* Pm&R, 2010. **2**(9): p. 858-861.

144. Wang, K., M.A. Johnstone, C. Xin, et al., *Estimating Human Trabecular Meshwork Stiffness by Numerical Modeling and Advanced OCT Imaging.* Invest Ophthalmol Vis Sci, 2017. **58**(11): p. 4809-4817.

145. Armentano, R.L., D.B. Santana, E.I. Cabrera Fischer, et al., *An in vitro study of cryopreserved and fresh human arteries: a comparison with ePTFE prostheses and human arteries studied non-invasively in vivo.* Cryobiology, 2006. **52**(1): p. 17-26.

146. Coudrillier, B., D.M. Geraldes, N.T. Vo, et al., *Phase-Contrast Micro-Computed Tomography Measurements of the Intraocular Pressure-Induced Deformation of the Porcine Lamina Cribrosa.* IEEE Trans Med Imaging, 2016. **35**(4): p. 988-99.

147. Overby, D.R., J. Bertrand, O.Y. Tektas, et al., *Ultrastructural Changes Associated With Dexamethasone-Induced Ocular Hypertension in Mice.* Investigative Ophthalmology & Visual Science, 2014. **55**(8): p. 4922-4933.

148. Agrahari, V., G. Li, V. Agrahari, et al., *Pentablock copolymer dexamethasone nanoformulations elevate MYOC: in vitro liberation, activity and safety in human trabecular meshwork cells.* Nanomedicine (Lond), 2017. **12**(16): p. 1911-1926.

149. Overby, D.R., J. Bertrand, O.Y. Tektas, et al., *Ultrastructural changes associated with dexamethasone-induced ocular hypertension in mice.* Invest Ophthalmol Vis Sci, 2014. **55**(8): p. 4922-33.

150. Vranka, J.A., M.J. Kelley, T.S. Acott, et al., *Extracellular matrix in the trabecular meshwork: intraocular pressure regulation and dysregulation in glaucoma.* Exp Eye Res, 2015. **133**: p. 112-25.

151. Singh, M., J.S. Li, Z.L. Han, et al., *Evaluating the Effects of Riboflavin/UV-A and Rose-Bengal/Green Light Cross-Linking of the Rabbit Cornea by Noncontact Optical Coherence Elastography.* Investigative Ophthalmology & Visual Science, 2016. **57**(9): p. Oct112-Oct120.

152. Han, Z.L., J.S. Li, M. Singh, et al., *Optical coherence elastography assessment of corneal viscoelasticity with a modified Rayleigh-Lamb wave model.* Journal of the Mechanical Behavior of Biomedical Materials, 2017. **66**: p. 87-94.

153. Wang, S. and K.V. Larin, *Shear wave imaging optical coherence tomography (SWI-OCT) for ocular tissue biomechanics.* Optics Letters, 2014. **39**(1): p. 41-44.

154. Park, S., H. Yoon, K.V. Larin, et al., *The impact of intraocular pressure on elastic wave velocity estimates in the crystalline lens.* Physics in Medicine and Biology, 2017. **62**(3): p. N45-N57.

155. Hogan, M.J.A., J. A.; Weddell, J.E., in *Histology of the Human Eye*. 1971, W.B. Saunders Company. p. 160.

156. Baraniak, P.R., M.T. Cooke, R. Saeed, et al., *Stiffening of human mesenchymal stem cell spheroid microenvironments induced by incorporation of gelatin microparticles.* J Mech Behav Biomed Mater, 2012. **11**: p. 63-71.

157. Quapp, K.M. and J.A. Weiss, *Material characterization of human medial collateral ligament.* Journal of Biomechanical Engineering-Transactions of the Asme, 1998. **120**(6): p. 757-763.

158. Yamamoto, E., K. Hayashi, and N. Yamamoto, *Mechanical properties of collagen fascicles from stress-shielded patellar tendons in the rabbit.* Clinical Biomechanics, 1999. **14**(6): p. 418-425.

159. Pant, A.D.K., L.; Schuman, J.S.; Sigal, I.A.; Amini, R., *An imaged-based inverse finite element method to determine in-vivo mechanical properties of the human trabecular meshwork.* Journal for Modeling in Ophthalmology, 2017. **3**: p. 100-111.

160. Mckay, M.D., R.J. Beckman, and W.J. Conover, *A Comparison of Three Methods for Selecting Values of Input Variables in the Analysis of Output from a Computer Code.* Technometrics, 1979. **21**(2): p. 239-245.

161. Blower, S.M. and H. Dowlatabadi, *Sensitivity and Uncertainty Analysis of Complex-Models of Disease Transmission - an Hiv Model, as an Example.* International Statistical Review, 1994. **62**(2): p. 229-243.

162. Tehrani, S., *Gender difference in the pathophysiology and treatment of glaucoma.* Curr Eye Res, 2015. **40**(2): p. 191-200.

163. Conover, W.J., *Practical Nonparametric Statistics*. Third ed. 1999.

164. al., S.T.P.e., *OMNITAB 80: An Interpretive System for Statistical and Numerical Data Analysis*. 1986: NBS Special Publication 701.

165. Ethier, C.R., A.T. Read, and D. Chan, *Biomechanics of Schlemm's canal endothelial cells: influence on F-actin architecture.* Biophys J, 2004. **87**(4): p. 2828-37.

166. Stamer, W.D., S.T. Braakman, E.H. Zhou, et al., *Biomechanics of Schlemm's canal endothelium and intraocular pressure reduction.* Prog Retin Eye Res, 2015. **44**: p. 86-98.

167. Last, J.A., T.R. Pan, Y.Z. Ding, et al., *Elastic Modulus Determination of Normal and Glaucomatous Human Trabecular Meshwork.* Investigative Ophthalmology & Visual Science, 2011. **52**(5): p. 2147-2152.

168. Last, J.A., S.J. Liliensiek, P.F. Nealey, et al., *Determining the mechanical properties of human corneal basement membranes with atomic force microscopy.* J Struct Biol, 2009. **167**(1): p. 19-24.

169. Yu, W.Y., C. Sheridan, I. Grierson, et al., *Progenitors for the corneal endothelium and trabecular meshwork: a potential source for personalized stem cell therapy in corneal endothelial diseases and glaucoma.* J Biomed Biotechnol, 2011. **2011**: p. 412743.

170. Thomasy, S.M., V.K. Raghunathan, M. Winkler, et al., *Elastic modulus and collagen organization of the rabbit cornea: epithelium to endothelium.* Acta Biomater, 2014. **10**(2): p. 785-91.